國立臺灣大學生命科學院植物科學研究所

碩士論文

Institute of Plant Biology

College of Life Science

National Taiwan University

Master's Thesis

阿拉伯芥熱休克轉錄因子 HsfA7a 和 HsfA7b 參與非生
物逆境反應之功能性研究

Functional study of heat shock transcription factors
HsfA7a and HsfA7b required for abiotic stress responses
in Arabidopsis

許宇豪

Xu, Yu-Hao

指導教授：靳宗洛 博士

Advisor: Tsung-Luo Jinn, Ph.D

中華民國 112 年 11 月

November, 2023

致謝

　　首先，我想先謝謝自己那麼努力的把實驗以及論文完成，在最艱困的時刻除了很感謝幫助我的人以外，自己的堅持與奮鬥功不可沒。再來，感謝靳宗洛老師在這三年來提供了實這麼多經費以及資源讓我可以做研究，也對我指導了許多研究上的問題、修改我的論文、進行數據的討論等等。另外，老師在我有困難的時候也給予我許多的關心與開導，我會銘記在心，希望老師的身體可以保持健康。也感謝我的母親不厭其煩的陪我聊天，抒發我的情緒，撐過情緒最為低落的時刻。

　　感謝一開始遇到的凌志學長、宥豪學弟在百忙之中帶我這個毫無經驗的新生做實驗；也感謝 Sandeep 在英文寫作與實驗上的許多幫助，在生活上陪我去爬爬山、聊天、吃飯，也以一位過來人的角度給予我許多人生經驗，讓我在台北有一位朋友可以訴苦、給予我支持。謝謝品萱、芷淇、胤榮、Silambu 在不同的事情給予我幫助，如實驗、帶學弟妹、處理實驗室雜事、陪我聊天等等，以後實驗室就靠你們了，也祝 Silambu 可以順利發表文章畢業。

　　僅此獻給曾經幫助我許多的各位朋友、老師以及家人，也謝謝中研院葉國禎老師實驗室的幫忙，讓我能順利的運用 CRISPR-Cas9 的技術。

i

摘要

植物熱休克轉錄因子（HSFs）調節包括高溫、乾旱、低溫、鹽度和氧化壓力逆境在內等非生物逆境反應。*HSFA7a* 和 *HSFA7b* 在演化上具有親緣關係，暗示著這兩個基因可能共同參與調控非生物逆境反應。利用 CRISPR-Cas9 技術建立 *HSFA7a* 和 *HSFA7b* 的雙突變株，其在 75 mM 氯化鈉或 100 mM 甘露醇瓊脂培養基上生長的根長度較野生型短。此外，*HSFA7b* 缺失株在滲透壓逆境下呈現不敏感的表現型。關於下胚軸延長的實驗結果顯示，雙突變植物對於先天耐熱性（BT）不敏感，但在後天短期耐熱性（SAT）條件下呈現敏感的表型。耐熱性分析的結果顯示，在 SAT 和梯度熱逆境（GHS）下，*HSFA7a* 和 *HSFA7b* 共同負調控植物耐熱性；然而 *HSFA7b* 單獨正向調控長期後天耐熱性（LAT)。有鑑於這些表型，植株在 GHS 和 LAT 熱處理後進行了 RNA-seq 轉錄體分析，以尋找由 *HSFA7a* 和 *HSFA7b* 所調控的下游基因。我們觀察到在兩個數據集中關於光合作用相關的上調差異表達基因（DEGs）重疊，暗示這兩個基因可能參與光合作用過程。總而言之，我們的結果突顯了 *HSFA7a* 和 *HSFA7b* 在不同非生物逆境下的複雜調控機制，並識別出潛在的下游基因，將進一步進行分析。

Abstract
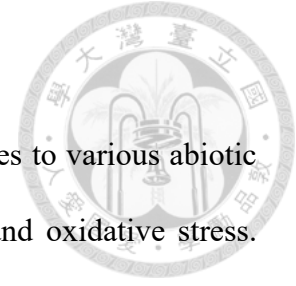
Plant heat shock factors (HSFs) are crucial in orchestrating responses to various abiotic stresses, including high and low temperatures, drought, salinity, and oxidative stress. *HSFA7a* and *HSFA7b* exhibit a shared evolutionary lineage, suggesting their possible collaboration in the regulation of abiotic stress responses. Leveraging CRISPR-Cas9 technology, we generated double mutant lines of *HSFA7a* and *HSFA7b*, which exhibited reduced root lengths when exposed to 75 mM sodium chloride or 100 mM mannitol treatments compared to wild-type plants. Furthermore, *HSFA7b*-deficient mutants displayed insensitivity to osmotic stress. Our experimental findings on hypocotyl elongation indicated that these double mutant plants were less responsive to basal thermotolerance (BT) yet displayed heightened sensitivity under short-term acquired thermotolerance (SAT) conditions. Heat tolerance analyses unveiled that *HSFA7a* and *HSFA7b* jointly exerted a negative regulatory influence on plant thermotolerance during SAT and gradient heat stress (GHS) scenarios, with *HSFA7b* demonstrating independent positive regulation of long-term acquired thermotolerance (LAT). Given these distinctive phenotypes, we conducted RNA-seq transcriptome analyses on plants subjected to GHS and LAT heat treatments to identify downstream genes under the regulatory influence of *HSFA7a* and *HSFA7b*. Remarkably, we observed a convergence of upregulated differentially expressed genes (DEGs) associated with photosynthesis in both datasets, suggesting the potential involvement of these genes in the photosynthesis process. In summary, our findings shed light on the complex regulatory mechanisms governing *HSFA7a* and *HSFA7b* responses to diverse abiotic stresses and identify candidate downstream genes warranting further investigation.

Table of contents

vi

List of figures

ix

List of tables

Abbreviations

AT   Acquired Thermotolerance

AZC   Azetidine-2-Carboxylic Acid

BT   Basal Thermotolerance

DBD   DNA Binding Domain

DEG   Differentially expressed gene

ER   Endoplasmic Reticulum

GHS   Gradient Heat Stress

HS   Heat Stress

HSF   Heat Shock Factor

HSP   Heat Shock Protein

HSR   Heat Shock/Heat Response

KD   Knockdown

KO   Knockout

LAT   Long-term Acquired Thermotolerance

OD   Oligomerization Domain

OE   Overexpression

PM   Plasma Membrane

ROS Reactive Oxygen Species

SAT Short-term Acquired Thermotolerance

UPR Unfold Protein Responses
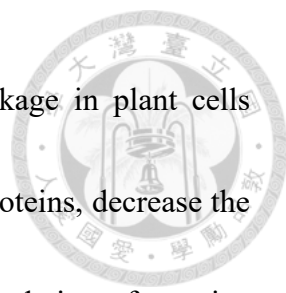
Introduction

Due to climate change, it can be predicted that more extreme natural disasters will occur, leading to severe reductions in crop yields (Tubiello et al., 2007). High temperatures, disastrous floods, and abnormal droughts would cause catastrophic impacts on plant survival. As sessile organisms, plants cannot prevent harmful situations by migrating to safer places. Hence, for survival, they have evolved numerous molecular mechanisms to sense and respond to enormous environmental stresses, such as heat, salinity, drought, and oxidative stress (Cheeseman, 1988; Demidchik, 2015; Fang and Xiong, 2015; Ohama et al., 2017). Nonetheless, although a large number of studies have been conducted to figure out how plants cope with abiotic stresses, many mechanisms require further investigation.

Heat Stress/ Shock (HS)

In general, heat stress or shock (HS) refers to an ambient temperature increase of 10-15°C above optimal growth (Wahid et al., 2007). HS can impair numerous physiological functions, such as plant growth, metabolism, photosynthesis, and membrane stability (Wahid et al., 2007; Allakhverdiev et al., 2008; Fahad et al., 2017). For instance, HS mostly damages leaves and results in curling, necrosis, and leaf senescence. Furthermore,

1
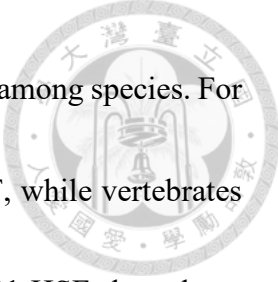
HS can change the membrane fluidity, leading to electrolytic leakage in plant cells (Savchenko et al., 2002). HS will lead to misfolding of functional proteins, decrease the activity of various critical enzymes in plants, and cause the accumulation of reactive oxygen species (ROS). Excess ROS induced by HS will interrupt the physiological activities and evaluate the oxidative stress in plants.

Naturally, plants have inherent capability to survive exposure to high temperatures without prior acclimation, which is considered as basal thermotolerance (BT). Additionally, acquired thermotolerance (AT) refers to the ability to survive lethal heat stress induced by a short acclimation period at moderately high but survivable temperature (Vierling, 1991; Larkindale et al., 2005).

Heat Shock Factors (HSFs)

Heat shock factors (HSFs) are the key signal transduction components activating gene expression in response to not only heat stress but other abiotic stress, and HSFs act as transcriptional regulators to encode heat shock proteins (HSPs) that maintain protein homeostasis (Nover et al., 2001; Ohama et al., 2015; Andrási et al., 2020). HSFs are evolutionarily conserved among eukaryotes; they have been found in *Saccharomyces cerevisiae* (Sorger and Pelham, 1988), *Drosophila buschii* (Clos et al., 1990), and *Homo*

2

sapiens (Goldenberg, 1988). However, the number of HSFs is diverse among species. For instance, Drosophila and *Caenorhabditis elegan*s have only one HSF, while vertebrates contain four HSFs (Nover et al., 2001). In the case of Arabidopsis, 21 HSFs have been discovered, and they can be categorized into three distinct classes based on their structural differences.

In general, HSFs typically contain four conserved regions: N-terminal DNA binding domain (DBD), oligomerization domain (OD) or HR-A/B region, nuclear localization and export signals (NLS and NES), and activator motifs (AHA motifs) (Wu, 1995; Nover et al., 2001).The DBD domain is located near the N-terminus of all HSFs, and it encompasses a helix-turn-helix motif responsible for recognizing and binding to the cis-elements of downstream genes. These *cis*-elements are known as heat shock elements (HSEs, 5'-AGAAnnTTCT-3'), and they are conserved in the promoter regions of HSPs and other genes involved in the heat stress response. The OD or HR-A/B region is involved in the trimerization of HSFs, and HSFs are divided into three classes (A, B, and C) based on the structural variations within the OD or HR-A/B region. In Arabidopsis, class A HSFs have 21 inserted amino acids between A and B segments, while class C HSF has only 7 amino acids inserted. On the other hand, class B HSFs have flexible

3

linkers between HR-A/B regions. The NLS and NES mediate the transportation of HSFs into or out of the nucleus, located at the C-terminal of HSFs. Only class A HSFs possess the AHA domain at their C-terminal end and function as transcriptional activators based on this unique domain. Class B HSFs, in contrast, carry a repression domain and act as transcriptional repressors (von Koskull-Döring et al., 2007).

Numerous studies have confirmed the pivotal role of *HSFA1s* (a, b, d, e) as master regulators in mediating heat stress response (HSR) and participating in other stress responses (Liu et al., 2011; Liu and Charng, 2013). Quadruple knockout (QK) mutant of *HSFA1s* shows severe defeat in basal and acquired thermotolerance. Additionally, the expression levels of many HS-related genes such as *DREB2A, HSFA2, HSFA3, HSFA7a,* and *HSFA7b* dramatically decrease in the QK mutant, resulting in heat sensitivity phenotypes (Liu et al., 2011). *HSFA2* is a highly inducible gene in HS and plays a critical role in HS transcriptional memory (Charng et al., 2007). *HSFA2* is also indispensable in activating plenty of downstream genes to regulate HSR (Schramm et al., 2006).

HSFA3 is a unique HSF gene induced by *DREB2A* and phylogenetically distinct from other HSFs. It contributes to the expression of heat shock proteins (HSPs) during heat stress, enhancing thermotolerance (Yoshida et al., 2008). Recent research has

4

demonstrated that HSFA2 and HSFA3 can form heterotrimers to regulate HS

transcriptional memory and maintain the expression of HS memory genes (Friedrich et

al., 2021). HSFA4 and HSFA5 have distinguished structural features of the

oligomerization domain from other HSFs, and HSFA5 specifically acts as the repressor

of HSFA4 which involved in HSR and oxidative stress responses (Baniwal et al., 2007;

Kotak et al., 2007).

HSFA6a is involved in ABA-dependent signaling pathway and positively regulates

salinity stress, osmotic stress, and drought stress responses (Hwang et al., 2014). On the

other hand, HSFA6b is dramatically induced by salinity, osmotic, and cold stresses.

HSFA6b acts as a critical role in ABA-mediated stress responses such as drought, salinity,

and thermotolerance (Huang et al., 2016; Wenjing et al., 2020). Both HSFA6a and

HSFA6b are activated by ABA-responsive element binding factor/ABA responsive

element binding protein, which are key regulators of the ABA signaling pathway (Hwang

et al., 2014). HSFA7a and HSFA7b are induced extensively by heat stress (Liu et al.,

2011). Interestingly, the expression level of HSFA7a can also be induced by azetidine-2-

carboxylic acid (AZC) treatment, which leads to the accumulation of misfolded proteins

and triggers the cytosolic protein response. This suggests the complex role of HSFA7a in

5

heat stress responses (Lin et al., 2018). HSFA7b also acts as a positive regulator and binds

to the E-box motifs to mediate in salinity tolerance (Zang et al., 2019). HSFA8 has been

validated that the conserved cysteinyl residues in HSFA8 act as redox sensors in plants.

Upon H_2O_2 treatment, HSFA8 will translocate from the cytosol to the nucleus to regulate

oxidate stress response (Giesguth et al., 2015; Andrasi et al., 2020). HSFA9 activates

specialized HSPs expression during the late stage of seed development (Kotak et al., 2007;

TEJEDOR-CANO et al., 2010).

HSFB1 and HSFB2b suppress HSR under non-heat-stress conditions, but they are

essential for expression of HSPs during HS and maintain acquired thermotolerance.

Moreover, HSFB1 and HSFB2b involve in pathogen resistance, which show the diverse

functions of HSFs (Ikeda et al., 2011; Pick et al., 2012). HSFB2a is required for

gametophyte development, and HSFB4 positively regulates root stem cell niche to control

cell identity (Begum et al., 2013; Wunderlich et al., 2014). HSFC1 may participate in

cold stress response and the expression level of *HSFC1* is induced by cold, ABA and

NaCl treatments (張凌誌, 2021).

6

Heat Stress Response

Heat stress response (HSR) is a protection mechanism which triggers transcription and translation of protective proteins or enzymes in plants to prevent from the damage from HS (Wahid et al., 2007). This evolutionarily conserved process is observed in both prokaryotic and eukaryotic organisms, and it involves the induction of a multitude of genes.

The initiation of HSR in plants begins with thermosensing. Recent reports indicate that DNA, RNA, proteins, and membrane fluidity can be thermosensors (Mittler et al., 2012; Vu et al., 2019). At low temperatures, a specific histone variant called H2A.Z is highly abundant in nucleosomes and occupies DNA structures. The occupancy hinders transcription by preventing RNA Polymerase II from binding to the cis-elements of target genes. Consequently, H2A.Z functions as a physical block to repress the expression of certain genes at low temperature and regulate the transcription activities. As the temperature rises, however, the occupancy of H2A.Z nucleosomes declines, which leads to increased expression of genes such as *HSP70* (Kumar and Wigge, 2010; Cortijo et al., 2017). Recent research highlights that the deposition of H2A.Z is regulated by POWERDRESS (PWR) and HISTONE DEACETYLASE 9 (HDA9) during high temperatures and these genes are involved in HSR (Tasset et al., 2018). In summary,

7

temperature-induced chromatin remodeling affects transcriptional activity, and this

process acts as a thermosensor to trigger downstream signaling pathways in response to

temperature fluctuation in plants.

Temperature will also affect the secondary structure of RNA, which in turn regulates

many RNA-related processes. In bacteria, elevated temperature can cause the "unzipping"

of mRNA stem-loop structures, resulting in ribosome binding and the translation process.

Although only little research has been conducted to figure out the detailed mechanism of

thermosensing at the RNA level in plants, the conformational changes in RNA suggest

the possibility that RNA might act as thermosensors to evoke HSR (Mittler et al., 2012;

Vu et al., 2019).

During heat stress, the stability and structure of various proteins are disturbed,

causing the aggregation or denaturation of proteins. These conformational changes in

proteins act as thermosensors, initiating diverse physiological responses. For instance,

recent reports demonstrated that phytochrome B (phyB), which is involved in red light

sensing, modulates thermomorphogenesis through its own conformational changes,

subsequently regulating downstream genes like the basic helix-loop-helix transcription

factor PHYTOCHROME-INTERACTING FACTOR 4 (PIF4). When subjected to far-

red light and high temperatures, phyB transitions from its active Pfr form to its inactive

Pr form, resulting in PIF4 accumulation and promoting cell elongation (Quint et al., 2016).
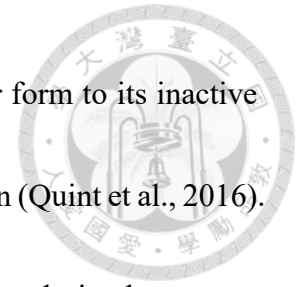
The plasma membrane (PM) plays a pivotal role in thermosensing during heat stress

(HS). Composed of two lipid layers, the PM houses various membrane-associated

proteins that regulate the exchange of compounds. HS enhances membrane fluidity and

evokes rapid calcium (Ca^{2+}) influx into the cell, controlled by heat-sensitive membrane-

associated Ca^{2+} channels such as PLANT CYCLIC NUCLEOTIDE-GATED

CHANNELLS (CNGCs) and trigger HSR. Moreover, membrane molecules such as

phospholipids, cholesterol can generate stress-induced second messengers when HS

strikes. Phospholipids are modified by PHOSPHATIDYLINOSITOLPHOSPHATE

KINASE (PIPK) and PHOSPHOLIPASE D (PLD), and this process eventually leads to

the accumulation of inositol 1,4,5-trisphosphate (IP3). IP3 regulates the influx of Ca^{2+}

and activates transcription of heat shock genes and trigger HSR during HS (Tang et al.,

2007).

Moreover, HS-induced accumulation of misfolded proteins in the endoplasmic

reticulum (ER) leads to ER stress, triggering the unfolded protein response (UPR) in

plants. ER is a crucial cytoplasmic membrane system of eukaryotic cells and involve in

protein synthesis, peptide chain folding and processing, post-translational modifications, lipid biosynthesis Ca^{2+} storage and homeostasis (Manghwar and Li, 2022). ER-stress causes imbalance of ER homeostasis and disrupts physiological functions of plants. The processes of UPR are regulated by intramembrane proteolysis of basic leucine zipper (bZIP) transcription factors like bZIP17/28/60. One pathway is mediated by bZIP17 and bZIP28. Under unstress conditions, bZIP17 and bZIP28 are anchored on the ER membrane by the interaction with binding protein (BiP). Once HS strikes and results in the accumulation of misfolding proteins, BiP aids in proper protein folding and releases bZIP17 and bZIP28 from the ER membrane. bZIP17 and bZIP28 then move to Golgi with the help of COAT PROTEIN II (COPII) vesicles, and SITE-1 and -2 proteases will process bZIP17 and bZIP28, which releases them from the Golgi into the nucleus. After bZIP17 and bZIP28 translocate into the nucleus, they can form a transcriptional complex to activate the genes related to UPR process (Nawkar et al., 2018; Howell, 2021; Manghwar and Li, 2022).

Another UPR pathway is mediated by bZIP60 and RNase INOSITOL-REQUIRING ENZYME 1 (IRE1). Although the detailed mechanism of this pathway needs further investigation, bZIP 60 will be spliced by IRE1, and this process leads to the translocation

into the nucleus of bZIP60 to mediate in UPR. In conclusion, the diversity of HSR in plants helps them conquer severe HS conditions; these processes decrease the damage from HS and maintain homeostasis in planta.
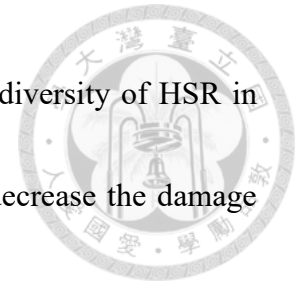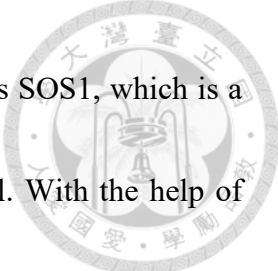
Salt Stress

Due to population growth, land overdevelopment, and the demand for food production, salt stress has emerged as a significant abiotic stress factor that severely limits plant growth and productivity. To date, approximately 20% of the world's cultivated land and nearly half of all irrigated areas are impacted by salinity (Zhu, 2001). The definition of salinity for soil is considered when the electric conductivity of the soil solution reaches 4 dS m^{-1} (equivalent to 40 mM NaCl), and leads to an osmotic pressure of about 0.2 MPa (Acosta-Motos et al., 2017). The effects of salt stress are initially felt by the root system, resulting in hyperosmotic and hyperionic conditions. These conditions hinder the plants growth by impairing plant absorption of water and nutrients from the soil. High salinity leads to the accumulation of Na^+ in the cytosol, causing a short-term reduction in water availability. Moreover, if plants continue to endure salt stress for a long duration, ion toxicity will occur and result in nutrient imbalances such as Ca^{2+} and K^+ deficiency, which

11

eventually causes damage to plants including inhibition of photosynthesis and generation

of excess reactive oxygen species (ROS).

When plants are subjected to salt stress, excess Na^+ will enter cells via nonselective

cation channels (NSCCs) or other unknown membrane transporters, which further

activate the signaling pathway such as Ca^{2+} influx and ROS burst to regulate physiological

behaviors to conquer high salinity. Plants primarily employ two major strategies to

maintain low cytoplasmic Na^+ concentrations in plant cells: Na^+ compartmentation and

Na^+ exclusion (Deinlein et al., 2014). Na^+ compartmentation involves transporting Na^+

from the cytosol into vacuoles, where excess Na^+ is stored to prevent cytosolic Na^+

toxicity. Ion transporter TONOPLAST-LOCALIZED Na^+/H^+ EXCHANGER 1(NHX1)

in Arabidopsis is mainly responsible for Na^+ compartmentation. Constitutive

overexpression of *NHX1* and its orthologs in Arabidopsis can increase plant salinity

tolerance (Apse et al., 1999). On the other hand, SALT OVERLY SENSITIVE (SOS)

genes *SOS1*, *SOS2*, and *SOS3* cascades take part in Na^+ exclusion process (Zhu et al.,

1998). *SOS3* is a calcineurin B-like protein (CBL) and known as CBL4 which senses salt-

elicited calcium signals during high salinity situations. As soon as SOS3 is activated by

high $[Ca^{2+}]_{cyt}$ under salt stress, SOS3 physically interacts with SOS2, a serine/threonine

12
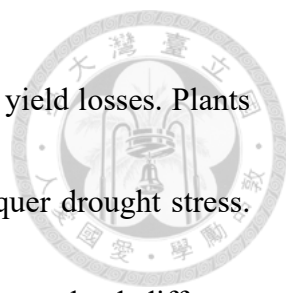
protein kinase. The downstream target of the SOS3-SOS2 complex is SOS1, which is a plasma membrane $Na^+- H^+$ antiporter that exports Na^+ from the cell. With the help of these *SOSs*, plants can effectively export excess Na^+ from the cell and maintain ionic homeostasis to increase salt tolerance.

One previous research suggested that heterotrimeric G-proteins in *Pisum sativum* played a role in signaling transduction under both heat and salt stress conditions. (Misra et al., 2007). The subunits of G-proteins, *PsGα1* and *PsGβ*, were observed to be induced by heat and salt treatments. Moreover, *Gα1*-overexpression lines exhibited higher salinity and heat tolerance compared to wild-type plants. Although there is limited research focusing on the cross-talk between salt and heat stress, investigating the signaling transduction of G-proteins could be a potential avenue to elucidate the detailed mechanisms of these two stress conditions.

Drought Stress

Drought stress occurs when the rate of transpiration in plants surpasses water uptake, resulting in a water deficit. The deficiency of water in plants triggers various changes in cell volume and membrane shape, concentration of solutes, loss of turgor, disruption of membrane integrity, and denaturation of protein (Bray, 1997). Drought stress severely

13

affects plant growth and productivity, leading to serious agricultural yield losses. Plants

have evolved different types of drought resistance strategies to conquer drought stress.

To overcome the challenges posed by drought stress, plants have evolved different

drought resistance strategies. These strategies can be categorized into four main types:

drought avoidance, drought tolerance, drought escape, and drought recovery (Fang and

Xiong, 2015).

Drought avoidance and drought tolerance are two major strategies for drought

resistance conferred by plants (Yue et al., 2006). Drought avoidance refers to the

capability of plants to maintain fundamental normal physiological processes under mild

or moderate drought stress conditions by adapting specific morphology or growth rates

to avoid the adverse effects of drought stress (Blum, 2005). Three major physiological

changes in plants can accomplish drought avoidance: (1) reducing water loss via rapidly

closing stomata; (2) enhancing the water uptake ability by increasing rooting depth,

rooting density or root/shoot ratio; (3) accelerating or decelerating the conversion from

vegetative growth to reproductive growth to avoid complete abortion at the severe

drought stress stage. Drought tolerance, on the other hand, refers to the ability of plants

to maintain specific level of physiological activities under severe drought stress

14
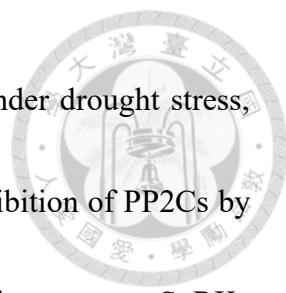
conditions by the regulation of considerable genes and numerous metabolic pathways to

reduce or repair the resulting stress damage. Many transcription factors including

APETALA2/ETHYLENE-RESPONSIVE ELEMENT BINDING PROTEIN

(AP2/EREBP), BASIC LEUCINE ZIPPER (bZIP), NAM-ATAF1/2-CUC2 (NAC)

are upregulated to mediate in downstream genes, leading to physiological changes that

contribute to drought tolerance (Fang and Xiong, 2015).

Abscisic acid (ABA), a plant hormone, plays a pivotal role in most abiotic stress

responses, including drought stress, by regulating plant water balance. For instance, the

ABA concentration of leaf can dramatically increase 10- to 50-fold within a few hours of

the onset of a water deficit (Bonetta and McCourt, 1998). The ABA biosynthesis genes

such as 9-cis-epoxycarotenoid dioxygenase (NCED), ABA DEFICIENT 1, 2, and 3

(ABA1, 2, 3) will be induced, strongly increasing ABA levels during drought stress (Zhu,

2002; Golldack et al., 2014). ABA signaling pathways are initiated by ABA receptors

known as REGULATORY COMPONENTS OF ABA RECEPTOR/PYRABACTIN

RESISTANCE PROTEIN1/PYR-LIKE PROTEINS (RCARs/PYR1/PYLs). Once ABA

binds to ABA receptors, this process will promote the receptors to bind to the catalytic

site of TYPE 2C PROTEIN PHOSPHATASES (PP2Cs), which results in inhibition of

PP2Cs' enzymatic activity and prevent them from dephosphorylating downstream targets such as SNF1-RELATED KINASES (SnRK2.2, 2.3, and 2.6) (Soon et al., 2012). SnRKs then activate downstream transcription factors, such as ABA-RESPONSIVE ELEMENT BINDING FACTORS (ABFs), which induce gene expression in response to ABA.

Both ABA-dependent and ABA-independent pathways play crucial roles in regulating drought and salt stress responses in plants. As for ABA-dependent pathways, many ABA-inducible genes contain a conserved ABA-responsive *cis*-acting element called ABA-responsive element (ABRE, 5'-ACGTGG/TC -3') in their promoter regions (Narusaka et al., 2003). A group of transcription factors such as ABRE-BIND PROTEINS (AREB) or ABA-RESPONSIVE ELEMENT BINDING FACTORS (ABFs) bind to the promoter regions of target genes which exist ABRE to regulate their expression in ABA-dependent manner (Narusaka et al., 2003; Yoshida et al., 2014). These transcription factors will be phosphorylated and activated by SnRKs and participate in ABA-dependent pathways to induce gene expression including RESPONSIVE TO DESICCATION 29 A/B (RD29A/B), which are responsible for the protection from drought and salt stresses (Msanne et al., 2011; Yoshida et al., 2014). In addition, stomata closure occurs during drought stress to reduce water loss, and this

16

process can be regulated by ABA-dependent signaling pathway. Under drought stress,

the concentration of ABA increases in leaf area and initiates the inhibition of PP2Cs by

interaction of ABA and its receptors RCARs/PYR1/PYLs. The downstream SnRKs

including OPEN STOMATA 1 (OST1) will be activated possibly by autophosphorylation,

and it activates downstream anion channels such as ANION CHANNEL-ACCOCIATED

1 (SLAC1) and QUICKLY ACTIVATING ANION CHANNEL 1 (QUAC1), which

results in the efflux of anion in stomata and eventually cause stomata closure (Munemasa

et al., 2015).

On the other hand, ABA-independent pathways play a pivotal role in drought and

salt stress responses (Narusaka et al., 2003). As mentioned earlier, the induction of the

RD29A gene is mediated by ABA-independent signal transduction cascades, enhancing

drought tolerance in plants (Msanne et al., 2011; Yoshida et al., 2014). In the promoter

region of *RD29A*, a conserved *cis*-acting element known as dehydration-responsive

element (DRE, 5'-TACCGACAT- 3') is present. Transcription factors called DRE-

binding proteins (DREB) can bind to the *cis*-acting element DRE and upregulate the

expression of *RD29A* under drought or salt stress. DREB1A and DREB2A are the major

transcription factors in ABA-independent signaling transduction pathway to induce

17

downstream genes to conquer drought and salt stresses (Sakuma et al., 2006; Huang et

al., 2012).

Objectives
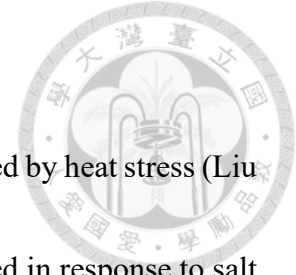
HSFA7a and *HSFA7b* have both been demonstrated to be induced by heat stress (Liu et al., 2011). Furthermore, *HSFA7b* has been shown to be upregulated in response to salt stress and is involved in salt tolerance by binding to an E-box-like motif to regulate downstream genes (Zang et al., 2019). Previous research has also identified an evolutionary relationship between these two genes (Nover et al., 2001).

Through the CRISPR-Cas9 strategy, we generated double mutant of *HSFA7a* and *HSFA7b* and conducted a series of phenotypic analyses to investigate whether these two genes exhibit functional redundancy in response to abiotic stresses. Additionally, there are only a limited number of studies that have explored the detailed relationship between these two genes and their mechanisms in regulating the heat stress response (HSR). We performed various thermotolerance assays to gain insights into the phenotypes of mutant lines following exposure to multiple heat stress conditions. To identify downstream genes influenced by these two genes, we also conducted RNA-seq and generated heat maps listing the differentially expressed genes (DEGs) in double mutant plants after heat treatments.

By employing these analyses, our aim is to uncover the functions and mechanisms of these two genes in the context of *Arabidopsis* HSR and other abiotic stress responses.

Material and Methods

Plant materials and growth conditions

In this study, the Arabidopsis (*Arabidopsis thaliana*) Columbia ecotype (Col) served as the wild-type (WT) plants. The T-DNA insertion lines of *HSFA7a* (AT3G51910) (SAIL_450_G04, *hsfa7a-1*; SALK_080138C, *hsfa7a-2*) and *HSFA7b* (AT3G63350) (GABI_498E08, *hsfa7b-1*; SALK_152004, *hsfa7b-2*), at the same chromosome 3, were obtained from the Arabidopsis Biological Resource Center (ABRC, Ohio State University) or Nottingham Arabidopsis Stock Center (NASC, Nottingham University). The homologous T-DNA insertion lines were isolated after being confirmed by PCR amplification. Seedlings were grown in growth chambers at 22°C to 23°C with 16 h light/8 h dark with a light intensity of 80 to 100 μmol m^{-2} s^{-1}. One-half Murashige and Skoog medium ($^1/_2$ MS, Sigma) containing 1% sucrose and 0.8% or 1% agar (Milipore) were used on the thermotolerance tests and root elongation assays, respectively .

Double mutant plants were generated in *hsfa7a-2* or in *hsfa7b-2* background by *Agrobacterium tumefaciens* GV3101-mediated transformation (Clough and Bent, 1998). A CRISPR-Cas9 mediated mutation vector pHEE401E **(Appendix 1)** (Wang et al., 2015) was constructed by Agricultural Biotechnology Research Center, Academia Sinica. Four single guide RNAs (sgRNAs) responsible for CRISPR-Cas9 mutation in *hsfa7a-2* and

20

hsfa7b-2 were designed on the CCTop- CRISPR/Cas9 target online predictor website (https://cctop.cos.uni-heidelberg.de:8043/), respectively **(Table 1)**. Four guide RNAs were designed at the 5'-UTR region and the first exon region of *HSFA7a* to mutate *HSFA7a* **(Supplemental Fig. 1)**, while 4 guide RNAs were designed at the second exon of *HSFA7b* to mutate *HSFA7b* to generate double mutant plants **(Supplemental Fig. 2)**. The sgRNA sequences were synthesized using overlapping PCR, and promoter sequences of AtU1, AtU26, and AtU29 were amplified from Arabidopsis wild-type plants **(Supplemental Fig. 3, 4)**. sgRNAs and promoter sequences linked with in reverse orientation by overlapping PCR, then the fragment was cloned into the pUC18 vector digested with *Bam*HI and *Hin*dIII, to establish the sgRNA intermediate vector sets, which were maintained in E. coli DH10B (Ma et al., 2015).

Golden Gate cloning method (Engler et al., 2008) was used to clone multiple sgRNA expression cassettes in the CRISPR-Cas9 binary vectors pHEE401E. Restriction–ligation reactions (15 μL) were set up with 1× *Bsa* I reaction buffer plus 1.0 mM ATP (or 1.5 μL of NEB 10× ligation buffer), 10 U of *Bsa* I, 35 U of T4 DNA ligase (Takara, China), 60–80 ng of the intact binary plasmid (pHEE401E/*HSFA7a* and pHEE401E/*HSFA7b*), and the purified PCR products (15 ng for each sgRNA expression cassette) amplified with the

21

site-specific primers. The reactions were incubated for 10–15 cycles (95°C, 10 s; 60°C, 15 s; 68°C, 20 s).
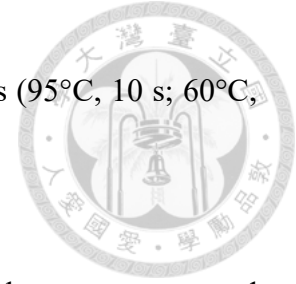
A 15μg/mL hygromycin was used to screen the T1 plants. T2 plants were screened by PCR amplification and then select the potential seedlings in which mutation occurred. T3 homozygous double mutant plants were confirmed by Sanger sequencing at the gDNA level. T4 double mutant plants were used to conduct the phenotypical analysis.

Generation of transgenic *HSFA7a* and *HSFA7b*-overexpression lines

The coding sequences (CDSs) of *HSFA7a* and *HSFA7b* without stop codon were amplified from total Col cDNA by PCR (the design of the primers was listed in **Table 1**), and CDSs were cloned into Gateway vector pCR8/GW/TOPO (Invitrogen) **(Appendix 2)** for sequencing. The CDS of *HSFA7a* was recombined into the pEarleyGate 201 vector (ABRC) **(Appendix 3)**, while the CDS of *HSFA7b* was recombined into the modified destination vector pCAMBIA3300 **(Appendix 4)** by Gateway LR reaction for overexpression. *35S::HSFA7a* conferred an HA tag at the N terminus, while *35S::HSFA7b* conferred a 3xFLAG tag at their C terminus. *35S::HSFA7a-HA* plants were under screening at T1 generation. *35S::HSFA7b-3xFLAG* was in T3, but HSFA7b was

22
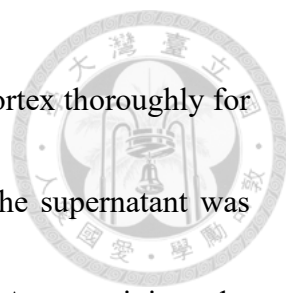
unable to detect in T3 generation, when checked by Western blotting **(Supplemental Fig.**

S5) at this moment.
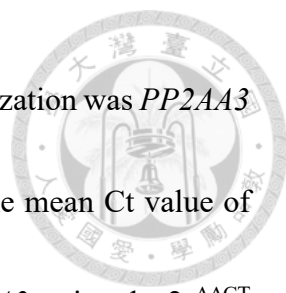
DNA/RNA preparation, cDNA synthesis and qRT-PCR

For DNA isolation, seedlings were ground in liquid nitrogen and mixed with Edward

buffer (Edwards et al., 1991) and phenol: chloroform: isoamyl alcohol (25:24:1). The

mixture was centrifuged at 12,000 rpm for 10 min to separate into two layers. After

centrifugation, upper water phase layer was added with equal volume of chloroform and

mixed well for the next separation. Transfer the upper water phase layer into new

eppendorf and added with equal volume of isopropanol (IPA) and incubated at -20°C for

1 h to precipitate DNA. After incubation, centrifuged the mixture at 12,000 rpm for 10

min again to obtain the DNA pellet. DNA pellet was washed with 75% ethanol for three

times. After being dried at room temperature for 10 min, the pellet was dissolved in

deionized water.

Total RNA was extracted by using TRIZOL reagent (Invitrogen) and TURBO DNA-

free kit (Applied Biosystems). Fifty 7-d-old seedlings were grown on $^1/_2$ MS plate and

collected in 1.5 mL eppendorf. After seedlings were harvested, seedlings were frozen in

liquid nitrogen and for grinding. Add 800 μL TRIzol reagent and mixed well the mixture

23

for 5 min waiting. The mixture was added 200 μL chloroform and vortex thoroughly for 10 sec. The mixture was centrifuged at 12,000 rpm for 20 min. The supernatant was transferred to a new 1.5 mL eppendorf and added equal volume of IPA to precipitate the RNA at -20°C for 2 hr. After precipitation, centrifuged at 12,000 rpm for 20 min and removed the supernatant and washed the pellet with 75% ethanol for three times. Discarded supernatant thoroughly and put it into cabinet drier for 10 min at room temperature. Add 35 μL DEPC-treated water to dissolve RNA pellet and incubated in dry bath at 55°C for 10 min. Transferred 25 μL mixture to new 1.5 mL eppendorf, and then added 0.5 μL TURBO DNase and its 10X buffer 2.5 μL. Incubated the mixture at 37°C for 30 min; add TURBO DNase inactivation reagent and waited for 5 min. Centrifuged at 12,000 rpm for 5 min and transferred the supernatant to a new 1.5 mL eppendorf. The cDNA was synthesized by using cDNA reverse transcription Kit (Applied Biosystems). qRT-PCR reactions were analyzed by 7500 Fast Real-Time PCR system (Applied Biosystems) with the PCR mix of iQ SYBR Green Supermix (BioRad). Reactions were performed in a total volume of 20 μL containing 10 μL iQ SYBR Green, 10 μM forward and reverse primers 0.4 μL, Low ROX 0.4 μL, 3.8 μL ddH$_2$O, and 2 ng/μL cDNA templates 5μL. Amplified using the following cycling conditions: 95°C for 3 min, 40

24
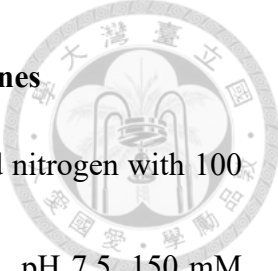
cycles of 95°C for 10 s, 60°C for 30 s. The internal control for normalization was *PP2AA3*

(*PP2A*; At1g13320) (Czechowski et al., 2005). For data analysis, the mean Ct value of

the target gene was normalized against the average Ct value of *PP2AA3*, using the $2^{-\Delta\Delta CT}$

method implemented in the 7500 Fast Real-Time PCR system software (Applied

Biosystems).

Thermotolerance tests

Forty 7-d-old seedlings were grown on 20 mL solid $^1/_2$ MS medium plates used for

thermotolerance tests. Heat treatments usually begin at 10 AM. The plates were sealed by

electric tape and were incubated in a water bath for basal thermotolerance (BT), short-

term acquired thermotolerance (SAT), long-term acquired thermotolerance (LAT), and

gradient heat stress (GHS) tests as previously described (Charng et al., 2007; Yeh et al.,

2012). During recovery from each HS treatment, the plate was removed from the water

bath and kept in the growth chamber under the same light/dark cycles. The healthy

growing seedlings were calculated 10 d after heat treatment. The survival rate was defined

as the condition in which seedlings did not exhibit complete bleaching and continued to

grow leaves after a 10-d recovery period.

Protein extraction and immunoblotting assay for *35S::HSFA7b* lines

Fifty 10-d-old seedlings were harvested and ground using liquid nitrogen with 100

µL of pre-cold, freshly prepared extraction buffer (50 mM Tris-HCl, pH 7.5, 150 mM

NaCl, 10 mM $MgCl_2$, 0.1% NP-40, 1 mM PMSF), along with a protease inhibitor cocktail.

The extract was centrifuged at 12,000 rpm for 10 min and repeated twice to obtain clear

protein extracts. Protein concentration was determined using a detergent-compatible

protein assay (Bio-Rad).

For immunoblotting, 50 µg of total protein was heated at 85°C for 10 min for non-

reducing conditions, and then loaded onto a 10% SDS-PAGE gel for separation. The total

proteins were transferred to a 0.45 µm Immobilon®-P PVDF Membrane (Millipore) using

a mini blot module (a wet tank blotting system; Bio-Rad). The membrane was blocked

with 1X PBST (25 mM KH_2PO_4, 0.15 M NaCl, 0.3% Tween-20; pH 7.2) containing 5%

low-fat dry milk for 30 min at room temperature and then incubated with the primary

antibody overnight at 4°C. The membrane was subsequently washed with 1x PBST three

times for 5 min each at room temperature. The secondary antibody was added to a

blocking solution, and the membrane was incubated for 1.5 h at room temperature for

further hybridization. The membrane was washed with 1X PBST two times for 5 min

each at room temperature. Finally, the membrane was soaked in 1X PBS buffer (25 mM

KH$_2$PO$_4$, 0.15 M NaCl; at pH 7.2) for temporary storage. Immobilon Western HRP

Substrate (Millipore) was applied to the membrane for chemiluminescent detection. The

luminescence signal was detected using the iBright™ CL750 Imaging System

(Invitrogen), and equal protein loading was confirmed by 0.1% Ponceau S staining.

Immunoblotting was performed using anti-FLAG antibody (Santa Cruz) at a 1:10,000

dilution.

Ponceau S staining

For the protein loading control assay, Immobilon®-P PVDF Membrane (Millipore)

membranes were stained by the solution of 0.1% Ponceau S in 5% acetate for 5 min, and

then membranes were washed with deionized water to eliminate the background. The

images were captured immediately after washing with deionized water. For further

western blotting, the membrane was completely washed by PBST three times.

Root elongation tests under acquired thermotolerance conditions

Sterilized seeds were vertically plated on $^1/_2$ MS mediums for 7 d. Before heat

treatments, plates were sealed with plastic electric tape and submerged in a water bath at

demanded temperature based on acquired thermotolerance tests. 4-d-old seedlings were

initially exposed to a 37°C non-lethal HS for 1 h, following by a 1-h recovery period at 22°C, and subsequently treated with a 44°C lethal HS for 30 min. After finishing all heat treatments, plates were recovered at 22°C for 3 d. Col and *hsp101* seedlings were used as controls. Primary root lengths of 7-d-old seedlings were measured by ImageJ software.

Root growth tests under salt and osmotic stresses either individually or in combination with heat stress.

For the control experiments (NaCl or Mannitol), seeds were directly sown and vertically plated on $^1/_2$ MS medium with 75 mM NaCl or 100 mM mannitol and allowed to grow for 7 d. For the experiments subjected to heat treatment (NaCl+HS or Mannitol+HS), 4-d-old seedlings were submerged in a water bath at 37°C for 1 h to induce the expression of the *HSFA7a* and *HSFA7b*. After the heat treatments, the plates were placed in a growth chamber at 22°C and allowed to recover for 3 d under the same light/dark cycles mentioned earlier. The primary root lengths of the 7-d-old seedlings were subsequently measured using ImageJ software.

Thermomorphogenesis analysis for different lines

4-d-old seedlings growing at 20°C were transferred to 28°C for further growth 3 d then photographed. Pictures were taken by Nikon digital cameras, and the hypocotyl lengths were then measured by ImageJ software. The experiments were repeated three times ($n > 30$).

Hypocotyl elongation

Sterilized seeds were sown onto $^1/_2$ MS agar medium and incubated in darkness for 2.5 d. Subsequently, these plates were placed within an opaque container covered with aluminum foil. Plants sealed with plastic electric tape were submerged in a water bath at the specified temperature as determined by basal or acquired thermotolerance tests, all while maintaining a dark environment. As controls, Col and *hsp101* seedlings were included. After heat treatments, the plates were returned to the opaque container and allowed to recover at 22°C for the prescribed duration. Hypocotyl lengths of 5-d-old seedlings were subsequently measured using ImageJ software.

29

RNA-seq analysis

Col and double mutant plants *hsfa7a^cas9-1* were grown at 22°C on ${}^{1}/_{2}$ MS medium for

7 d. For LAT heat treatment, plates were subjected to a 1 h priming at 37°C for non-lethal

heat stress, followed by a 2-d recovery at 22°C, and then treated with 44°C lethal heat

stress (LHS) for 90 min. For GHS heat treatment, the temperature was gradually increased

from 22°C to 44°C over a 6-h period for acclimation, followed by exposure to LHS at

44°C for 180 min. After exposure to both LAT and GHS heat treatments, seedlings were

immediately collected, and total RNA was extracted using the same method as mentioned

earlier. Two independent biological repeats were conducted in this analysis. For library

sequencing, the library quality was assessed on the Qubit® 2.0 Fluorometer (Thermo

Scientific) and Agilent Bioanalyzer 2100 system. At last, the library was sequenced on an

Illumina NovaSeq6000 (BioTools) platform and 150 bp paired-end reads were generated.

The raw data for RNA-seq were converted into raw sequenced reads using CASAVA

base calling and were stored in FASTQ format. FastQC and MultiQC (Ewels et al., 2016)

were used to perform quality checks on the fastq files to ensure data quality. To filter out

low-quality reads and trim adapter sequences, Trimmomatic (Bolger et al., 2014) tool was

used with the following parameters: LEADING: 3; TRAILING: 3; SLIDINGWINDOW:

4:20; MINLEN: 36 to remove low-quality bases from the raw paired-end reads. After

eliminating poor-quality reads, the resulting high-quality data, referred to as "clean reads", was used for downstream analysis. The read pairs from each sample were then mapped to TAIR10 using HISAT2 (Kim et al., 2015), and the number of reads mapped to individual genes was counted using featureCounts (Liao et al., 2014) with default settings.

To normalize gene expression, the "Relative Log Expression" (RLE) normalization method, which was performed using DESeq2 (Love et al., 2014), was selected for experiments with biological repeats. To find differentially expressed genes (DEGs), RNA-seq data from two biological repeats were used DESeq2 method (R packages based on the negative binomial distribution and Poisson distribution model) to determine the DEGs (Wang et al., 2010; Anders et al., 2013). The fold change ≥ 2 or $\leq$ -2, and *P.adjust* < 0.05 were set as the threshold for significantly differential expression. *P.adjust* values were adjusted using Benjamini and Hochberg's approach to control the false discovery rate (FDR). ClusterProfiler (Yu et al., 2012) was used to conduct Gene Ontology (GO) and KEGG pathway (Kanehisa et al., 2008; Kanehisa et al., 2019) enrichment analysis of DEGs. Heat maps were made using BioTools Cloud (https://cloud.toolsbiotech.com/app/biotools_rnaseq) platform.

31

Results

Transcription profiling of *HSFA7a* and *HSFA7b* in response to heat shock (HS)

To understand the expression levels of *HSFA7a* and *HSFA7b* in response to HS, we conducted real-time quantitative PCR (qRT-PCR) to assess the expression of *HSFA7a* and *HSFA7b* under 37°C-HS treatment for different times **(Figure 1)**.

In this study, 7-d-old wild-type (Col) seedlings cultivated on agar plates were subjected to 37°C HS for durations ranging from 15 min to 3 h, followed by a recovery period at 22°C for 1 h and 3 h **(Figure 1A)**. Subsequently, we analyzed the transcriptional levels of *HSFA7a* and *HSFA7b* using qRT-PCR **(Figure 1B)**. The results indicated that both genes were rapidly induced by the 37°C HS, with their expression peaking after 1 h of HS treatment. Moreover, during the recovery phase, the expression of both genes notably decreased compared to the HS stage. The heat-inducible marker gene, *HSP18.2* (AT5G59720), was used as a reference for these analyses **(Figure 1C)**.

Identification and characterization of the single mutants and double mutants of *HSFA7a* and *HSFA7b*

To shed light on the roles of *HSFA7a* and *HSFA7b*, we acquired the following T-DNA insertion mutant lines from ABRC: *hsfa7a-1* (SAIL_450_G04), *hsfa7a-2*

32

(SALK_080138C), as well as *hsfa7b-1* (GABI_498E08), and *hsfa7b-2* (SALK_152004) **(Figures 2A, 3A)**.
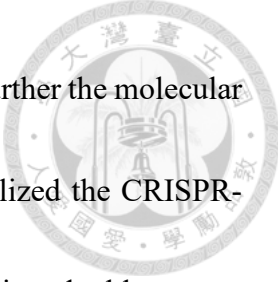
The T-DNA insertion of *hsfa7a-1* was located in the promoter region of *HSFA7a*, while the T-DNA insertion of *hsfa7a-2* was in the second exon of *HSFA7a* **(Figure 2A)**. Similarly, *hsfa7b-1* contained a T-DNA insertion in the 5'-UTR region, whereas *hsfa7b-2* had a T-DNA insertion in the second exon of *HSFA7b* **(Figure 3A)**. We utilized PCR-base genotyping to demonstrated that all the T-DNA insertion lines were homozygous mutant lines **(Figures 2B, 3B)**.

Based on the qRT-PCR results, we concluded that the *hsfa7a-1* was a knockdown (KD) mutant, whereas *hsfa7a-2* was a knockout (KO) mutant **(Figure 2C)**. Likewise, *hsfa7b-1* was identified as a knockdown (KD) mutant, and *hsfa7b-2* was categorized as a knockout (KO) mutant **(Figure 3C)**. We found that *hsfa7a-1* was unable to respond to HS, and the expression level of *HSFA7b* in *hsf7b-1* was lower than that of WT after exposure to HS. *HSP18.2*, a heat-responsive marker gene, was used as a reference. Moreover, the RT-PCR confirmed that the expression of *HSFA7a* and *HSFA7b* was detectable under normal growth conditions **(Figures 2D, 3D)**.

Additionally, we generated double mutant plants to investigate further the molecular mechanisms of *HSFA7a* and *HSFA7b* under abiotic stresses. We utilized the CRISPR-Cas9 strategy to mutate *HSFA7a* in a *hsfa7b-2* background, resulting in a double mutant line of the *hsfa7a^{cas9-1}/hsfa7b-2* (referred to as *hsfa7a^{cas9-1}*) **(Figure 4A)**. To achieve this, four sgRNAs were designed using the CCTop-CRISPR/Cas9 target online predictor website (https://cctop.cos.uni-heidelberg.de:8043/) targeting to the 5' untranslated region (5'-UTR) and the first exon of *HSFA7a* **(Supplemental Fig. S1)**. The final constructed pHEE401E/*HSFA7a* vector (Wang et al., 2015), was used for plant transformation **(Supplemental Fig. S3)**.

Sanger sequencing results showed that the double mutant *hsfa7a^{cas9-1}* line conferred the insertion of one adenine at the first exon of *HSFA7a* in *hsfa7b-2* background **(Figures 4B, 4C)**, which led to a premature stop codon **(Figure 4D)**.

We also generated the double mutant plant with a mutate *HSFA7b* in a *hsfa7a-2* background, *hsfa7b^{cas9-1}/hsfa7a-2* (referred to as *hsfa7b^{cas9-1}*) **(Figure 5A)**. As mentioned above, four sgRNAs were designed to target the second exon of *HSFA7b* **(Supplemental Fig. S2)**. The final constructed pHEE401E/*HSFA7b* vector was used for plant

34

transformation **(Supplemental Fig. S4)**. Sanger sequencing results demonstrated that a 236-base pair deletion in the second exon of *HSFA7b* **(Figure 5B)**.

Phenotyping of mutants by quantitation of the root elongation in response to different abiotic stresses

To investigate the potential involvement of *HSFA7a* and *HSFA7b* in root growth, we thus analyzed the root length and elongation rates of 4-d-old seedlings in *hsfa7a-2*, *hsfa7b-2*, *hsfa7a^{cas9-1}*, and *hsfa7b^{cas9-1}* under normal growth conditions, and in response to heat, salt, and osmotic stress **(Figures 6 to 8)**.

Under normal growth conditions **(Figures 6B, C; CK)**, we observed that the root length of 7-d-old single knockout mutants *hsfa7a* and *hsfa7b* was significantly longer compared to Col; however, the root length of double mutant plants was significantly shorter **(Figure 6C; CK)**. Intriguingly, following exposure to the HS **(Figures 6B, C; AT)**, only the root length of *hsfa7a-2* was longer than that of Col. In contrast, the other mutant lines exhibited no significant differences when compared to the Col **(Figure 6C; AT)**. The root elongation rate (%) compared to the control treatment was calculated as the root elongation length of the AT test (4th d to 7th d) / CK (4th d to 7th d). We found that

35

the elongation rate of *hsfa7a-2*, *hsfa7a^(cas9-1)*, and *hsfa7b^(cas9-1)* was higher compared to Col, while that of *hsfa7b-2* was lower compared to Col **(Figure 6D)**.

We also examined the root elongation rate under 75 mM NaCl salt stress to assess the roles of *HSFA7a* and *HSFA7b* **(Figure 7)**. Single and double mutant seeds were sown on $^1/_2$ MS plates containing 75 mM NaCl for 7 d (NaCl). To investigate whether the heat induced *HSFA7a* and *HSFA7b* influenced root growth under salt stress, we subjected 4-d-old seedlings growth in NaCl to a 1 h 37°C HS treatment (NaCl+HS), followed by a 3-d recovery period **(Figure 7A)**.

For NaCl treatment, we measured the root length of 7-d-old seedlings that continuously grew under 75 mM NaCl. The results indicated that the root length of *hsfa7b-2* was longer than that of the Col, while the root length of both two double mutants was shorter compared to the Col **(Figures 7B, C; NaCl)**. In contrast, the results of NaCl+HS treatment revealed that only the root lengths of the double mutant plants were significantly affected compared to Col **(Figures 7B, C; NaCl+HS)**.

The root elongation rate (%) was measured by the root elongation length under NaCl or NaCl+HS treatments (4th d to 7th d) / CK (4th d to 7th d) **(Figures 7D, E)**. Under NaCl treatments, the results showed that the root elongation rate of *hsfa7b-2* was higher than

36

that of Col, while those of two double mutants were lower compared to Col **(Figure 7D)**.

On the other hand, under NaCl+HS treatments, only the elongation rate of *hsfa7a-2* was

higher compared to Col, whereas that of *hsfa7b-2*, *hsfa7a^{cas9-1}*, and *hsfa7b^{cas9-1}* was lower

compared to Col **(Figure 7E)**.

To further explore the phenotypes related to root growth in single and double

mutants under osmotic stress, we analyzed the root length of 7-d-old seedlings grown on

$^1/_2$ MS medium containing 100 mM mannitol (Mannitol). Similarly, as mentioned earlier,

we subjected 4-d-old seedlings to a 1 h exposure at 37°C to induce gene expression,

followed by a 3-d recovery period (Mannitol+HS) **(Figure 8)**.

For mannitol treatment, we observed that the root length of *hsfa7b-2* was longer than

that of the Col, while the root length of two double mutant plants was shorter compared

to Col **(Figures 8B, C; Mannitol)**. Conversely, in the Mannitol+HS treatment, the root

lengths of the single mutant plants did not differ significantly from Col, but the root

lengths of the double mutant plants were notably shorter than that of Col **(Figures 8B, C;**

Mannitol+HS).

As mentioned earlier, the root elongation rate (%) was measured by the root

elongation length under Mannitol or Mannitol+HS treatments (4th to 7th d) / CK (4th to 7th

37
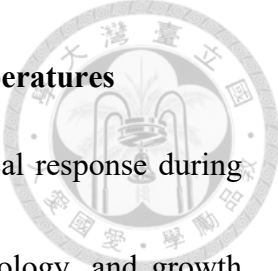
d) **(Figures 8D, E)**. We found that the mutation of *HSFA7a* and *HSFA7b* resulted in a lower root elongation rate compared to Col. Moreover, the loss of function of *HSFA7b* had a greater impact on the elongation rate, which was also observed in double mutant plants **(Figures 8D, E)**.

Phenotyping of mutants by quantitation of the hypocotyl elongation in response to HS

We conducted further analysis of hypocotyl elongation rates in single and double mutant plants to gain insights into the molecular mechanisms governed by *HSFA7a* and *HSFA7b* during basal thermotolerance (BT) and acquired thermotolerance (AT) tests **(Figures 9, 10)**. To quantify this, we calculated the hypocotyl elongation rate (%) as the ratio of the hypocotyl length from the (2.5^{th} d to 5th d) / 5th d **(Figures 9D, 10D)**, as indicated.

For BT test, our results showed that the hypocotyl elongation rate of *hsfa7b-2* and two double mutants was significantly higher than that of the wild-type plants **(Figure 9D)**. On the other hand, the hypocotyl elongation rate of *hsfa7b-2* under AT test was still higher compared to Col, while two double mutants showed significantly lower than that of Col **(Figure 10D)**.

38

Thermomorphogenesis analysis for mutant lines under high temperatures

Thermomorphogenesis was recognized as a crucial physiological response during plant growth, encompassing changes in plant development, morphology, and growth patterns under elevated temperatures (Stavang et al., 2009). In previous studies, the basic-helix-loop-helix (bHLH) transcription factor PHYTOCHROME INTERACTING FACTOR 4 (PIF4) has been demonstrated as a key player promoting thermomorphogenesis (Koini et al., 2009; Franklin et al., 2011). Given this context, we sought to determine whether *HSFA7a* and *HSFA7b* were involved in this process and conducted tests using various mutant lines under warm temperatures (28°C) **(Figure 11)**.

Seedlings were initially cultivated at 20°C for 4 d and subsequently shifted to 28°C for 3 d **(Figures 11A, B)**. Our results indicated that *hsfa7b-2* its hypocotyl length was significantly longer compared to wild-type (Col) plants after being transferred to 28°C **(Figure 11C; 28°C)**. However, the hypocotyl length of double mutant *hsfa7a^{cas9-1}* was shorter than that of Col, while another double mutant *hsfa7b^{cas9-1}* exhibited opposite phenotypes. Specifically, the hypocotyl lengths of *hsfa7b^{cas9-1}* were longer compared to Col **(Figure 11C; 28°C)**. For comparative analysis of thermomorphogenesis, *pif4* was as a reference.

39

We also examined the relative hypocotyl length rate (%) to further elucidate the mechanisms of *HSFA7a* and *HSFA7b* for thermomorphogenesis **(Figure 11D)**. The relative hypocotyl length rate (%) was calculated as the ratio of the hypocotyl length from 28°C (7th d) / 20°C (7th d). The results indicated that the relative hypocotyl length rate (%) of *hsfa7a-2*, *hsfa7b-2*, and *hsfa7b^{cas9-1}* was higher compared to Col, while that of *hsfa7a-1* and *hsfa7a^{cas9-1}* was lower compared to Col.

Basal thermotolerance and short-term acquired thermotolerance analysis for mutants

To further elucidate the roles of *HSFA7a* and *HSFA7b* in heat shock response (HSR), we conducted basal thermotolerance and short-term acquired thermotolerance assays by sowing mutant lines on agar plates together with Col and heat-sensitive mutant *hsp101* **(Figure 12)**. For basal thermotolerance (BT) assay, 7-d-old seedlings grown on plates were exposed to a 44°C lethal HS (LHS) for 25 min. The results showed that there was no significant difference between mutant plants and Col **(Figure 12 A)**.

Regarding the short-term acquired thermotolerance (SAT) assay, 7-d-old seedlings grown on plates were initially exposed to a 37°C non-lethal HS for 1 h, followed by a 2-h recovery period at 22°C, and subsequently treated with a 44°C lethal HS (LHS) for 180

40

min. Remarkably, the survival rate (%) of the double mutant *hsfa7a^cas9-1* exceeded 90%

(Figure 12B).

Long-term acquired thermotolerance and gradient heat stress analysis for mutants

We extended our investigation by conducting long-term acquired thermotolerance

and gradient heat stress tests to further explore the roles of *HSFA7a* and *HSFA7b* in HSR

(Figure 13).

In the long-term acquired thermotolerance (LAT) assay, 7-d-old seedlings grown on

plates were subjected to a 37°C non-lethal HS for 1 h, followed by a 2-d recovery period

at 22°C, and subsequently treated with a 44°C lethal HS (LHS) for 90 min. The results

revealed a significant reduction in survival rate (%) compared to Col when *HSFA7b* was

mutated. Intriguingly, the survival rate (%) of the double mutant *hsfa7b^cas9-1* did not

exhibit a major difference compared to Col **(Figure 13A)**.

For the gradient heat stress (GHS) assay, the temperature was gradually increased

from 22°C to 44°C over a 6-h period for acclimation, followed by exposure to lethal heat

stress (LHS) at 44°C for 180 min. The results showed that the survival rate (%) of single

mutants did not significantly differ from the Col. Remarkably, the survival rate (%) of

hsfa7a^cas9-1 was nearly 100%, while the survival rate of the Col was approximately 25%.

However, the other double mutant, *hsfa7b*[cas9-1], did not display the same phenotypic response as *hsfa7a*[cas9-1] **(Figure 13B)**.

RNA-seq transcriptome analysis under LAT test in *hsfa7a*[cas9-1]

As previously mentioned, we observed unique phenotypes in the double mutant plant, *hsfa7a*[cas9-1], during SAT, LAT, and GHS thermotolerance tests. To gain a deeper understanding of the downstream genes influenced by *HSFA7a* and *HSFA7b* in these thermotolerance assays, we focused on the LAT and GHS tests to explore the transcriptome differences between Col and *hsfa7a*[cas9-1] **(Figures 14 to 18)**.

In LAT assay, 7-d-old seedlings of both Col and *hsfa7a*[cas9-1] were subjected to a 1 h priming at 37°C for non-lethal heat stress, followed by a 2-d recovery at 22°C, and then treated with 44°C lethal heat stress (LHS) for 90 min. Once the LHS was completed, samples were promptly collected and total RNA was extracted **(Figure 14A)**. We identified 48 differentially expressed genes (DEGs) based on fold changes ≥ 2.0 or ≤ -2.0 and *P.adjust* < 0.05. Out of these 48 DEGs, 37 DEGs showed upregulation in *hsfa7a*[cas9-1] after LHS treatment, while 11 DEGs showed downregulation **(Figure 14B)**. To understand the functions of these DEGs, we performed gene ontology (GO) analysis, revealing that the top 20 enriched GO terms were related to DNA-templated transcription,

42

photosynthesis, and oxidation-reduction processes **(Figure 14C)**. We also did a Kyoto

Encyclopedia of Genes and Genomes (KEGG) analysis to investigate which metabolic

pathways were significantly affected in $hsfa7a^{cas9-1}$. The results revealed that only the

pathway of sesquiterpenoid and triterpenoid biosynthesis showed upregulation, while

others were downregulation **(Figure 14D)**.
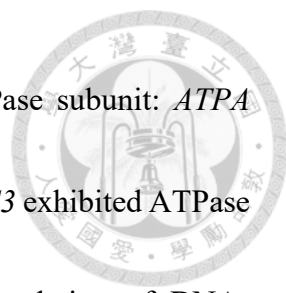
To further understand the DEGs in $hsfa7a^{cas9-1}$ under LAT test, we compiled a list

of the top 20 significant DEGs and generated a heat map to visualize the gene expression

changes after treatment **(Figure 15)**. Among these 20 DEGs, five exhibited

downregulated in $hsfa7a^{cas9-1}$: AT2G01422, CHLOROPLAST GLUTAMYL

PEPTIDASE (AT2G47390), *DEG5* (AT3G05945), FAD/NAD(P)- FAD/NAD(P)-

BINDING OXIDOREDUCTASE (AT5G11330), and QUA-QUINE STARCH (QQS,

AT3G30720). AT2G47390 played a role in maintaining the chloroplast proteome and is

likely involved in starch metabolism(Bhuiyan et al., 2020), while *QQS* might take part in

starch metabolism in leaves (Li et al., 2009). *DEG5* was involved in the final step of the

linear photosynthetic electron transport chain. Conversely, among the other 15

upregulated DEGs, many were related to DNA-templated transcription, elongation, and

photosynthesis.

43

RNA-seq transcriptome analysis under GHS test in *hsfa7a^{cas9-1}*

As noted earlier, after LHS was completed, samples were collected immediately and total RNA was extracted **(Figure 16A)**. For GHS test, we identified 350 differentially expressed genes (DEGs) (fold change ≥ 2.0 or ≤ -2.0, and *P.adjust* < 0.05). Among these, 184 DEGs showed downregulation in *hsfa7a^{cas9-1}*, while 166 DEGs showed upregulation in *hsfa7a^{cas9-1}* in GHS test **(Figure 16B)**. The results of gene ontology (GO) analysis revealed that most of these DEGs were related to DNA-templated transcription, elongation, and photosynthesis **(Figure 16C)**. Furthermore, the majority of the top 20 significant GO terms showed upregulation in *hsfa7a^{cas9-1}*. Kyoto Encyclopedia of Genes and Genomes (KEGG) analysis indicated a significant impact on the plant hormone signal transduction pathway in *hsfa7a^{cas9-1}* **(Figure 16D)**.

We also created a heat map to further investigate the most affected DEGs in *hsfa7a^{cas9-1}* after GHS test **(Figures 17, 18)**. First, we listed top 30 significant upregulated DEGs depicted by heat map **(Figure 17B)**. These upregulated DEGs were briefly categorized based on their functions. Among the top 30 DEGs, ten DEGs related to photosynthesis had the highest proportion among the top 30 DEGs: *PSBB* (ATCG00680), *RBCL* (ATCG00490), *PSBC* (ATCG00280), *NDHA* (ATCG01100), *PSBT* (ATCG00690), *PSAC* (ATCG01060), *PSBN* (ATCG00700), *PETB* (ATCG00720), *PSAB*

44

(ATCG00340), and *PSBH* (ATCG00710). Three DEGs were ATPase subunit: *ATPA*

(ATCG00120), *ATPH* (ATCG00140), and *AHA9* (AT1G80660). *APS3* exhibited ATPase

sulfurylase enzyme activity. Three DEGs were related to the regulation of DNA-

templated transcription: *ATHB25* (AT5G65410), *bHLH071* (AT5G46690), and

AT1G75860. *ATGPAT2* (AT1G02390) and AT3G01345 were associated with the

metabolism of organic matter. ATCG01210 and ATCG00920 were ribosomal RNA in

chloroplast. *GA2OX2* (AT1G30040) was involved in GA biosynthesis process, while

CKX7 (AT5G21482) was related to cytokinin biosynthesis. *TRX* (AT3G06730) acted as

a reductase in the photosynthesis process, and *TCP10* (AT2G31070) played a role in leaf

differentiation. *ATIDD6* (AT1G14580) was a C2H2-like zinc finger protein involved in

plant growth. *IQD24* (AT5G07240), the most significantly upregulated DEGs in

hsfa7a^{cas9-1}, was a CaM/CML-binding proteins related to Ca^{2+} signaling.

We also examined top 30 downregulated DEGs in *hsfa7a^{cas9-1}* after GHS, which

were presented by heat map **(Figure 18B)**. Two DEGs, AT2G47390 and AT2G47410,

were responsible for proteolysis. *QQS* (AT3G30720) was involved in starch metabolism

in leaves. *NIT2* (AT3G44300) participated in IAA signaling pathway. *GSTF3*

(AT2G02930) was a glutathione transferase. AT3G54830 was responsible for amino acid

45

transmembrane transportation. Two DEGs, *SPP1* (AT1G51420) and *IGMT1* (AT1G21100), were related to metabolism of organic matters. *GAT* (AT1G15040) regulated secondary shoot formation. AT4G36430 and AT4G37520 were peroxidase superfamily protein. *DIOX1* (AT3G01420) was responsible for oxidative stress responses. AT4G11650 participated in ABA signaling pathway, while *ST2A* (AT5G07010) took part in JA signaling. The functions of the remaining DEGs remained unclear.

The expression level of *HSFA7a* and *HSFA7b* under SAT and LAT tests

We extended our analysis to examine the expression levels of *HSFA7a* and *HSFA7b* under short-term acquired thermotolerance (SAT) and long-term acquired thermotolerance (LAT) tests **(Figure 19)**.

In the context of SAT analysis **(Figure 19A)**, the results highlighted that HS treatment had a substantial effect on inducing the expression of both genes, while lethal heat shock (LHS) did not lead to their upregulation. Intriguingly, during the HSR and LHSR phases, the expression level of *HSFA7b* was higher compared to CK **(Figure 19B)**.

For the LAT analysis **(Figure 19C)**, we observed that the expression levels of both *HSFA7a* and *HSFA7b* were primarily elevated during the HS phase. Throughout the other phases, the expression levels of *HSFA7a* did not exhibit significant differences compared

46

to CK. Conversely, for *HSFA7b*, its expression level experienced a decline specifically during the HSR phase **(Figure 19D)**.

***HSFA7a* and *HSFA7b* did not affect each other's expression levels.**

To further understand whether two genes would affect each other's expression levels, we performed qRT-PCR to measure their expression in *hsfa7a-2* and *hsfa7b-2* **(Figure 20)**. The expression level of *HSFA7a* would not be affected by the loss of *HSFA7b* expression under normal conditions (CK) or heat stress (HS) **(Figure 20A)**. In a similar manner, the expression of *HSFA7b* would not be influenced by the absence of *HSFA7a* expression under normal CK or HS **(Figure 20B)**.

***HSFA7a* and *HSFA7b* were not heat-memory genes**

In nature, plants frequently encounter chronic or recurring abiotic stresses. Therefore, the mechanism known as "stress memory" helped plants respond and acclimate rapidly to subsequent stresses (Liu et al., 2022). Pre-exposure to stress may alter plants' subsequent responses by producing faster and stronger reactions implying that plants exercise a form of stress memory (Ding et al., 2012). For heat stress, moderate heat stress allowed plants to acquire thermotolerance and subsequently withstand high temperatures

47

which were lethal to plants in the naïve state (Mittler et al., 2012). The heat stress memory referred to as a phenomenon that after returning to non-stress temperatures, acquired thermotolerance continued for several days (Charng et al., 2006; Charng et al., 2007).

Heat-responsive and -memory genes have been demonstrated that they played critical roles for plants against HS. These genes assist plants in retaining a memory of past HS exposures and enable them to react swiftly to subsequent incidents (Lamke et al., 2016). Previous studies have shown that *HSFA2* was required for HS memory and governed various downstream genes to regulate this process (Charng et al., 2007; Lamke et al., 2016; Friedrich et al., 2021). Moreover, a HSP known as Hsa32 acted as a crucial factor essential for acquired thermotolerance. As a result, we were curious about whether *HSFA7a* and *HSFA7b* were HS-memory genes. We carried out qRT-PCR analysis using the established method to validate this hypothesis (Liu et al., 2018). Our results demonstrated that the expression level of *HSFA7a* and *HSFA7b* increased their transcripts to about the same level during triggered (T) and primed+triggered (P+T) phases, suggesting that *HSFA7a* and *HSFA7b* were not HS-memory genes **(Figure 21)**. However, more experiments needed to be conducted to analyze whether *HSFA7a* and *HSFA7b* would take part in HS-memory, including quantification of downstream HS-

48

memory genes expression level or the analysis for trimethylated histone H3 Lys4

(H3K4me3) levels (Ding et al., 2012; Friedrich et al., 2021). *AZF3*, a HS-memory gene,

was used as a positive control for HS-memory analysis (Liu et al., 2018).
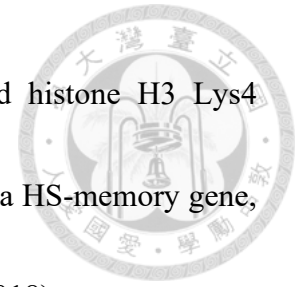
Discussion

HSFA7a and _HSFA7b_ were HS-induced genes and exhibited expression under normal conditions.

Previous studies have been demonstrated that both _HSFA7a_ and _HSFA7b_ genes are heat-inducible and upregulated by _HSFA1s_ (Lin et al., 2018; Andrasi et al., 2020). Our transcriptional profiling analysis demonstrated that _HSFA7a_ and _HSFA7b_ were rapidly induced by the 37°C heat stress, with their expression peaking after 1 h of treatment **(Figure 1)**. We screened T-DNA insertion mutant lines to gain insights into the function and mechanism of these two genes under abiotic stresses. **(Figures 2 and 3)**. We found that _HSFA7a_ expression level in response to HS may be dependent on its promoter region. Our qRT-PCR results revealed that _hsfa7a-1_, carrying a T-DNA insertion at the promoter region, was unable to respond to heat stress **(Figure 2C)**. This suggested that the T-DNA insertion disrupted the promoter region of _hsfa7a-1_, preventing proper induction of _HSFA7a_ expression in response to heat stress. Therefore, promoter analysis of _HSFA7a_ and _HSFA7b_ were conducted for further investigation of _cis_-elements present in the promoter regions of two genes **(Supplemental Figs. S6, S7)**. We focused on their 2-kb potential promoter regions including 5'-UTR regions and analyzed the _cis_-elements by

50

using Plant Promoter Analysis Navigator (PlantPAN4.0;

(http://plantpan.itps.ncku.edu.tw/plantpan4/index.html).

The results revealed that there were two predicted HS-responsive elements in the

HSFA7a promoter and one in the 5'-UTR sequences. For the analysis of *HSFA7b*, five

predicted HS-responsive elements presented in the *HSFA7b* promoter regions. Moreover,

the HSEs existing in the promoter region of *HFSA7a* were closed to the T-DAN insertion

site of *hsfa7a-1*, which might result in the disruption of the HSEs. In summary, these

findings supported the idea that *HSFA7a* and *HSFA7b* were regulated by *HSFA1s*, and

the promoter regions of *HSFA7a* were responsive to HS, leading to an increase in its

expression level.

In addition, we also analyzed ABA-responsive elements (ABRE; ACGTGG/TC) and

dehydration-responsive elements (DRE; TACCGACAT) to further investigate the

promoter regions of *HSFA7a* and *HSFA7b* (Narusaka et al., 2003). In the *HSFA7a*

promoter region, two ABRE elements were identified, along with one DREs in the

promoter region and another in the 5'-UTR sequences. In the *HSFA7b* promoter region,

five ABREs and five DREs were identified. These findings suggested that *HSFA7a* and

HSFA7b might be involved in ABA and drought response signaling pathways. To gain

51

further insight to their specific functions in response to ABA and drought stress, further

investigations are warranted.
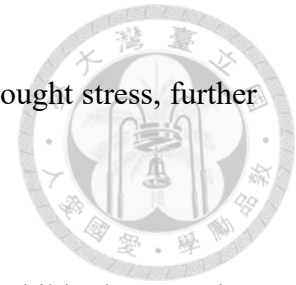
Moreover, it is interesting to note that *HSFA7a* and *HSFA7b* exhibited expression

under normal, non-stress conditions **(Figures 2D, 3D)**. These results might suggest that

HSFA7a and *HSFA7b* have roles or functions beyond their involvement in stress

responses.

Generation of double mutant plants was difficult by crossing strategy

To elucidate whether *HSFA7a* and *HSFA7b* collaborated in response to abiotic

stresses, it was necessary to generate double mutant lines and analyze their phenotypes.

The typical approach for generating double mutants involves crossing two independent

single mutants and screening their offspring to obtain homozygous double mutant lines.
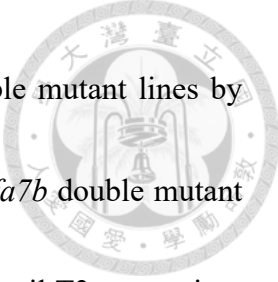
According to Mendelian inheritance, specifically the Law of Segregation, during the

formation of gametes (sperm and egg cells) in sexually reproducing organisms, the two

alleles for each gene segregate or separate from each other and end up in different gametes.

However, the Law of Segregation applied only when genes were not on the same

chromosome. If genes were located on the same chromosome, the process of synapsis

during meiosis allows for the matching-up of homologous pairs before their eventual

52

separation, resulting in the segregation of genes. In other words, if we would like to cross

two single mutants whose genes were on the same chromosome, we needed to screen

plenty of offerings to find cases where successful synapsis occurred at the specific region

of the chromosome. We then aimed to determine the probability of synapsis occurring in

this specific region.
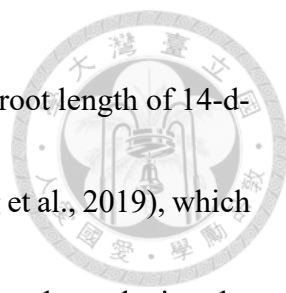
One unit, known as CentiMorgan (cM), was used to quantify the relative distance

between two genes or genetic markers on a chromosome. One cM represents a 1% chance

of them becoming separated due to genetic recombination during meiosis. A previous

study indicated that the average recombination rate of two genes in Arabidopsis could be

calculated based on their distance (Singer et al., 2006). *HSFA7a* and *HSFA7b* were both

located on chromosome 3, with a distance of approximately 4.2 Mb between them.

According to this study, the average recombination rate was 3.2 cM per Mb on

chromosome 3 in Arabidopsis. Consequently, we calculated that the recombination rate

between *HSFA7a* and *HSFA7b* during meiosis was 4.2 Mb multiplied by 3.2 cM, resulting

in 13.44 cM during the generation of one gamete. To determine the final probability of

synapsis successfully occurring twice, we need to multiply this probability by itself.

Therefore, 13.44% multiplied by 13.44% equals approximately1.8%. As a result, we

53

obtain a final probability of 1.8% for obtaining *hsfa7a hsfa7b* double mutant lines by crossing. In fact, one senior student attempted to generate *hsfa7a hsfa7b* double mutant lines through crossing, but she could not obtain double mutant lines until T3 generation. Consequently, we opted to employ the CRISPR-Cas9 strategy to establish the double mutant lines.

HSFA7a and HSFA7b might participate in root development.

Phenotypic analysis of root elongation assays showed that knockout mutants *hsfa7a-2* and *hsfa7b-2* had longer root lengths compared to Col under normal growth conditions (CK) **(Figure 6C; CK)**. As mentioned earlier, we noticed that both genes were expressed under CK **(Figures 2D, 3D)**. These results indicated that both genes might be involved in root growth control. Intriguingly, the single knockout mutants had longer root length, while the double-mutant plants had shorter root length, exhibiting opposite phenotypes compared to Col **(Figure 6C; CK)**. These findings suggested that *HSFA7a* and *HSFA7b* might act as negative regulators of root development individually. On the other hand, when both genes were mutated, the plants conferred a positive effect phenotype that affected plant root growth.

However, a previous study reported no significant difference in root length of 14-d-old *hsfa7b-2* mutants under normal conditions compared to Col (Zang et al., 2019), which was inconsistent with our findings. Additionally, there has been no study analyzing the root development of the *hsfa7a* knockout plants. Therefore, further analysis is required to determine whether both genes are involved in root development.
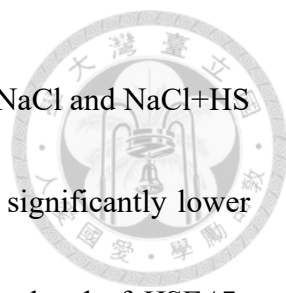
The root elongation phenotypical analysis for mutants in response to abiotic stress

Based on our results, we observed that the root elongation rate of *hsfa7b-2* under heat stress (HS) was lower compared to Col, while that of *hsfa7a-2*, *hsfa7a^cas9-1*, and *hsfa7b^cas9-1* was higher **(Figure 6D)**. From these findings, we inferred that *hsfa7b-2* was sensitive to HS, while *hsfa7a-2* appeared to be insensitive to HS. However, it's noteworthy that the root length of *hsfa7b-2* after the AT test showed no significant difference compared to Col **(Figure 6C; AT)**. Moreover, when both genes were mutated, two double mutants appeared to be insensitive to HS, indicating that *HSFA7a* and *HSFA7b* functioned together in response to HS **(Figure 6D)**. To confirm our findings, generating more double-mutant lines through CRISPR-Cas9 strategy and performing the same root elongation assay are necessary to confirm these results and analyze the phenotypes of mutants under heat stress.

55

Regarding root elongation in response to NaCl treatment, the root length of 7-d-old

hsfa7b-2 was higher than that of Col, while that of two double mutants was lower

(Figures 7C; NaCl). However, a previous study indicated that 7-d-old *hsfa7b-2* seedlings

grown on a normal $^1/_2$ MS plate and then transferred to 125 mM NaCl for one more week

exhibited shorter phenotypes in root length compared to Col (Zang et al., 2019). This

paper demonstrated that *HSFA7b* acted as a positive regulator in response to salt stress

by binding to the E-box-like motif of downstream genes, and overexpression of *HSFA7b*

exhibited more tolerance in response to salt stress. Our results were inconsistent with

previous paper. One possible explanation could be the varying growth conditions,

specifically whether the plants were transferred from a normal $^1/_2$ MS plate or not.

Although the mutation of *HSFA7b* has been shown to lead to low germination rates under

125 mM NaCl compared to Col (Zang et al., 2019), it is still uncertain how the mutation

of *HSFA7b* influences the salt tolerance of plants under continuous NaCl treatments.

Furthermore, it would be necessary to perform this assay with various NaCl

concentrations, including increasing levels, to validate these results.

Interestingly, under both NaCl and NaCl+HS treatments, the root length of two

double mutants was significantly shorter compared to Col **(Figure 7C)**. Likewise, the

results of root elongation rate (%) also demonstrated that under both NaCl and NaCl+HS

treatments, the root elongation rate (%) of two double mutants was significantly lower

compared to Col **(Figures 7D, E)**. During heat stress, the expression level of *HSFA7a*

increased in Col, and we attempted to determine whether the mutation of *HSFA7a* in

double mutant plants had an impact on salt tolerance. The root length results suggested

that *HSFA7a* and *HSFA7b* might function together not only under normal conditions but

also under salt stress. In previous microarray data, *HSFA7a* was not induced by salt stress

(Huang et al., 2016; Andrasi et al., 2020). However, whether *HSFA7a* participates in salt

tolerance remains unknown. For instance, *HSFA6b* was not induced by HS, but HSFA6b

took part in thermotolerance by activating the transcriptional activity of HSR-related

genes including *HSP18.1-CI*, *DREB2A*, and *APX2* (Huang et al., 2016). Similar

mechanism might be found in *HSFA7a* regulating salt tolerance in plants. Moreover,

HSFA7a and *HSFA7b* shared an evolutionary relationship and might have similar

functions in response to abiotic stresses (Nover et al., 2001). Under salt stress, HSFA7b

upregulated downstream target genes including SOSs, NHXs, pCSs to enhance salt

tolerance (Zang et al., 2019). It is possible that both genes collaborate to regulate salt

tolerance. Once again, more double mutant lines should be screened and generated to
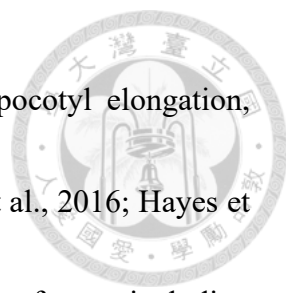
perform this assay. Additionally, other transgenic plants including complementary or overexpression lines should be established and analyzed the phenotypes to elucidate the mechanism under salt stress.

In the phenotypical analysis in response to osmotic stress, we observed that under Mannitol and Mannitol+HS treatments, the root length of the two double mutants was shorter than that of Col **(Figure 8C)**. According to root length analysis, the root length of two double mutants was shorter than that of Col under salt and osmotic stress **(Figures 7C, 8C)**. Specifically, under both Mannitol and Mannitol+HS treatments, it was observed that the root elongation rate of *hsfa7b-2*, as well as that of the two double mutant plants, was significantly lower than Col **(Figures 8D, E)**. These results suggest that the mutation of *HSFA7b* had a negative effect on plants in response to osmotic stress. Moreover, it's worth knowing that the mutation of *HSFA7a* also negatively influenced the root elongation rate, suggesting that *HSFA7a* might also play a role in osmotic stress **(Figures 8D, E)**.

HSFA7a and HSFA7b might play a role in thermomorphogenesis process.

Thermomorphogenesis is a process that alters plant morphology and development in response to elevated temperatures, typically occurring between approximately 24°C and

58

30°C in Arabidopsis. This response includes features such as hypocotyl elongation, petiole elongation, early flowering, and hyponastic growth. (Quint et al., 2016; Hayes et al., 2021). Plant hormone such as indole-3-acetic acid (IAA) and key factors including PHYTOCHROME B and PHYTOCHROME INTERACTING FACTORS (PIFs) are responsible for thermomorphogenesis (Quint et al., 2016; Ding et al., 2020). The conformational changes between active form of phytochrome (Pfr) and inactive from of phytochrome (Pr) are not only light-dependent but temperature-dependent. High temperature promotes the reversion to the inactive form Pr, resulting in the accumulation of PIFs, including PIF4, PIF5, and PIF7, and subsequently increasing auxin levels to extend hypocotyl growth (Hayes et al., 2021).

Our results demonstrated that the hypocotyl length of *hsfa7b-2* was longer than that of Col, while that of *hsfa7a^{cas9-1}* was shorter at both 20°C and 28°C **(Figure 11D)**. These results suggested that *HSFA7*b might negatively regulate thermomorphogenesis individually, while the mutation of both *HSFA7a* and *HSFA7b* had a positive and collaborative effect on this process. Additionally, the knockdown mutant *hsfa7b-1* and the knockout mutant *hsfa7b-2* exhibited elongated hypocotyl lengths at 20°C in a dose-dependent manner, indicating that the accumulation of HSFA7b may participated in this

59

process. It was interesting to note that the phenotypes of the two double mutants were different compared to Col **(Figures 11D, E)**. Again, more double mutant lines should be generated to confirm our data.
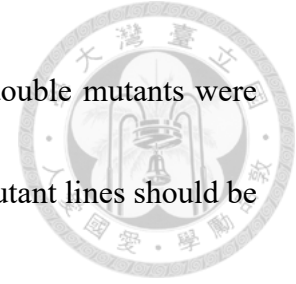
The complex mechanisms of *HSFA7a* and *HSFA7b* regulated plant's thermotolerance

Heat shock factors in plants regulate the thermotolerance and heat shock responses with the activation cycle model (Hasanuzzaman et al., 2013; Guo et al., 2016). Under normal conditions, the inactive HSFs are retained in the cytoplasm in complexes with HSP70 and HSP90. When plants are exposed to heat stress, the accumulation of misfolded proteins binds to HSP70 and HSP90 within the complexes. This binding results in the dissociation of HSFs from these complexes, allowing them to translocate into the nuclei where they form active trimers and carry out their functions (Gomez-Pastor et al., 2018). The activation cycle is mainly valid for HSFA1-type factors, and they form inactive complexes with HSP70 and HSP90.

HSFA7a and *HSFA7b* are downstream genes of *HSFA1s*, and the expression level of *HSFA7a* and *HSFA7b* decreases in the quadruple *hsfa1a,1b,1d,1e* mutant. *HSFA7a* and *HSFA7b* are heat-induced, and they will continue to activate downstream heat-relative

60

genes to participate in thermotolerance (Andrasi et al., 2020). Our thermotolerance assays indicated that *HSFA7a* and *HSFA7b* functioned together to negatively regulate heat stresses of SAT and GHS **(Figures 12B , 13B)**. This is the first observation of double mutant plants showing a high survival rate under HS. Single knockout mutants of the two genes did not influence SAT and GHS **(Figures 12B, 13B)**, suggesting potential compensation between the genes when one was mutated. Our qRT-PCR results demonstrate that *HSFA7a* and *HSFA7b* did not affect each other's expression levels **(Figure 20)**. In summary, these findings indicated that *HSFA7a* and *HSFA7b* were part of a complex mechanism in response to HS.

Nonetheless, in tomato, the knockout mutant of *HSFA7* led to a decrease in acquired and long-term mild HS thermotolerance. Temperature-dependent alternative splicing of *HSFA7* also occurred, generating different splice variants to regulate thermotolerance in tomato. (Mesihovic et al., 2022). Additionally, the T-DNA insertion in *hsfa7a-2* occurred at the end of the second exon. We cannot exclude the possibility of truncated HSFA7a being translated and potentially exhibiting partial functionality in regulating thermotolerance in plants. Whether *hsfa7a-2* is a knockout mutant needs more evidence to confirm. Furthermore, the precise function of the truncated HSFA7a remains unknown.

It could play a negative role in regulating thermotolerance, or there may be other possibilities. Further research is necessary to address these questions.

In our preliminary BiFC (Bimolecular Fluorescence Complementation) data obtained from a senior student (data not shown), the results suggest that HSFA7a and HSFA7b might interact with each other. However, in the STRING protein-protein interaction database (STRING: functional protein association networks (string-db.org), there was no evidence of interaction between these two HSFs. Whether HSFA7a and HSFA7b interact with each other to collaboratively regulate thermotolerance in plant HSR responses remains an interesting question to investigate.
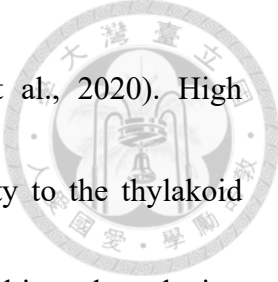
For long-term acquired thermotolerance, *HSFA2* has been validated as a critical heat shock factor in control of this process (Charng et al., 2007). In our analysis for long-term acquired thermotolerance assay **(Figures 13A, C)**, we observed that the mutation of *HSFA7b* resulted in low survival rate of seedlings, including in knockdown, knockout, and double mutant *hsfa7a^{cas9-1}*. Although our qRT-PCR results showed that the expression pattern of *HSFA7b* was not an HS-memory gene **(Figure 21)**, *HSFA7b* still played a role in long-term acquired thermotolerance. Further investigation of the downstream genes regulated by *HSFA7b* after heat treatments is required to elucidate the

62

detailed mechanism by which *HSFA7b* regulates thermotolerance. Moreover, the

establishment of complementary lines or overexpression lines are also necessary to

confirm our thermotolerance analysis.
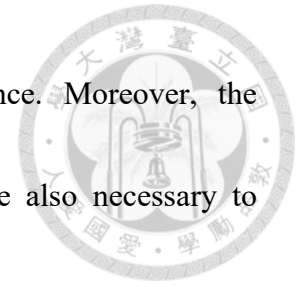
RNA-seq analysis in LAT and GHS test

We compiled lists of all upregulated and downregulated DEGs in **Tables 2 to 5**. It

was observed that following two heat treatments, a portion of the upregulated genes were

related to photosynthesis **(Figures 14C, 16C)**. Therefore, to gain further insight, Venn

diagrams were constructed to illustrate the overlap DEGs between the two datasets

(Supplemental Fig. S8). The results showed that among all the upregulated DEGs, there

were 30 DEGs overlapped. These overlapping DEGs included the subunits of

photosystem I and photosystem II (*PSAA*, *PSAB*, *PSAC*; *PSBA*, *PSBB*, *PSBC*, etc.), as

well as the genes responsible for the assembly and stability of photosystem I (*YCF3*,

YCF4, *YCF10*). Extensive research pointed out that heat stress will disrupt photosynthetic

processes, and chloroplasts as a key component in these processes is highly sensitive to

high temperature (Salvucci and Crafts-Brandner, 2004; Allakhverdiev et al., 2008; Hu et

al., 2020). Heat stress influences many photosynthesis-associated processes including

electron transport, CO_2 assimilation, photophosphorylation, chlorophyll biosynthesis,

63

thylakoid membrane fluidity and photochemical reactions (Hu et al., 2020). High temperature will result in the damage to chloroplasts, the instability to the thylakoid membrane, and the inactivation of crucial enzymes like Rubisco, ultimately reducing photosynthesis efficiency (Eamus et al., 1995; Salvucci and Crafts-Brandner, 2004; Allakhverdiev et al., 2008).

It is worth noting that many photosynthesis-related DEGs were upregulated with the mutation of *HSFA7a* and *HSFA7b* in LAT and GHS tests, which might suggest that *HSFA7a* and *HSFA7b* participate in the regulation of photosynthesis process. The upregulation of photosystem I and II subunit genes in the double mutant after HS indicated the possibility that *HSFA7a* and *HSFA7b* may act as negative regulators affecting photosynthetic processes. However, these upregulation DEGs related to photosynthesis cannot explain the opposite phenotypes observed between the LAT and GHS thermotolerance tests. **(Figure 13)**. Whether increasing or decreasing photosynthetic processes affected thermotolerance in plants remained unrevealed. Further experiments such as measuring the ratio of variable fluorescence to maximum fluorescence (F_v/F_m) should be conducted to elucidate whether the mutation of *HSFA7a* and *HSFA7b* disrupted the photosynthetic processes.

64

On the other hand, we also generated another Venn diagram to observe the overlapping downregulated DEGs. Due to the smaller number of downregulated DEGs in the LAT test, only 6 DEGs overlapped between the two datasets (**Supplemental Fig. S8**). These genes included CHLOROPLAST STROMA LOCALIZED GLUTAMYL PEPTIDASE (*CEGP*, AT2G47390), QUA-QUINE STARCH (*QQS*, AT3G30720), AT3G05945, AT2G01422, AT1G19530, and GLUTATHIONE S-TRANSFERASE 16 (*GST16*, AT2G02930). Interestingly, we found that *IQD24* (AT5G07240) exhibited downregulation in LAT test, whereas it showed upregulation in GHS test. As mentioned earlier in result part, *IQD24* was a CaM/CML-binding proteins related to Ca^{2+} signaling. With different types of heat treatments, this Ca^{2+} signaling-related genes exhibited opposite expression, suggesting that *IQD24* may a potential target for further elucidating its functions under HS.

Moreover, altering the time of sample collection could offer another approach to uncover more DEGs in *hsfa7a^{cas9-1}*. Our initial decision to collect samples after exposure to 44°C may not have been optimal for elucidating the downstream genes regulated by *HSFA7a* and *HSFA7b*. Many genes are likely to be influenced during the recovery stage after mild heat stress (i.e., 37°C). Therefore, if we collect samples immediately after the

65

conclusion of mild heat stress, more DEGs can be identified to analyze the effects caused by the mutation of *HSFA7a* and *HSFA7b*.
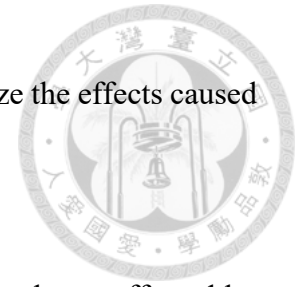
In addition, we would like to further investigate the signaling pathway affected by *HSFA7a* and *HSFA7b*. We selected some interested DEGs and ordered their T-DNA insertion lines from the Arabidopsis Biological Resource Center (ABRC, Ohio State University). These genes included transcription factors with zinc finger motifs such as *IDD6* (AT1G14580), and *ZFP8* (AT2G41940). Two transcription factors belonged to ERF/AP2 transcription factor family and they were members of the DREB subfamily: *DEAR2* (AT5G67190), and *DREB26* (AT1G21910). One transcription factor belonging to WRKY family was selected: *WRKY45* (AT3G01970). We hope to conduct phenotypical analysis under abiotic stresses for these mutant lines in the future and figure out whether *HSFA7a* and *HSFA7b* regulate these genes or not.

66

Tables

Table 1. List of primer sequences for genotyping, RT-PCR, qPCR, and sgRNAs for CRISPR-Cas9
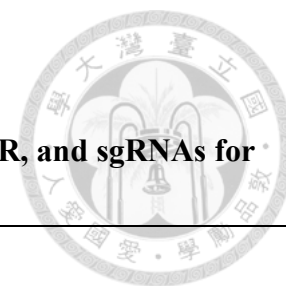
	Primer	Sequence (5' to 3')
	Genotyping	
hsfa7a-1	HSFA7a-SAIL-Fw	TTTTAGCCTTAACCAATCCGGT
	HSFA7a-SAIL-Rv	CCTGAGGTAACGGGTTTTGA
hsfa7a-2	A7a-2nd exon medium-Fw	AGTCAGCAAAGAGGAAAAGAGGTTC
	A7a-3'-UTR-Rv	GAATTAACCATTTTTTTGTTTACAC
hsfa7b-1	HSFA7b-GABI-Fw	GCCACATTTCCTGCCCCAACTGCCAT
	HSFA7b-GABI-Rv	GGGCTGAGACTGAGAGTAGTTA
hsfa7b-2	HSFA7b-2nd exon-Fw	GGATTCAGAAAGATCGAGGCAGA
	HSFA7b-dstop-Rv	ATCTTGCTTCACATTCGCCTCTT
	LBb1.3-ROK2	GGGATTTTGCCGATTTCGGAAC
	pCSA110-LB1	GCCTTTTCAGAAATGGATAAATAGCCTTGCTTCC
	GABI-LB	GGGCTACACTGAATTGGTAGCTC
	RT-PCR	
HSFA7a	A7a-2nd exon medium-Fw	AGTCAGCAAAGAGGAAAAGAGGTTC
	A7a-3'-UTR-Rv	GAATTAACCATTTTTTTGTTTACAC
HSFA7b	*HSFA7b*-CDS-Fw short	ATGGACCCGTCGTCAAGC
	HSFA7b-dstop-Rv	ATCTTGCTTCACATTCGCCTCTT
ACTIN2	ACTIN2-RT-Fw	ATGAAGCACAATCCAAGAGAGGTATTCTTA
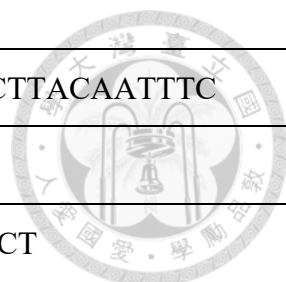
ACTIN2	ACTIN2-RT-Rv	GAGCTTCTCCTTGATGTCTCTTACAATTTC
Real-time Quantitative PCR		
PP2AA3	PP2AA3-qFw	CCTGCGGTAATAACTGCATCT
	PP2AA3-qRv	CTTCACTTAGCTCCACCAAGCA
HSFA7a	HSFA7a-2nd exon-qFw	ATGTCGGAATTGGAAGTTTTG
	HSFA7a-2nd exon-qRv	TCTCTCTCTACCACCAGTTGA
HSFA7b	HSFA7b-qFw	GGTGGAGAATCCTTCCCTTC
	HSFA7b-qRv	CCGTCCATATCCTTGCATCT
HSP18.2	HSP18.2-qFw	AAGGCAACAATGGAGAATGG
	HSP18.2-qRv	GCACACAAGCTTTTTATTTGACA
AZF3	AZF3-qFw	CGAAGTGATGAGTCCGATGG
	AZF3-qRv	GGAATTGAATCGTATTGTGTATTGG
sgRNAs for CRISPR-Cas9		
HSFA7a	HSFA7a-sgRNA1	TCTTGTCTTTAATTTCCAAT
	HSFA7a-sgRNA2	ACCACCACCACAACCAATGG
	HSFA7a-sgRNA3	TCTGACCAAGACATTTGAGA
	HSFA7a-sgRNA4	TGTGTTTGAAATGACGAGGA
HSFA7b	HSFA7b-sgRNA1	CTACTCTCAGTCTCAGCCCG
	HSFA7b-sgRNA2	GAGAGGCTACGTCCAAGCCA
	HSFA7b-sgRNA3	GCAGAAGAGAGACCGAGAGG
	HSFA7b-sgRNA4	GGAAGAGGTGGAGCACCTGT
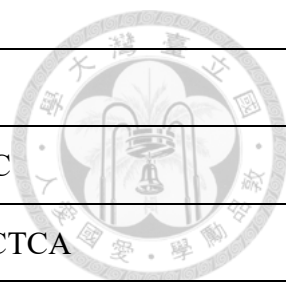
Cloning		
HSFA7a	HSFA7a-CDS-Fw	ATGATGAACCCGTTTCTCCC
	HSFA7a-dstop-Rv	GGAGGTGGAAGCCAAACTCTCA
HSFA7b	HSFA7b-CDS-Fw	ATGGACCCGTCGTCAAGCTCCAGA
	HSFA7b-dstop-Rv	ATCTTGCTTCACATTCGCCTCTT

69

Table 2. All upregulated differentially expressed genes (DEGs) whose expression changed more than 2 fold (log$_2$ > 1) compared to that of Col and *P. adjust* < 0.05 in LAT test

ensembl_gene_id	symbol	log2 Fold Change	*P.adjust*	WT.norm.count.mean	dou.norm.count.mean
AT3G01345		9.3853	6.7E-15	3.8176	2576.7213
ATCG00690	PSBT|PSBTC	2.0621	1E-09	173.0266	722.372
AT1G64795		6.6908	2.3E-08	1.0619	110.8613
ATCG00120	ATPA	1.9066	4.7E-08	482.165	1807.0492
ATCG00360	YCF3	2.2713	6.4E-08	202.4695	976.948
ATCG00340	PSAB	1.9779	1.6E-07	2792.8897	11001.7836
ATCG00680	PSBB	1.8214	3.1E-07	6538.4436	23107.6733
ATCG00710	PSBH	1.936	4.1E-07	137.7544	526.6867
AT1G75945		4.4576	5.3E-07	4.7349	103.3492
ATCG01070	NDHE	1.9992	3.5E-06	126.5298	505.3013
ATCG01090	NDHI	2.1287	5.9E-06	135.2251	590.7198
ATCG00130	ATPF	1.8016	6E-06	342.9433	1194.8345
ATCG00070	PSBK	1.8384	2E-05	302.0474	1079.8146
ATCG00700	PSBN	2.05	2.4E-05	91.4918	378.7231
ATCG00730	PETD	1.7452	2.4E-05	227.0023	760.3996
ATCG00290		1.6073	0.00015	133.796	407.7143
ATCG01080	NDHG	1.9258	0.00021	214.6892	815.1954
ATCG00140	ATPH	1.8097	0.00022	724.5897	2539.8041
ATCG00520	YCF4	1.5513	0.00024	254.7248	745.9612
ATCG00720	PETB	1.7378	0.00038	1486.1909	4956.155
ATCG01100	NDHA	1.6163	0.00073	837.027	2565.5958
ATCG00920		2.7629	0.00118	568.7761	3859.7004
ATCG00180	RPOC1	1.6014	0.00139	799.7925	2426.2987
AT1G29090		3.4337	0.00178	9.7572	104.9989
ATCG01060	PSAC	1.6739	0.00221	359.9816	1148.2126
AT4G11485	LCR11	1.6638	0.00273	47.728	151.1705
ATCG01050	NDHD	1.9394	0.00284	292.2273	1120.3171
AT4G19690	ATIRT1|IRT1	2.5305	0.00418	54.9254	316.9599
ATCG00170	RPOC2	1.5477	0.00481	672.0315	1964.0276
AT5G42600	MRN1	1.9486	0.01146	213.3665	823.4905
ATCG00280	PSBC	1.089	0.01345	6881.2319	14637.7147
AT4G36880	CP1|RDL1	1.8275	0.01499	74.2135	262.8382
ATCG00300	YCF9	1.4009	0.01533	211.4216	558.0391
ATCG00065	RPS12|RPS12A	1.2832	0.02347	189.0068	459.5994
ATCG00530	YCF10	1.2327	0.02762	350.4034	822.9218
ATCG00350	PSAA	1.4119	0.0307	14312.1145	38082.8745
ATCG00540	PETA	1.2206	0.03847	299.2346	696.8268

Table 3. All downregulated differentially expressed genes (DEGs) whose expression changed more than 2 fold (log₂ < -1) compared to that of Col and *P. adjust* < 0.05 in LAT test

ensembl_gene_id	symbol	log2 Fold Change	*P.adjust*	WT.norm.count.mean	dou.norm.count.mean
AT2G47390		-4.3458	2.3E-26	1805.5314	89.2662
AT3G30720	QQS	-3.197	2.2E-17	482.3836	52.715
AT3G05945		-4.1081	3.3E-15	447.6713	26.19
AT5G11330		-1.6976	1.5E-07	1794.2563	553.0114
AT2G01422		-6.5498	1.7E-07	113.7087	1.3265
AT2G05510		-1.3909	0.00054	3138.4357	1196.9967
AT5G55700	BAM4|BMY6	-1.2141	0.00151	465.5451	200.5193
AT1G19530		-1.114	0.00221	299.3319	138.6512
AT3G14130	HAOX1	-2.0773	0.00284	308.748	73.1774
AT5G07240	IQD24	-1.1758	0.00881	641.4357	284.1012
AT2G02930	ATGSTF3|GST1	-2.269	0.02871	104.1513	21.6841

71
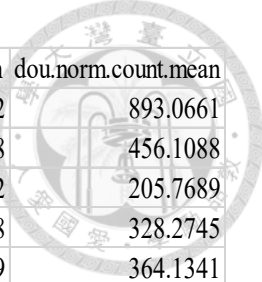
Table 4. All upregulated differentially expressed genes (DEGs) whose expression changed more than 2 fold (log$_2$ > 1) compared to that of Col and *P. adjust* < 0.05 in GHS test

ensembl_gene_id	symbol	log2 Fold Change	*P.adjust*	WT.norm.count.mean	dou.norm.count.mean
AT5G07240	IQD24	3.222	1.2E-28	471.9143	4395.7397
ATCG01210		4.6108	3.4E-25	210.8711	5148.1357
AT1G76740		3.8672	1.6E-10	25.4957	383.2751
ATCG00680	PSBB	2.0823	6.8E-10	3927.6597	16637.1632
ATCG00920		3.9448	4.1E-08	70.9511	1091.6796
ATCG00490	RBCL	2.2893	4.6E-08	8512.265	41612.9607
ATCG00280	PSBC	1.6923	9.5E-08	3674.9647	11876.2691
AT3G01345		7.7706	2E-06	1.6405	392.9998
AT1G02390	ATGPAT2|GPAT2	1.9539	3.4E-06	102.8722	398.8752
AT1G75860		1.2555	5E-06	7684.111	18346.1886
AT5G65410	HB25	1.393	8.3E-06	254.6172	668.861
AT1G75945		5.235	1.1E-05	2.8025	97.973
AT5G46690	bHLH071	2.298	1.2E-05	37.3212	181.5061
ATCG01100	NDHA	1.897	1.6E-05	180.3166	673.2255
ATCG00690	PSBT|PSBTC	1.7355	1.7E-05	70.6776	235.4129
AT1G30040	GA2OX2	1.6273	2.6E-05	237.187	733.2741
ATCG00170	RPOC2	2.0081	4.5E-05	75.9408	306.7707
AT5G21482	ATCKX5|CKX7	1.8268	5E-05	70.131	247.1463
ATCG01060	PSAC	2.0203	6.5E-05	82.5028	335.2893
ATCG00700	PSBN	2.1265	6.6E-05	40.6702	181.0714
ATCG00720	PETB	1.8089	7.3E-05	1055.3092	3700.2388
AT4G14680	APS3	1.6166	9.2E-05	127.8214	391.1803
ATCG00340	PSAB	1.589	9.2E-05	721.7439	2174.4101
ATCG00120	ATPA	1.5551	9.9E-05	136.6388	402.3774
AT3G06730	TRX	1.4354	0.0001	143.6112	386.2723
ATCG00140	ATPH	1.8289	0.0001	287.2895	1023.6382
AT2G31070	TCP10	1.6353	0.0001	204.4459	633.8113
AT1G80660	AHA9|HA9	1.5641	0.00011	367.4696	1085.0964
AT1G14580		1.4778	0.00016	119.3454	332.6566
ATCG00710	PSBH	1.6296	0.00019	89.4064	277.9927
AT1G62180	APR2|APSR	1.2232	0.00021	1484.7745	3469.2122
AT3G05600		1.996	0.00023	18.3188	73.2265
ATCG00350	PSAA	1.734	0.0003	2229.9605	7421.6315
ATCG00130	ATPF	1.6268	0.0003	92.6876	285.1653
AT1G64795	ATEH1	7.1296	0.00037	0.7519	89.8118
AT2G41940	ZFP8	1.2711	0.00037	394.8109	951.7652
AT1G76750	EC1.1	7.5244	0.00038	0.7519	118.4602
ATCG00180	RPOC1	1.9256	0.00039	35.4072	133.6923
AT1G26230	Cpn60beta4	1.5645	0.0004	86.604	256.0718
AT2G46870	NGA1	1.8394	0.00043	43.3364	152.3144
AT4G03400	DFL2|GH3-10	1.2529	0.00043	865.904	2063.3573
AT2G33330	PDLP3	1.4214	0.00047	120.029	321.0528
AT5G05740	EGY2	1.3229	0.00055	323.1767	806.0694
AT5G39080		1.1037	0.00068	521.4693	1121.9199
AT1G24580		3.7733	0.00076	3.2809	49.8401
AT4G32790		1.3174	0.00097	233.7007	583.9291
AT2G46320	MTM2	1.1712	0.00105	234.7265	527.8629
ATCG00580	PSBE	1.5802	0.00112	586.5428	1753.5293
AT2G32230	PRORP1	1.2724	0.00129	213.6055	513.8367
ATCG00730	PETD	1.4506	0.00165	128.573	352.7441

72

ensembl_gene_id	symbol	log2 Fold Change	P.adjust	WT.norm.count.mean	dou.norm.count.mean
AT1G34245	EPF2	1.8932	0.0019	93.7814	346.7423
AT1G65800	ARK2|RK2	1.3238	0.00208	63.9105	161.1452
AT4G17810	EMB3022	1.4709	0.0023	66.5083	182.1792
AT5G55220		1.1325	0.0025	566.1735	1240.5763
AT1G76110		1.0948	0.0027	394.8793	842.1884
AT4G27820	BGLU9	1.1781	0.00272	112.6466	256.4959
AT3G47450	ATNOA1|ATNOS1	1.0109	0.00278	632.8183	1274.406
ATCG01080	NDHG	1.6915	0.00286	76.8292	250.6484
ATCG00070	PSBK	1.4258	0.00286	223.1066	598.3373
AT1G35730	APUM9|PUM9	1.3453	0.00286	318.5966	808.5129
ATCG00570	PSBF	1.5835	0.00328	115.5176	346.2726
ATCG00270	PSBD	1.1521	0.00328	6735.4319	14968.8737
AT4G04350	EMB2369	1.0155	0.00328	471.0932	952.0142
AT2G31725		1.0979	0.00336	543.4802	1162.3683
AT1G61300		1.6988	0.00348	28.0933	91.5787
AT3G51870		1.1547	0.00351	342.9307	761.926
AT1G63360		1.2492	0.00359	55.093	131.5959
AT1G21520		2.6057	0.00368	38.0729	232.4014
AT5G24570		1.3174	0.00405	194.7398	484.0876
AT3G24000		1.0691	0.0041	238.4857	500.5993
ATCG00520	YCF4	1.4149	0.00445	60.8347	162.7718
AT2G35130		1.1809	0.00505	105.0596	237.355
AT5G36120	atylmg3|CCB3|YLMG3	1.7598	0.00506	16.9516	58.9444
AT1G59710		1.0809	0.0052	445.3924	941.9246
ATCG00360	YCF3	1.5452	0.00531	55.2981	161.9409
ATCG00150	ATPI	1.3238	0.00575	721.6104	1805.2346
ATCG00540	PETA	1.367	0.00581	89.2015	230.2489
AT5G07020		1.1404	0.00593	1330.3685	2931.2983
AT4G29590		1.1184	0.00607	166.4411	361.2173
AT3G61970	NGA2	1.5537	0.00637	69.5841	203.0485
AT5G28300	AtGT2L|GT2L	1.2446	0.00639	359.4042	849.8166
ATCG00020	PSBA	1.3782	0.00649	25162.8461	65412.8546
AT2G07042		1.7206	0.0067	50.7184	167.1679
AT4G39940	AKN2|APK2	1.6011	0.00676	128.7786	388.7929
AT1G02380		1.1863	0.0074	304.926	692.6329
AT1G31540		1.0324	0.0074	310.8727	634.6667
AT1G32990	PRPL11	1.0228	0.00859	1638.6449	3327.3866
AT1G13270	MAP1B|MAP1C	1.0593	0.00878	590.3711	1228.8919
AT2G36630		1.0406	0.00893	177.1729	362.6231
AT5G43270	SPL2	1.0681	0.00914	181.4791	379.4188
ATCG01050	NDHD	1.7176	0.00956	83.3227	276.8568
AT2G41980		1.1098	0.00956	171.5673	371.7238
AT1G11785		2.2173	0.0099	19.0707	88.6058
AT5G20130		1.1037	0.01009	450.0409	966.0436
ATCG00065	RPS12|RPS12A	1.3577	0.01026	61.9969	157.3836
AT1G72430	SAUR78	1.0327	0.01045	3068.8082	6277.275
AT3G25480		1.1305	0.01147	132.9476	292.4256
ATCG00040	MATK	1.2654	0.01149	161.8616	388.3266
AT1G32220		1.2461	0.01193	431.1069	1021.64
AT1G31550		1.9998	0.0124	14.6961	57.2231

73

ensembl_gene_id	symbol	log2 Fold Change	P.adjust	WT.norm.count.mean	dou.norm.count.mean
AT1G16720	HCF173	1.0809	0.0129	1336.179	2825.1638
AT5G61390		1.2454	0.0129	133.4266	314.8198
ATCG01070	NDHE	1.3889	0.013	58.5106	154.6141
AT2G37450	UMAMIT13	1.1681	0.013	108.2724	241.2813
AT1G44830		2.2915	0.0135	15.0378	72.7041
AT2G22870	EMB2001	1.2002	0.0135	176.0106	404.5859
AT2G41990		1.1346	0.0135	340.333	746.5327
AT5G18660	PCB2	1.2587	0.0138	437.943	1045.8081
AT1G72190		1.1202	0.0146	98.4977	212.7206
AT3G55630	ATDFD|DFD|FPGS3	1.2216	0.0151	120.2343	278.9918
AT1G27960	ECT9	1.1726	0.0152	236.6402	533.8365
AT4G34900	ATXDH2|XDH2	1.4191	0.0153	63.2956	167.841
AT1G33720	CYP76C6	1.3724	0.0155	70.0625	180.7664
AT3G16750		1.4046	0.0157	46.8906	123.5434
AT5G51600	ATMAP65-3|MAP65-3	1.3472	0.0157	93.5762	237.4041
ATCG01090	NDHI	1.4532	0.0165	57.9638	159.9497
AT3G50270		1.2919	0.017	30.8958	75.8943
ATCG00160	RPS2	1.2764	0.0179	82.2979	198.7084
AT3G18110	EMB1270	1.0685	0.0183	113.7405	237.9299
AT3G57520	AtSIP2|RS2|SIP2	1.0938	0.0186	1425.3777	3042.3795
AT1G29070		1.0508	0.0187	5024.8232	10407.8914
AT3G53900	PYRR|UPP	1.0686	0.0191	141.9708	295.9312
ATCG00440	NDHC	1.0807	0.0199	1189.9017	2515.6552
AT3G51080	GATA6	1.0717	0.0199	125.2238	263.5599
AT1G63860		1.152	0.0211	399.2534	887.5027
ATCG00190	RPOB	1.1349	0.0213	118.4567	260.9972
AT3G62030	CYP20-3|ROC4	1.3267	0.0225	5213.1378	13074.4087
AT3G12685		1.6855	0.0229	22.5568	70.1415
AT1G22570		1.4503	0.0232	136.5708	372.2741
AT1G10225		1.2737	0.0253	161.5878	391.296
AT1G76620		1.1131	0.0257	259.6073	560.8583
AT4G13500		1.2877	0.0258	510.1925	1244.3132
AT5G44870	LAZ5|TTR1	1.1528	0.0259	91.6624	202.3614
AT2G45150	CDS4	1.1097	0.0259	90.4318	195.5639
ATCG00420	NDHJ	1.062	0.0263	1133.92	2366.3383
AT5G62730		1.641	0.0264	466.174	1451.5509
AT5G11950	LOG8	1.0071	0.0274	264.8022	531.6384
AT4G18390	TCP2	1.0902	0.0279	102.3255	216.7942
AT4G36870	BLH2|BLH2|SAW1|SA`	1.0632	0.0285	490.2326	1023.6806
AT4G29400		1.0738	0.0286	154.8212	325.0843
AT3G28270	AFL1	1.2614	0.029	90.3635	216.6574
AT3G13850	LBD22	1.9704	0.0302	23.3086	91.4244
AT3G04550		1.0772	0.0316	746.0132	1572.5177
AT2G09150		1.4745	0.0324	69.584	193.478
ATCG00530	YCF10	1.1197	0.0331	121.9429	265.1865
AT1G22380	AtUGT85A3|UGT85A3	1.2252	0.034	107.7252	252.6292
AT3G47430	PEX11B	1.2655	0.0364	173.6871	415.9899
ATCG00210	YCF6	2.1567	0.0366	39.7818	177.6498
AT3G25770	AOC2	1.84	0.0372	63.4326	224.7204
AT1G51080		1.7659	0.0372	18.5238	62.9268

ensembl_gene_id	symbol	log2 Fold Change	P.adjust	WT.norm.count.mean	dou.norm.count.mean
AT5G67190	DEAR2	1.0177	0.0399	440.9492	893.0661
ATCG00080	PSBI	1.063	0.0409	218.1848	456.1088
AT4G04880		1.0468	0.0409	99.5912	205.7689
AT1G62780		1.2203	0.0429	141.5608	328.2745
AT1G80080	AtRLP17|TMM	1.0918	0.0429	171.9099	364.1341
AT1G64500		1.15	0.04352	42.5161	93.051
AT4G16563		1.049	0.04389	1936.3909	4006.1337
ATCG00500	ACCD	1.2828	0.04437	320.7151	780.7864
AT5G39210	CRR7	1.5562	0.04511	41.0123	119.8343
AT1G21910	DREB26	1.0591	0.04511	1373.7054	2861.1248
ATCG00380	RPS4	1.1953	0.04592	97.814	224.5487
AT3G27540		1.2383	0.04641	47.5057	112.6652
AT2G47910	CRR6	1.079	0.04879	463.5074	977.1741
ATCG00810	RPL22	1.0503	0.04999	197.6791	408.039
ATCG00560	PSBL	1.3174	0.05	87.9712	219.1114
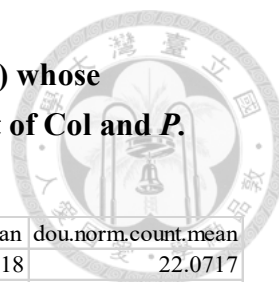
Table 5. All downregulated differentially expressed genes (DEGs) whose expression changed more than 2 fold (log$_2$ < -1) compared to that of Col and *P. adjust* < 0.05 in GHS test
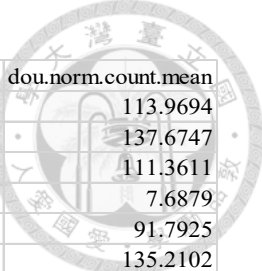
ensembl_gene_id	symbol	log2 Fold Change	*P.adjust*	WT.norm.count.mean	dou.norm.count.mean
AT2G47390		-6.12	2E-39	1539.118	22.0717
AT2G47410		-3.5112	2.9E-22	3211.5923	281.544
AT3G30720	QQS	-3.3362	5E-18	575.5383	57.0127
AT3G63350	AT-HSFA7B|HSFA7B	-2.2841	5.4E-13	6248.271	1282.7217
AT3G44300	AtNIT2|NIT2	-2.1216	6.3E-12	2868.8716	658.9015
AT3G05945		-3.2614	4.7E-09	374.6463	39.2845
AT2G02930	GST16|GSTF3	-3.7895	4.1E-08	422.9059	30.7062
AT3G54830		-1.943	2.3E-07	308.8215	80.4446
AT2G43510	ATTI1|TI1	-2.8817	2.9E-07	582.7854	79.0879
AT1G26390		-4.167	6.3E-07	517.2348	28.9288
AT1G51420	ATSPP1|SPP1	-2.0483	1.7E-06	251.1996	60.7252
AT1G15040	GAT|GAT1_2.1	-3.154	1.9E-06	145.9353	16.3715
AT4G23700	ATCHX17|CHX17	-1.94	2.9E-06	381.9606	99.2701
AT2G15220		-3.4033	3.8E-06	1431.7437	135.431
AT1G74590	ATGSTU10|GSTU10	-2.0422	4.8E-06	337.5309	81.8574
AT1G11080	scpl31	-2.2045	5.2E-06	159.811	34.5729
AT5G04980		-1.3799	1.1E-05	933.9149	359.1244
AT4G36430		-4.1179	1.2E-05	102.6675	5.9106
AT1G03220		-1.3701	1.6E-05	10707.6733	4142.0137
AT1G21310	ATEXT3|EXT3|RSH	-2.1359	1.7E-05	21655.0458	4926.9719
AT4G37520		-1.6839	2E-05	3320.2853	1033.3104
AT3G51910	AT-HSFA7A|HSFA7A	-1.5561	2.7E-05	8345.7533	2838.4158
AT1G30190		-2.5825	7.6E-05	197.8152	32.9498
AT5G53680		-1.9788	7.6E-05	4022.4144	1020.5707
AT4G11650	ATOSM34|OSM34	-1.9827	9.2E-05	12875.8248	3257.6864
AT3G01420	DOX1|PADOX-1	-1.1724	9.6E-05	29240.0357	12973.535
AT5G07010	ATST2A|ST2A	-1.9043	0.0001	1452.2451	387.9024
AT4G20110	VSR3;1|VSR7	-1.4581	0.00011	2171.3238	790.2833
AT1G21100	IGMT1	-2.0471	0.00012	353.6622	85.626
AT4G33720		-3.6427	0.0002	113.6038	9.0481
AT5G37690		-1.6709	0.00021	211.6226	66.5832
AT1G30730		-2.8222	0.00028	1056.6845	149.5028
AT3G50930	BCS1	-1.9819	0.00028	191.5267	48.6447
AT3G14990	AtDJ1A|DJ-1a|DJ1A	-1.2178	0.00034	15084.2545	6485.3973
AT5G44380		-1.3186	0.00039	4970.2048	1992.462
AT2G47400	CP12|CP12-1	-15.3959	0.00043	10364.3517	0
AT5G58350	WNK4|ZIK2	-1.2878	0.00043	1572.0683	643.6166
AT5G07250	ATRBL3|RBL3	-1.4566	0.00047	879.5067	320.4744
AT2G39310	JAL22	-1.5582	0.0005	13510.0163	4587.8822
AT1G62810	CuAO1	-1.4127	0.00051	321.4677	120.5635
AT1G58320		-4.0973	0.00053	78.9489	4.6029
AT1G02920	GST11|GSTF7	-2.5955	0.00055	8782.9333	1453.2718
AT2G20550		-1.4324	0.00057	306.2239	113.6574
AT3G01970	WRKY45	-1.8262	0.00057	1003.3658	282.9286
AT5G43580	UPI	-1.3659	0.00057	701.171	272.0822
AT5G49350		-2.0857	0.00057	110.4593	26.0997
AT1G68620		-1.329	0.00064	548.6061	218.3683
AT4G01350		-1.9387	0.00068	141.9705	36.9252
AT3G45710		-2.301	0.00069	110.8699	22.545
AT1G21110	IGMT3	-3.101	0.0007	131.6497	15.432

76

ensembl_gene_id	symbol	log2 Fold Change	P.adjust	WT.norm.count.mean	dou.norm.count.mean
AT1G19530		-1.035	0.0007	4506.4881	2199.0619
AT5G19530	ACL5	-1.2482	0.0008	1778.1479	748.8815
AT1G30720		-1.8385	0.00082	3629.6598	1014.8144
AT1G02220	ANAC003|NAC003	-1.0136	0.00099	975.4748	483.0815
AT1G28190		-1.9042	0.00101	171.0893	45.6088
AT4G36540	BEE2	-1.1407	0.00102	506.7735	230.0351
AT5G25930		-1.525	0.00115	795.1578	276.3801
AT1G76930	EXT1|EXT4|ORG5	-2.0667	0.00122	20821.8172	4970.1326
AT5G48540		-1.8492	0.00134	125.8393	34.8884
AT2G39855		-1.9391	0.00146	160.4258	41.9489
AT1G26410		-3.7924	0.0015	63.9794	4.6029
AT4G28250	EXPB3	-1.3251	0.00167	350.2435	139.8027
AT3G29370	P1R3	-1.7724	0.00232	313.6746	91.9537
AT1G65370		-1.5626	0.0027	229.8734	77.9906
AT5G24090	ATCHIA|CHIA	-1.1915	0.0027	406.7724	178.2563
AT1G78490	CYP708A3	-1.2021	0.0027	440.2661	191.2799
AT1G15380	GLYI4	-1.4089	0.00328	1080.668	407.2328
AT1G30910		-10.9136	0.00328	463.6435	0
AT2G23170	GH3.3	-1.5121	0.00328	1473.7053	516.6658
AT5G40780	LHT1	-1.5581	0.00328	167.8768	56.855
AT5G63560	FACT	-1.0561	0.00348	1027.4223	494.2085
AT3G21352		-3.6274	0.00359	106.4273	8.631
AT4G37010	CEN2	-1.5813	0.00379	1094.3435	365.7291
AT5G10180	AST68|SULTR2;1	-1.2035	0.00418	2126.6132	923.6638
AT1G01190	CYP78A8	-3.331	0.00428	39.987	3.9754
AT2G38870		-1.7167	0.00428	1669.6816	507.7824
AT3G53180	NodGS	-1.0057	0.00428	1602.2772	797.7716
AT3G15450		-1.0092	0.00466	13902.5968	6906.6034
AT2G03360		-1.9787	0.00475	182.1627	46.0785
AT3G49780	PSK4	-1.0918	0.00495	3476.7427	1631.08
AT2G01422		-6.4518	0.00504	20.8478	0
AT3G62040		-1.8442	0.0051	526.3889	146.6493
AT2G43590		-1.3014	0.00531	994.5455	403.5308
AT1G67980	CCOAMT	-2.8492	0.00545	52.0173	7.1656
AT2G24180	CYP71B6	-1.2175	0.00578	1258.803	541.1003
AT1G77145		-1.2328	0.00589	378.6113	160.7806
AT2G28780		-1.9931	0.00593	227.9589	57.3247
AT3G45160		-1.7142	0.00593	630.0849	192.0161
AT4G09890		-1.3357	0.00593	171.4309	67.8908
AT5G09480		-1.1655	0.00593	1656.7541	738.7465
AT1G30700		-1.3653	0.00603	711.6993	276.1767
AT5G57790		-1.3655	0.00607	426.1164	165.4396
AT1G01720	ANAC002|ATAF1	-1.1543	0.00611	16923.7572	7603.1384
AT3G56260		-1.1562	0.00619	443.2731	198.8031
AT1G20160	ATSBT5.2	-1.1831	0.00649	1186.2091	522.2469
AT3G63380		-1.6144	0.0074	590.7827	192.8014
AT5G54370		-1.5585	0.0074	700.0809	237.2463
AT5G42440		-2.3605	0.00806	44.2249	8.5784
AT2G43570	CHI	-1.3724	0.00822	1776.856	686.1334
AT4G21120	AAT1|CAT1	-1.8056	0.00845	87.2194	24.8447

ensembl_gene_id	symbol	log2 Fold Change	P.adjust	WT.norm.count.mean	dou.norm.count.mean
AT5G01180	NPF8.2|PTR5	-1.1746	0.00845	9187.9513	4070.2352
AT1G60730		-1.0349	0.00878	1751.3593	854.5073
AT3G13750	BGAL1	-1.0677	0.00878	14061.7715	6708.4669
AT5G54510	DFL1|GH3.6	-1.3545	0.00878	4915.161	1922.314
AT4G37070	AtPLAIVA|PLA|PLP1	-1.3586	0.00938	764.6734	298.2589
AT2G25940	ALPHAVPE	-1.3323	0.00973	271.6377	107.6942
AT1G14870	AtPCR2|PCR2	-1.5411	0.00977	1612.3278	554.0852
AT2G37900		-3.2248	0.01027	30.349	3.1902
AT5G43700	ATAUX2-11|IAA4	-1.0419	0.01034	1438.7073	698.9641
AT3G16450	JAL33	-1.4946	0.01051	8040.1785	2853.1393
AT4G26120		-2.1593	0.01051	82.9132	18.5695
AT2G46750	AtGulLO2|GulLO2	-1.6986	0.01129	1012.184	311.8048
AT3G01175		-1.4873	0.01158	128.0949	45.5036
AT4G13310	CYP71A20	-3.2197	0.01169	30.4174	3.1902
AT4G14060		-2.3217	0.01193	55.093	10.9833
AT4G14630	GLP9	-2.9752	0.01285	73.4804	9.4162
AT2G38860	DJ-1e|DJ1E|YLS5	-1.6569	0.01303	1218.1353	386.1846
AT4G33550		-1.2431	0.0135	483.6015	204.4577
AT1G29510	SAUR67	-1.8696	0.01353	197.269	53.9803
AT4G39675		-1.0367	0.01353	828.5831	403.7341
AT4G21650		-1.6094	0.0136	260.5649	85.3666
AT3G52060	AtGnTL|GnTL	-1.1808	0.0136	5062.3271	2233.0778
AT4G37900		-1.3461	0.01405	178.1299	69.826
AT1G26420		-2.5535	0.01482	50.7869	8.6835
AT3G16400	NSP1	-1.0835	0.01484	6756.2846	3187.8611
AT3G08065		-2.3561	0.01518	40.1235	7.8983
AT3G01670	SEOR2	-1.0303	0.0152	896.0467	438.8224
AT4G12490		-2.8289	0.01616	335.9612	47.288
AT5G48430		-2.4056	0.01645	146.619	27.6703
AT5G01500	TAAC	-1.2601	0.01817	175.1906	72.911
AT1G30420	MRP12	-1.9211	0.01862	61.5867	16.056
AT3G54260	TBL36	-1.339	0.01875	778.2059	307.6542
AT5G23020	IMS2|MAM-L|MAM3	-1.1888	0.01907	385.1727	168.9418
AT5G45380	ATDUR3|DUR3	-1.2718	0.01907	372.2547	153.934
AT4G05200	CRK25	-2.3601	0.0206	194.8773	37.9769
AT4G37370	CYP81D8	-1.2605	0.02099	392.4868	163.9287
AT1G19250	FMO1	-3.6403	0.02141	58.2377	4.7081
AT2G02120	LCR70|PDF2.1	-2.0192	0.02141	192.0737	47.3336
AT1G18970	GLP4	-2.6609	0.02191	70.5411	11.141
AT3G26590		-1.3156	0.02251	101.3	40.5852
AT1G26380		-2.6588	0.02265	446.0782	70.7269
AT2G37870		-1.0747	0.02544	619.0094	294.266
AT3G26830	CYP71B15|PAD3	-2.5342	0.02586	123.1735	21.3425
AT3G55880	SUE4	-1.083	0.02586	335.821	158.7438
AT2G04100		-1.612	0.02654	129.7352	42.2048
AT3G43190	ATSUS4|SUS4	-1.0955	0.02743	323.5181	151.1049
AT1G67750		-1.112	0.02744	153.4536	71.3965
AT3G44716		-2.1511	0.02853	94.1233	21.1848
AT3G51330		-1.2687	0.02853	1063.5168	441.2552
AT1G72200		-1.2206	0.02863	253.0454	108.4269

78

ensembl_gene_id	symbol	log2 Fold Change	P.adjust	WT.norm.count.mean	dou.norm.count.mean
AT3G05640		-1.1384	0.02889	250.4473	113.9694
AT5G14200	ATIMD1|IMD1	-1.4716	0.02889	381.619	137.6747
AT4G32280	IAA29	-1.4026	0.03071	294.468	111.3611
AT4G16000		-2.3573	0.03296	40.1237	7.6879
AT2G47860	SETH6	-1.176	0.03307	207.1796	91.7925
AT3G49110	PRXCA	-1.3951	0.03383	355.2336	135.2102
AT3G49120	PRX34|PRXCB	-1.3876	0.0345	2523.5542	964.2769
AT3G22850		-1.0583	0.03478	1005.5511	482.773
AT2G44370		-1.9181	0.03578	94.6019	24.8973
AT3G26210	CYP71B23	-1.4607	0.03605	377.5182	137.1523
AT1G52060		-1.251	0.03632	434.4566	182.1687
AT1G47670		-1.0988	0.03635	329.9425	154.0813
AT5G47580	ASG7	-1.2842	0.03637	155.9829	63.8593
AT4G32870		-1.1774	0.03644	200.5499	88.5007
AT1G21120	IGMT2	-5.1782	0.0399	24.2657	0.6801
AT5G38900		-2.3779	0.04066	163.2974	31.4914
AT1G04240	IAA3|SHY2	-1.1906	0.0409	310.5978	136.5669
AT2G41780		-1.2929	0.0409	131.6491	53.77
AT3G26760		-1.2279	0.04159	104.0342	44.4063
AT2G40480		-1.3165	0.04162	83.6647	33.6299
AT3G07130	ATPAP15|PAP15	-1.0804	0.04167	230.7617	109.3173
AT3G55500	|EXP16|EXPA16	-1.7559	0.04187	213.9464	63.4456
AT4G22690	CYP706A1	-1.0433	0.04261	476.9035	231.5075
AT1G29770		-1.2167	0.04261	265.0066	114.2323
AT1G49570		-2.713	0.043	54.4776	8.2629
AT1G32450	NPF7.3|NRT1.5	-1.4681	0.04318	5256.1731	1899.9759
AT3G09260	BGLU23	-1.0615	0.0434	43343.1709	20766.5531
AT3G25900	ATHMT-1|HMT-1	-1.0595	0.04352	395.2891	189.6568
AT5G01870		-1.2499	0.04413	196.9955	82.7478
AT2G29330	TRI	-1.9359	0.04511	166.3047	43.4668
AT1G27020		-1.5909	0.04554	1181.9759	392.3721
AT1G52200		-1.4744	0.04971	307.1139	110.4742
AT3G46490		-1.3558	0.04984	121.1912	47.2319
AT5G06570		-1.4029	0.04999	243.7497	92.0589

Figures
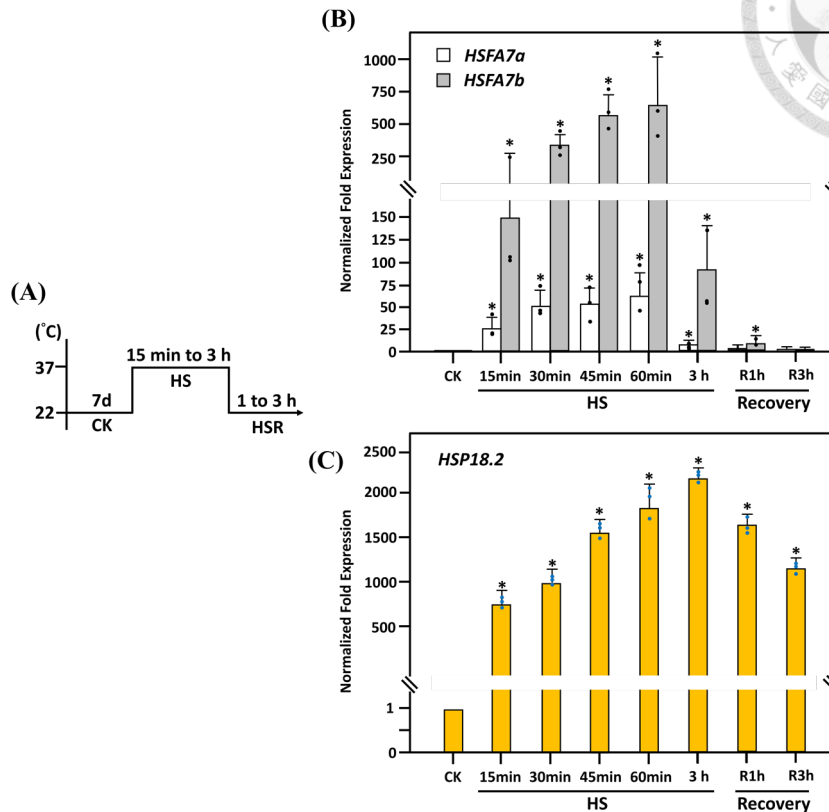
Figure 1. Transcription profiling of *HSFA7a* and *HSFA7b* in response to heat shock (HS).

7-d-old WT (Col) seedlings were treated without (control; CK) or with a sublethal HS (37°C) for 15 min to 3 h then recovery from the HS for 1 to 3 h. **(A)** Pictogram illustrated the scheme for treatments and recovery time. **(B and C)** Expression levels of *HSFA7a*, *HSFA7b*, and *HSP18.2* were analyzed by qRT-CR. *HSP18.2,* an HS-responsive marker gene, was used as a reference. Data were mean ± SD (*n* = 3). The qRT-PCR assays were repeated for three times. Expression level of each gene was normalized to the CK. The star mark (*) indicated significance at *P* < 0.05 (Student's *t* test) compared to the CK. *PP2A* was used as reference gene.

80
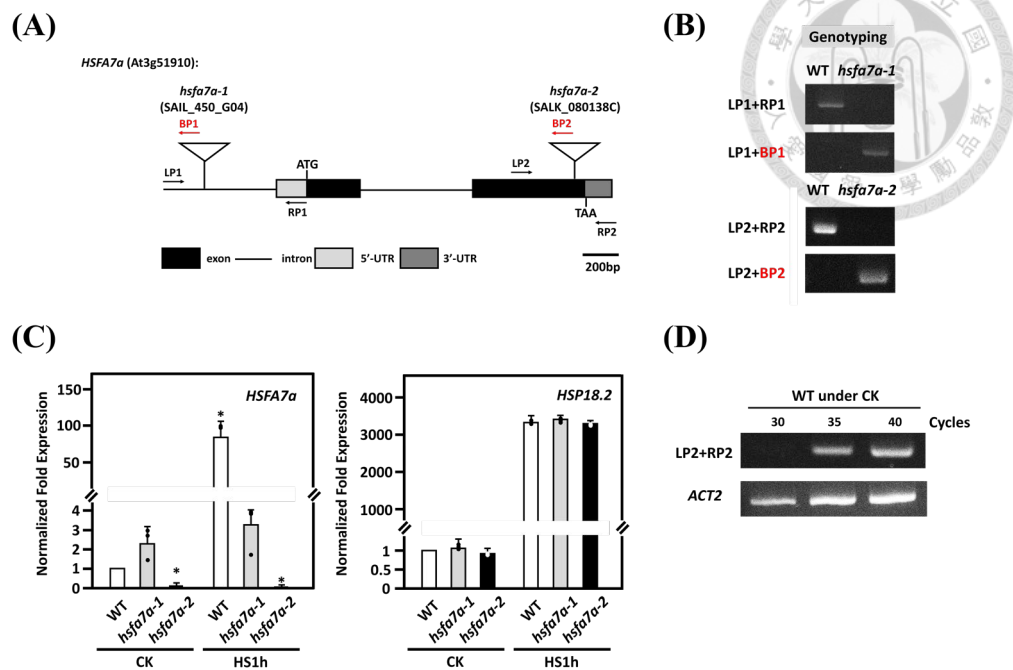
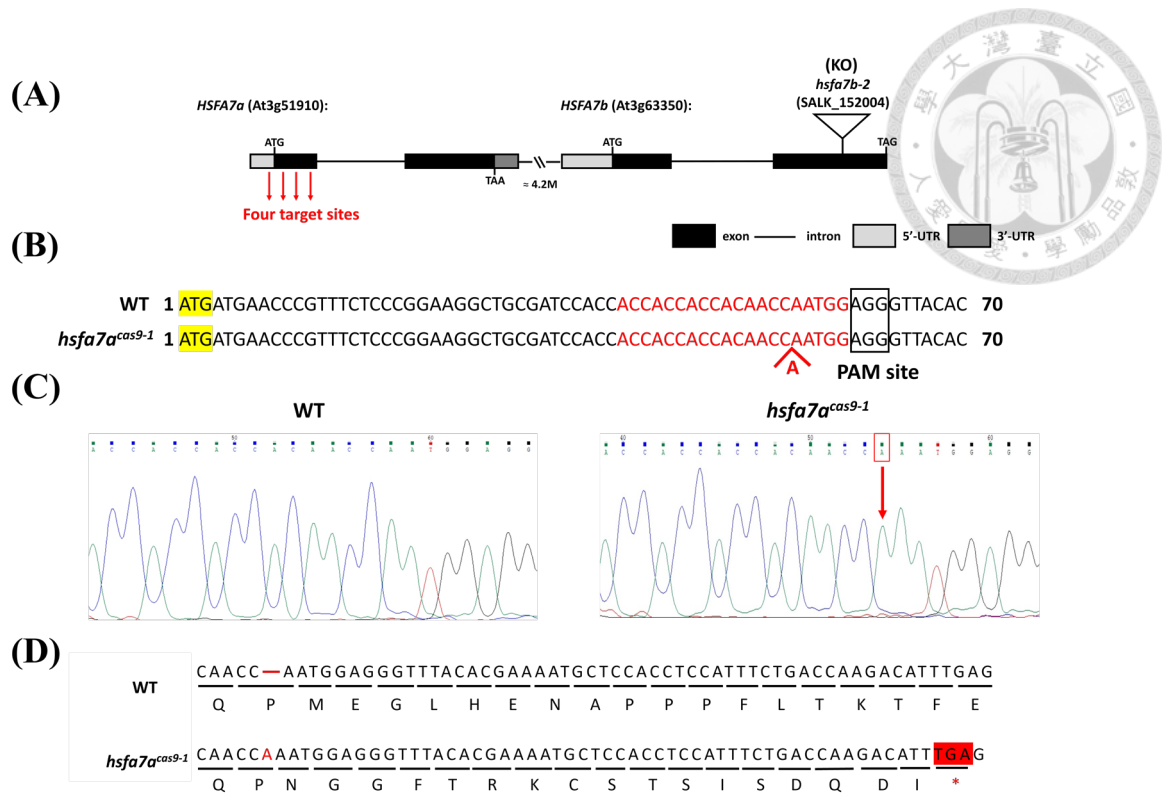**Figure 2. Genotyping and characterization of *HSFA7a* T-DNA insertion lines.**

(A) The inverted triangle represented the T-DNA insertion site in *hsfa7a-1* (SAIL_450_G04) and *hsfa7a-2* (SALK_080138C) lines. ATG and TAG showed the position of the start and stop codons, respectively. Arrows indicated the positions of the specific primers designed for genotyping. **(B)** Genotyping results demonstrated that *hsfa7a-1* and *hsfa7a-2* were homozygous mutants. **(C)** The expression levels of *HSFA7a* and *HSP18.2* in *hsfa7a-1* and *hsfa7a-2* were analyzed by qRT-PCR under CK or 37°C for 1 h, respectively. Gene expression level was normalized to the CK of WT. **(D)** The RT-PCR results of *HSFA7a* under CK with different cycles are shown here. Data were mean ± SD (*n* =3). The qRT-PCR assays were repeated for three times. The star mark (*) indicated significance at *P* < 0.05 (Student's *t* test) compared to the CK. *PP2A* was used as reference gene.
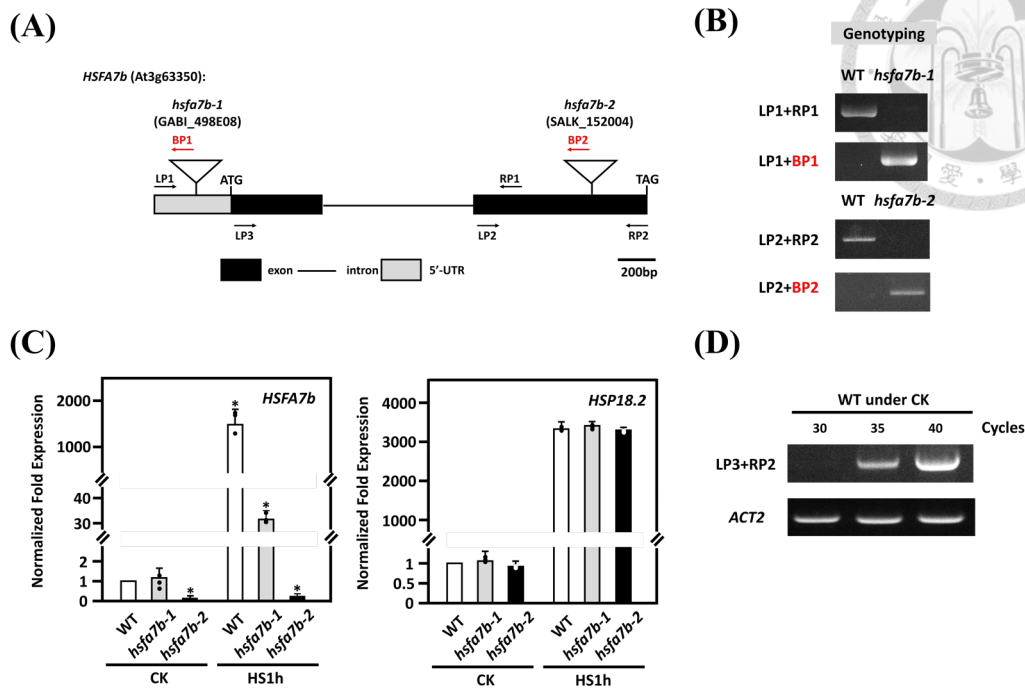
Figure 3. Genotyping and characterization of *HSFA7b* T-DNA insertion lines.

(A) The inverted triangle represented the T-DNA insertion site in *hsfa7b-1* (GABI_498E08) and *hsfa7b-2* (SALK_152004) lines. ATG and TAG showed the position of the start and stop codons, respectively. Arrows indicated the positions of the specific primers designed for genotyping. **(B)** Genotyping results demonstrated that *hsfa7b-1* and *hsfa7b-2* were homozygous mutants. **(C)** The expression levels of *HSFA7b* and *HSP18.2* in *hsfa7b-1* and *hsfa7b-2* were analyzed by qRT-PCR, respectively. Gene expression level was normalized to the CK of WT. **(D)** The RT-PCR results of *HSFA7b* under CK with different cycles are shown here. Data were mean ± SD (*n* =3). The qRT-PCR assays were repeated for three times. The star mark (*) indicated significance at *P* < 0.05 (Student's *t* test) compared to the CK. *PP2A* was used as reference gene.

82

Figure 4. Characterization of *hsfa7a^cas9-1*/*hsfa7b-2* double mutant plant.

(A) Schematic illustration showed the mutation for *hsfa7a^cas9-1*/*hsfa7b-2* (i.e., *hsfa7a^cas9-1*) double mutant plant mutated by different strategies. Target sites of CRISPR-Cas9 in *HSFA7a* were represented by red arrows, and inverted triangle represented the T-DNA insertion site in *hsfa7b-2* (SALK_152004) line. **(B and C)** The pictogram illustrated the Sanger sequencing results from the first *HSFA7a* exon of wild-type plants and *hsfa7a^cas9-1* at gDNA level. ATG with yellow background represented the start codon at the first exon of *HSFA7a*, and red letters represented one of the sgRNA used to mutated *HSFA7a* by CRISPR-Cas9. Red letter in bond (**A**) represented the inserted nucleotide, and the black box represented protospacer-adjacent motif (PAM) sequences. **(D)** One nucleotide insertion led to frame shift in *hsfa7a^cas9-1* plant, resulting in a premature stop codon.

(A)

HSFA7a (At3g51910): (KO) hsfa7a-2 (SALK_080138C) HSFA7b (At3g63350):

ATG TAA ≈ 4.2M ATG TAG Four target sites

■ exon — intron ▢ 5′-UTR ▨ 3′-UTR

(B)

WT	1 GGATTCAGAAAGATCGAGGCAGAGAGATGGGAGTTTATGAATGAAGGTTTCTTGATGGGTCAGAGGGACCTTCTCAAA
hsfa7b^cas9-1	1 GGATTCAGAAAGATCGAGGCAGAGAGATGGGAGTTTATGAATGAAGGTTTCTTGATGGGTCAGAGGGACCTTCTCAAA
WT	79 AGCATCAAGCGACGAACCTCCTCTTCTTCCCCTCCTTCGCTTAACTACTCTCAGTCTCAGCCCGAGGCTCATGACCCAGGC
hsfa7b^cas9-1	79 AGCATCAAGCGACGAACCTCCTCTTCTTCCCCTCCTTCGCTTAACTACTCTCAGTCTCAGC---|---|-------------- PAM
WT	160 GTCGAGCTTCCGCAGCTCCGAGAAGAGAGGCATGTCCTAATGATGGAGATCTCGACGCTCAGACAGGAGGAGCAAAGA
hsfa7b^cas9-1	160 --
WT	238 GCGAGAGGCTACGTCCAAGCCATGGAGCAGAGGATTAATGGAGCAGAGAAGAAACAGAGGCATATGATGTCCTTCTTG PAM
hsfa7b^cas9-1	238 ---
WT	238 AGGCGTGCGGTGGAGAATCCTTCCCTTCTGCAGCAGATTTTCGAGCAGAAGAGAGACCGAGAGGAGG PAM
hsfa7b^cas9-1	238 --GAGGAGG PAM

Figure 5. Characterization of *hsfa7b^cas9-1*/*hsfa7a-2* double mutant plant.

(A) Schematic illustration showed the mutation for *hsfa7b^cas9-1*/*hsfa7a-2* (i.e., *hsfa7b^cas9-1*) double mutant plant mutated by different strategies. Target sites of CRISPR-Cas9 in *HSFA7b* were represented by red arrows, and inverted triangle represented the T-DNA insertion site in *hsfa7a-2* (SALK_080138C) line. **(B)** The pictogram illustrated the Sanger sequencing results from the second *HSFA7b* exon of wild-type plants and *hsfa7b^cas9-1* at gDNA level. There were 236 bp deleted at the second exon of *HSFA7b* in *hsfa7b^cas9-1*. Red letters represented three of four sgRNAs used to mutate *HSFA7b* by CRISPR-Cas9, and the black boxes represented protospacer-adjacent motif (PAM) sequences.

84

Figure 6. Root elongation analysis of the mutant plants in response to HS.

(A) Schematic diagram of a short-term AT test is shown here. **(B)** Photos were 4-d-old

seedlings (control; CK) and 3 d later following the AT test. The root lengths of 4-d-old

seedlings were marked by black lines on the plates. **(C)** The root length (mm) was shown

by box plots, and mean values were represented by rhombus, as indicated. The relative

root length (%) of 7-d-old seedlings under CK and AT test compared to WT under normal

conditions is shown here. **(D)** The root elongation rate (%) was measured by the root

elongation length of the AT test (4th d to 7th d) / CK (4th d to 7th d). The heat-sensitive

HSP101-mutant plants (*hsp101*) were used as reference. Data were mean ± SD (*n* > 30

seedlings). The root quantitative elongation assays were repeated for three times.

Statistically significant differences between each line were represented by different upper

and lowercase letters (ANVOA, Tukey-Kramer test, *P* < 0.05).
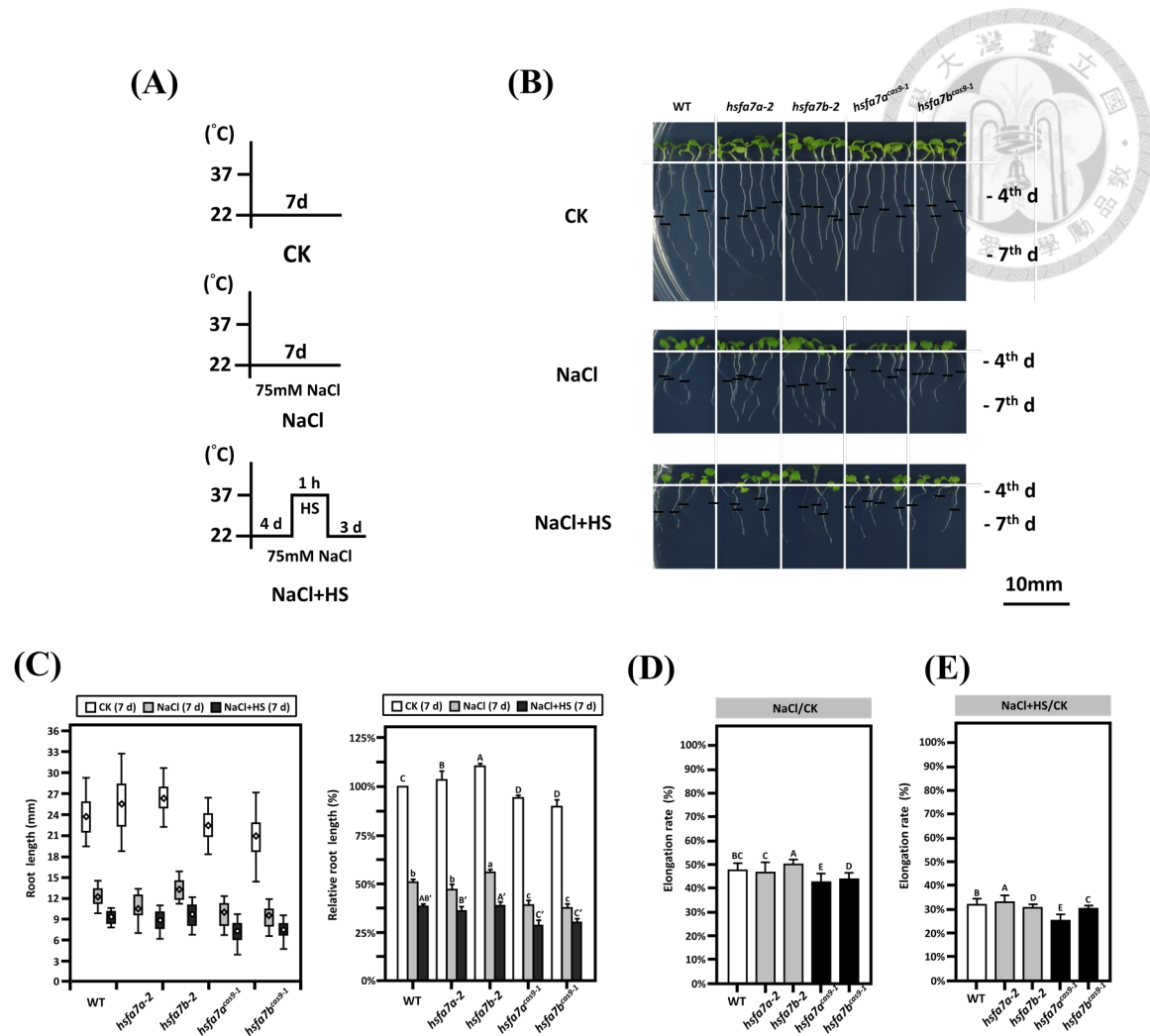
Figure 7. Root elongation analysis of the mutant plants in response to salinity.

Seeds were germinated on mediums with 75 mM NaCl. **(A)** Schematic diagrams of CK, NaCl, and NaCl+HS are shown here. **(B)** Photos were 7-d-old seedlings (CK), 7-d-old seedlings sown on 75 mM NaCl plates (NaCl), 4-d-old seedlings sown on 75 mM NaCl plate, and 3 d later following the HS test (NaCl+HS). The root lengths of 4-d-old seedlings were marked by black lines on the plates. **(C)** The root length (mm) of 7-d-old seedlings was shown by box plots, and mean values were represented by rhombus, as indicated. The relative root length (%) of 7-d-old seedlings under CK, NaCl, and NaCl+HS compared to WT under normal conditions is shown here. **(D and E)** The root elongation rate (%) of each plant was measured by the root elongation length under NaCl or

86

NaCl+HS treatments (4th d to 7th d) / CK (4th d to 7th d). Data were mean ± SD ($n > 30$ seedlings). The root quantitative elongation assays were repeated for three times. Statistically significant differences between each line were represented by different upper and lowercase letters (One-way ANVOA, Tukey-Kramer test, $P < 0.05$).
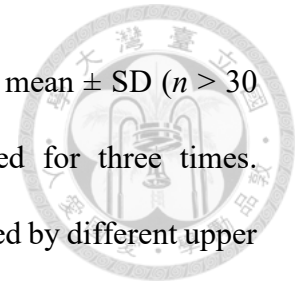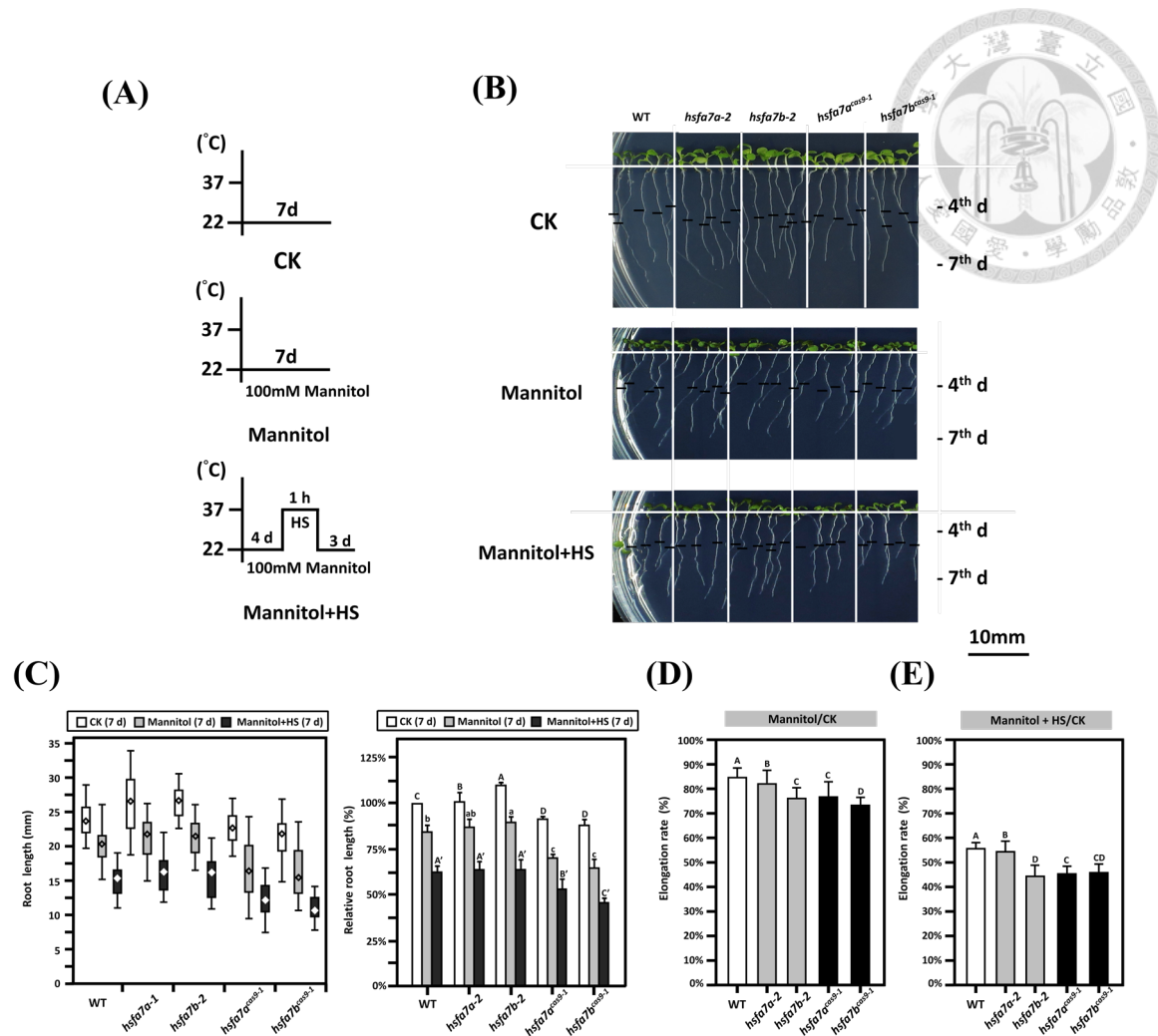
Figure 8. Root elongation analysis of the mutant plants in response to osmotic stress.

Seeds were germinated in mediums with 100 mM mannitol. **(A)** Schematic diagrams of CK, Mannitol, and Mannitol+HS are shown here. **(B)** Photos were 7-d-old seedlings (CK), 7-old seedlings sown on 100 mM mannitol plates (Mannitol), 4-d-old seedlings sown on 100 mM mannitol plate, and 3 d later following the HS test (Mannitol+HS). The root lengths of 4-d-old seedlings were marked by black lines on the plates. **(C)** The root length (mm) of 7-d-old seedlings was shown by box plots, and mean values were represented by rhombus, as indicated. The relative root length (%) of 7-d-old seedlings under CK, Mannitol, and Mannitol+HS compared to WT under normal conditions is shown here. **(D and E)** The root elongation rate (%) of each plant was measured by the root elongation

88

length under Mannitol or Mannitol+HS treatments (4th to 7th d) / CK (4th to 7th d). Data were mean ± SD ($n > 30$ seedlings). The root quantitative elongation assays were repeated for three times. Statistically significant differences between each line were represented by different upper and lowercase letters (One-way ANVOA, Tukey-Kramer test, $P <$ 0.05).
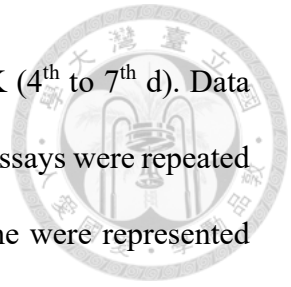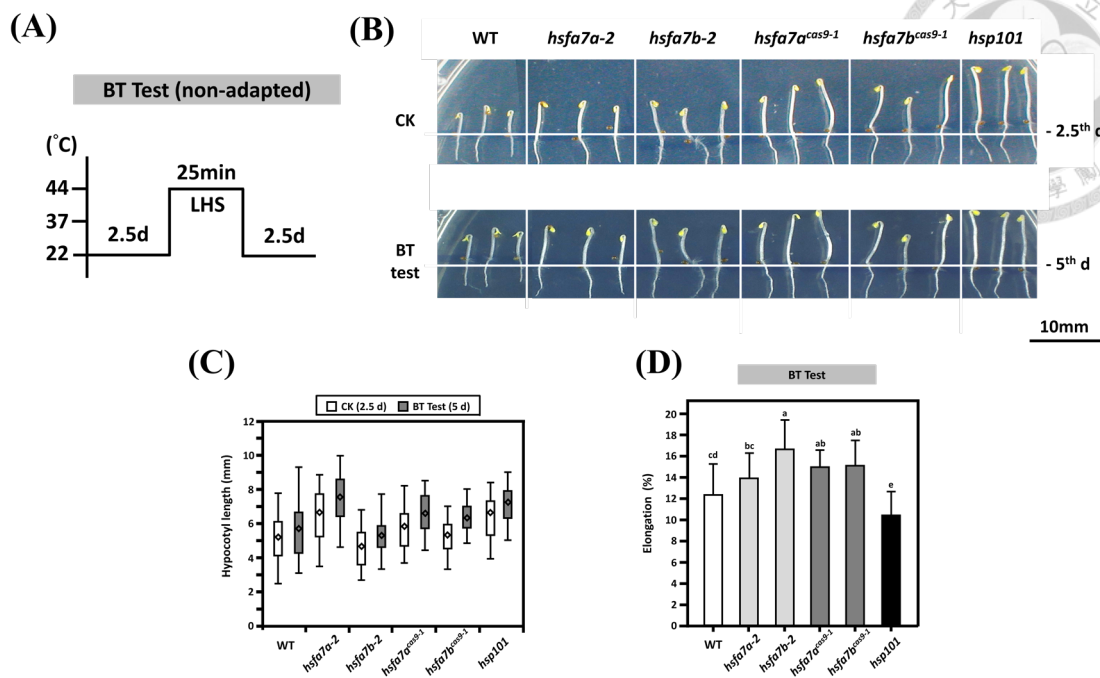
Figure 9. Phenotype of the thermo-responsive hypocotyl growth in mutant plants under basal thermotolerance (BT) test.

(A) Schematic diagram of a BT test is shown here. **(B)** Photos were 2.5-d-old etiolated seedlings (control; CK) and 2.5 d later following the BT test (BT test; 5th d). **(C)** The hypocotyl length (mm) was shown by box plots, and mean values were represented by rhombus. **(D)** The hypocotyl elongation rate (%) was measured by the hypocotyl length of (2.5th d to 5th d) / 5th d. The heat-sensitive *HSP101*-mutant plants (*hsp101*) were used as reference. Data were mean ± SD (*n* > 30 seedlings). The hypocotyl quantitative elongation assays were repeated for three times. Statistically significant differences between each line were represented by different letters (One-way ANVOA, Tukey-Kramer test, *P* < 0.05).
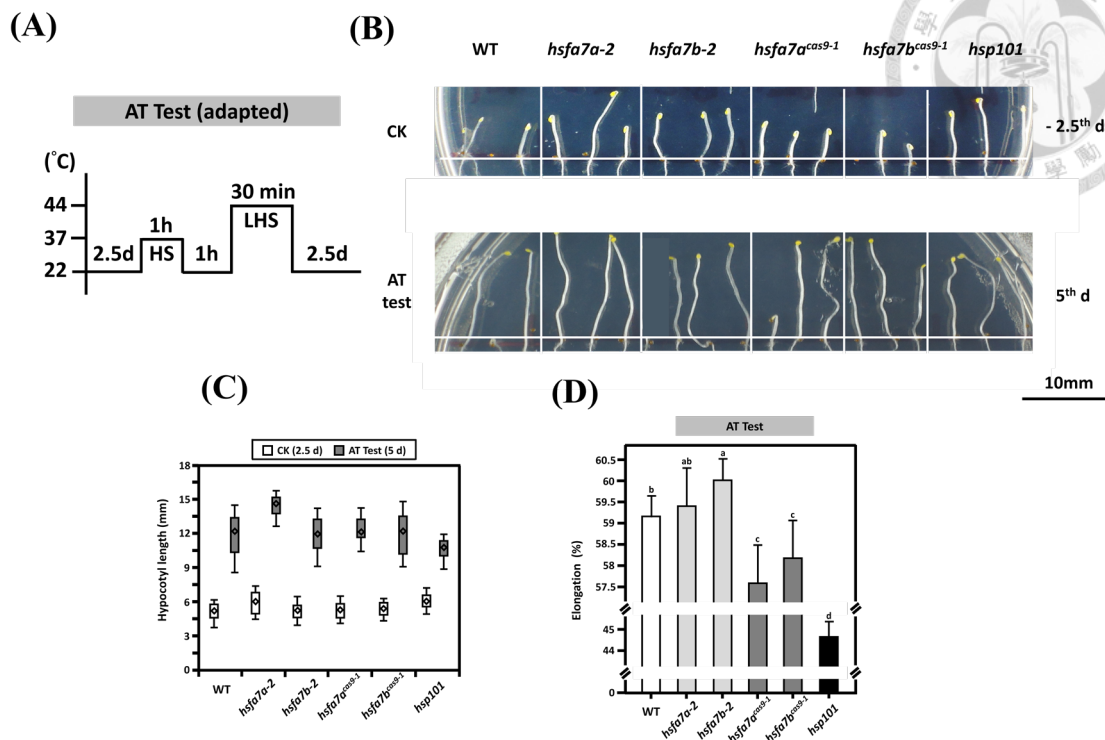
Figure 10. Phenotype of the thermo-responsive hypocotyl growth in mutant plants under acquired thermotolerance (AT) test.

(A) Schematic diagram of a AT test is shown here. (B) Photos were 2.5-d-old etiolated seedlings (control; CK) and 2.5 d later following the AT test (AT test; 5th d). (C) The hypocotyl length (mm) was shown by box plots, and mean values were represented by rhombus. (D) The hypocotyl elongation rate (%) was measured by the hypocotyl length of (2.5th d to 5th d) / 5th d. The heat-sensitive *HSP101*-mutant plants (*hsp101*) were used as reference. Data were mean ± SD ($n > 30$). The hypocotyl quantitative elongation assays were repeated for three times. Statistically significant differences between each line were represented by different letters (One-way ANVOA, Tukey-Kramer test, $P < 0.05$).
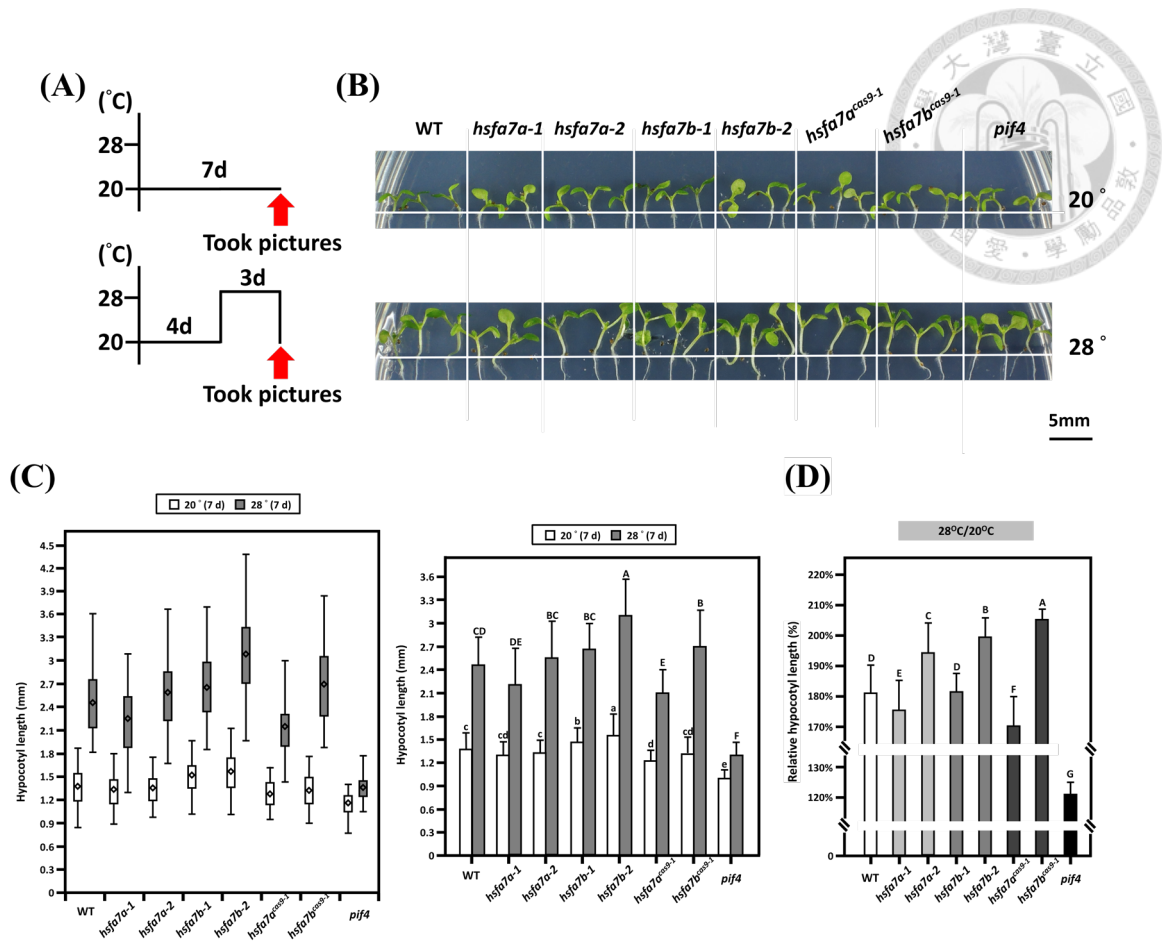
Figure 11. Thermomorphogenesis analysis for mutant plants under high temperature.

(A) Schematic diagrams of thermomorphogenesis analysis are shown here. Seedling were grown continuously at 20°C for 4 d before being transferred to 28°C for 3 d. **(B)** Phenotypes of 7-d-old seedling wild-type plants, single mutants, double mutants under 20°C for 7 d were shown in the top of panel. The bottom of panel showed that the seedlings continuously grown at 20°C for 4 d, and then being transferred to 28°C for 3 d. **(C)** The hypocotyl length (mm) of 7-d-old seedlings under 20°C or 28°C was shown by box plots, and mean values were represented by rhombus, as indicated. The statistical analysis of mean values of hypocotyl length (mm) is shown here. **(D)** The relative hypocotyl length (%) was measured by the hypocotyl length of 28°C (7th d) / 20°C (7th

92

d). Data represented the mean ± SD ($n > 30$) of three biological replicates. *pif4* was used as a reference for thermomorphogenesis analysis. Statistically significant differences between each line were represented by different uppercase and lowercase letters (One-way ANVOA, Tukey-Kramer test, $P < 0.05$).
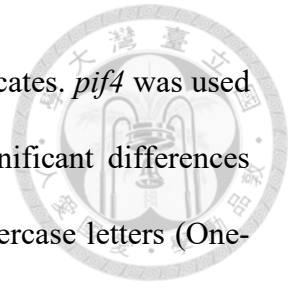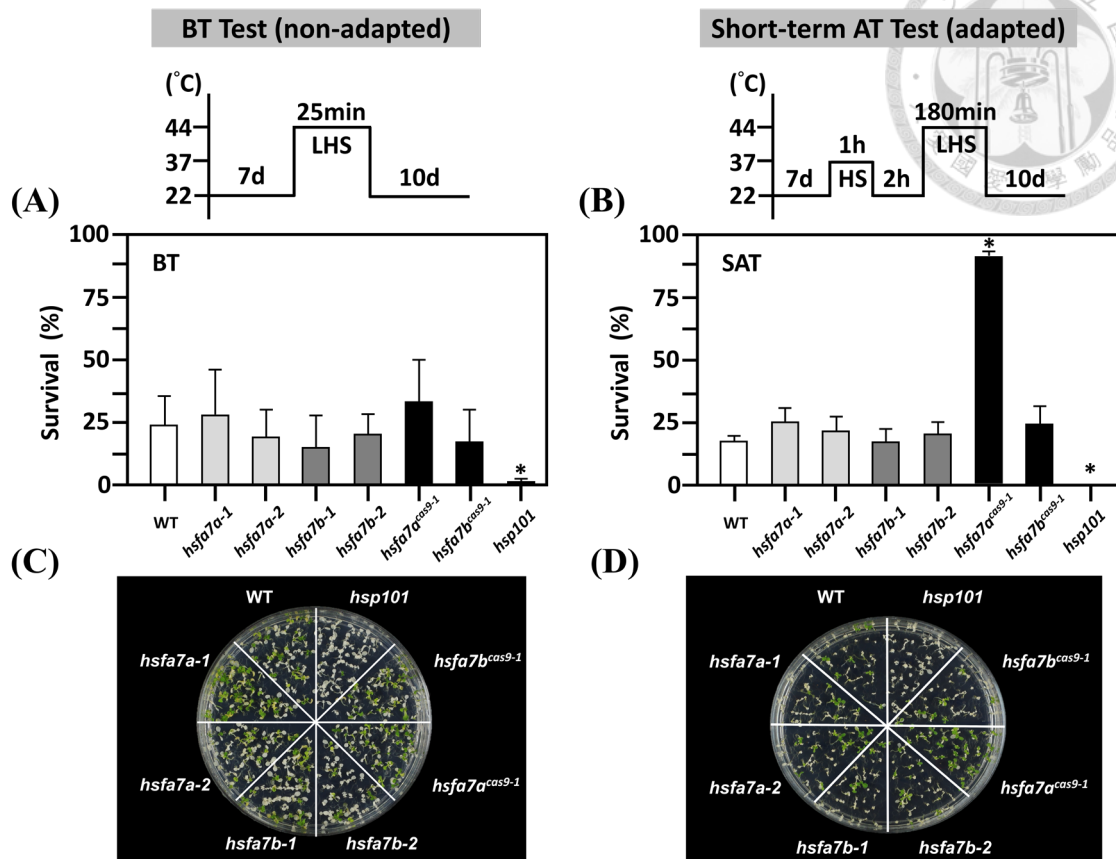
Figure 12. Thermotolerance analysis of *hsfa7a*, *hsfa7b*, and double mutant plants.

The regimes of BT and SAT tests are schematically shown on the top of each. 7-d-old seedlings were challenged with BT and SAT test, respectively. The survival rates were measured at 10 d after the HS treatment **(A and B)** and seedlings were photographed **(C and D)**. The heat-sensitive *hsp101* was used as a reference. Data were mean ± SD (*n* = 40). The thermotolerance tests were repeated for three times. The asterisk (*) indicated significance at $P < 0.05$ (Student's *t* test) compared to the WT.
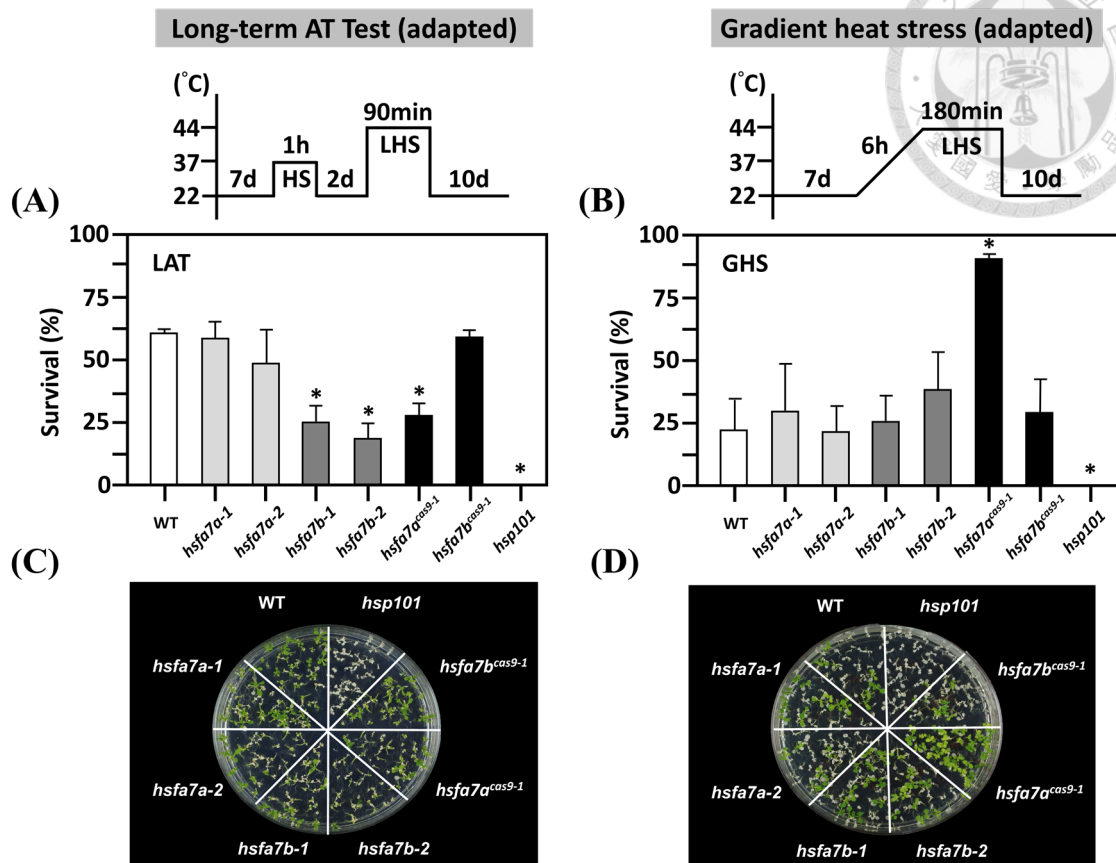
Figure 13. Thermotolerance analysis of *hsfa7a*, *hsfa7b*, and double mutant plants.

The regimes of LAT and GHS tests are schematically shown on the top of each penal. 7-d-old seedlings were challenged with LAT and GHS test, respectively. The survival rates were measured at 10 d after the HS treatment **(A and B)** and seedlings were photographed **(C and D)**. The heat-sensitive *hsp101* was used as a reference. Data were mean ± SD (*n* = 40). The thermotolerance tests were repeated for three times. The asterisk (*) indicated significance at *P* < 0.05 (Student's *t* test) compared to the WT.

95
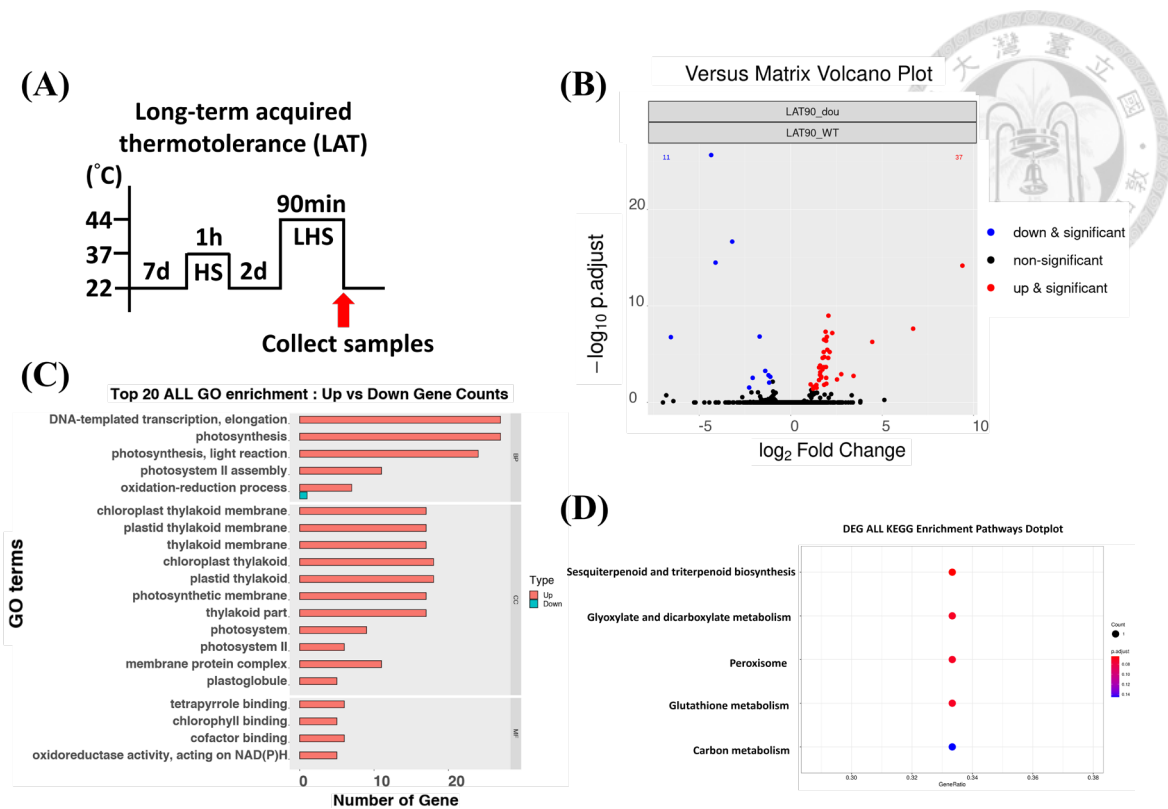
Figure 14. RNA-seq and gene ontology (GO) analysis of *hsfa7a^cas9-1* with respect to Col Arabidopsis plants after long-term acquired thermotolerance test.**

(A) The regime indicated a long-term acquired thermotolerance test. After LHS finished, samples were collected and extracted total RNA. **(B)** Volcano plot illustrated the number of differentially expressed genes (DEGs) in *hsfa7a^cas9-1* compared to WT (Col) after LAT test. **(C)** Gene ontology (GO) enrichment of up-and down-regulated genes in *hsfa7a^cas9-1* after LAT test. BP represented biology process, CC represented cellular component, and MF represented molecular function. **(D)** KEGG analysis of upregulated and downregulated pathways from RNA-seq data of *hsfa7a^cas9-1* compared to WT. Only "Sesquiterpenoid and triterpenoid biosynthesis" showed upregulation in *hsfa7a^cas9-1*, while other pathways were downregulated. Each experiment was conducted with two biological repeats.

96
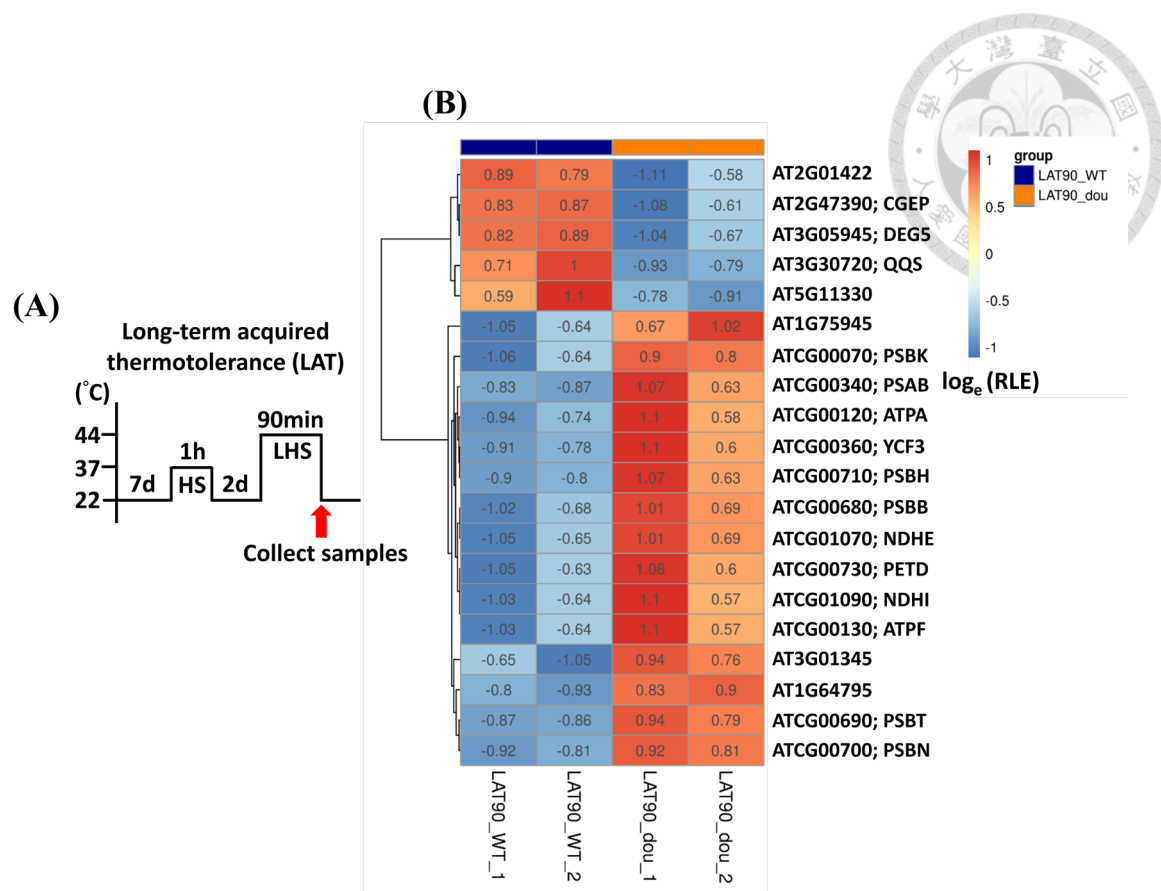
Figure 15. Heat map of top 20 significant DEGs under long-term acquired thermotolerance (LAT) test.

(A) The regime indicated a long-term acquired thermotolerance test. (B) The heat map illustrated top 20 DEGs whose fold changes ≥ 2.0 or ≤ -2.0 and *P.adjust* < 0.05 compared to the WT group. Relative log expression (RLE) method was used to normalize read counts. Color corresponded to per-gene z-score that was computed from $\log_e$ RLE (after adding 1).

97
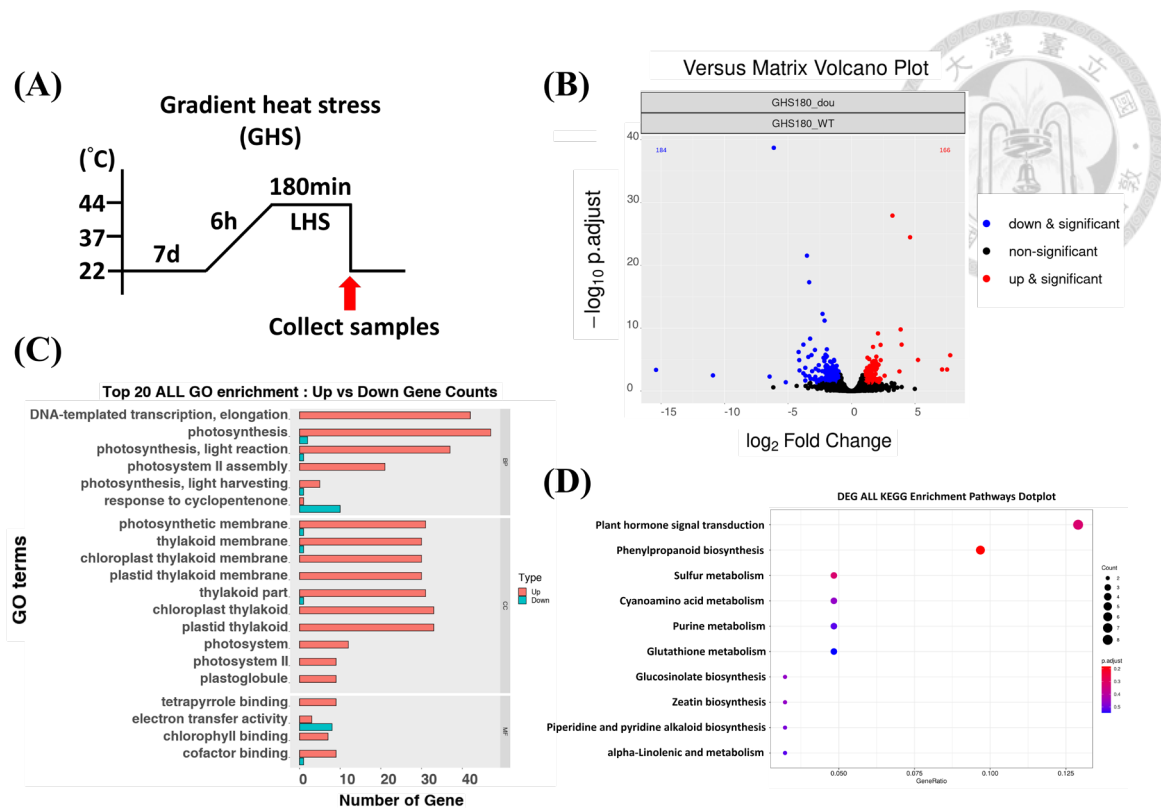
Figure 16. RNA-seq and gene ontology (GO) analysis of *hsfa7a^cas9-1^* with respect to Col Arabidopsis plants after gradient heat stress (GHS) test.

(A) The regime indicated a gradient heat stress test. After LHS finished, samples were collected and extracted total RNA. **(B)** Volcano plot illustrated the number of differentially expressed genes (DEGs) in *hsfa7a^cas9-1^* compared to WT (Col) after GHS test. **(C)** Gene ontology (GO) enrichment of upregulated and downregulated genes in *hsfa7a^cas9-1^* after GHS test. BP represented biology process, CC represented cellular component, and MF represented molecular function. **(D)** KEGG analysis of upregulated and downregulated pathways from RNA-seq data of *hsfa7a^cas9-1^* compared to WT. Each experiment was conducted with two biological repeats.

98
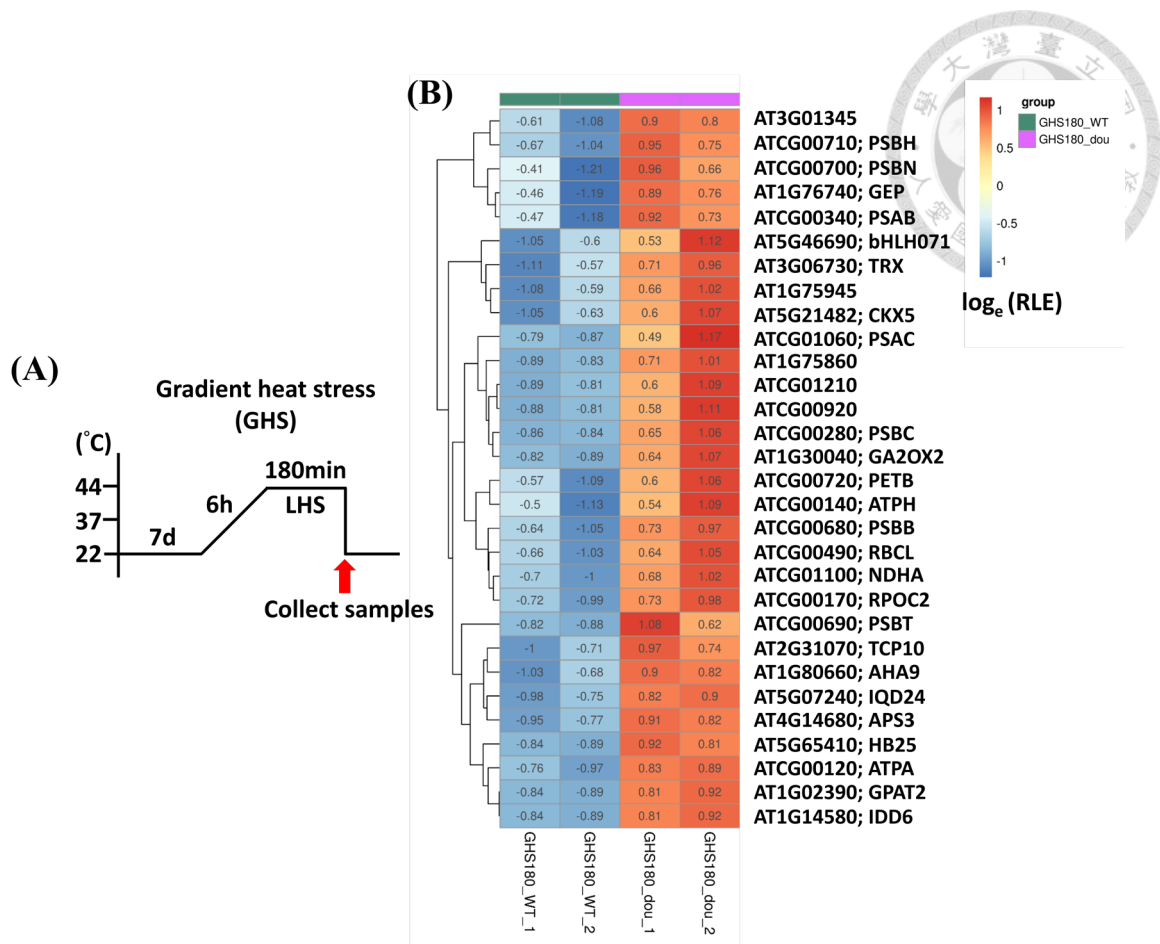
Figure 17. Heat map of top 30 significantly upregulated DEGs under gradient heat stress (GHS) test.

(A) The regime indicated a gradient heat stress (GHS) test. **(B)** The heat map illustrated top 30 upregulated DEGs whose fold changes ≥ 2.0 or ≤ -2.0 and *P.adjust* < 0.05 compared to the WT group. Relative log expression (RLE) method was used to normalize read counts. Color corresponded to per-gene z-score that was computed from $\log_e$ RLE (after adding 1).
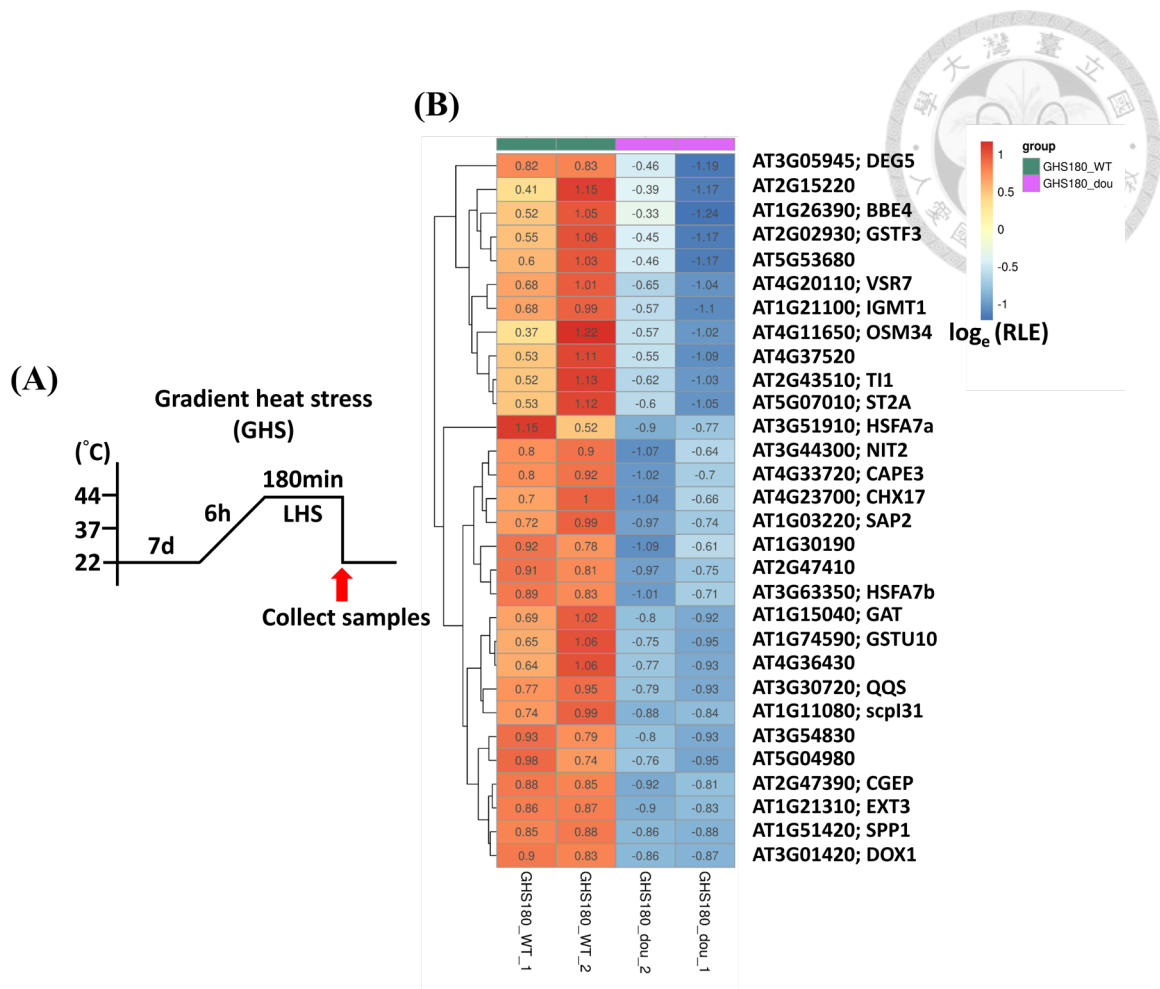
Figure 18. Heat map of top 30 significantly downregulated DEGs under gradient heat stress (GHS) test.

(A) The regime indicated a gradient heat stress (GHS) test. **(B)** The heat map illustrated top 30 downregulated DEGs whose fold changes ≥ 2.0 or ≤ -2.0 and *P.adjust* < 0.05 compared to the WT group. Relative log expression (RLE) method was used to normalize read counts. Color corresponded to per-gene z-score that was computed from $\log_e$ RLE (after adding 1).
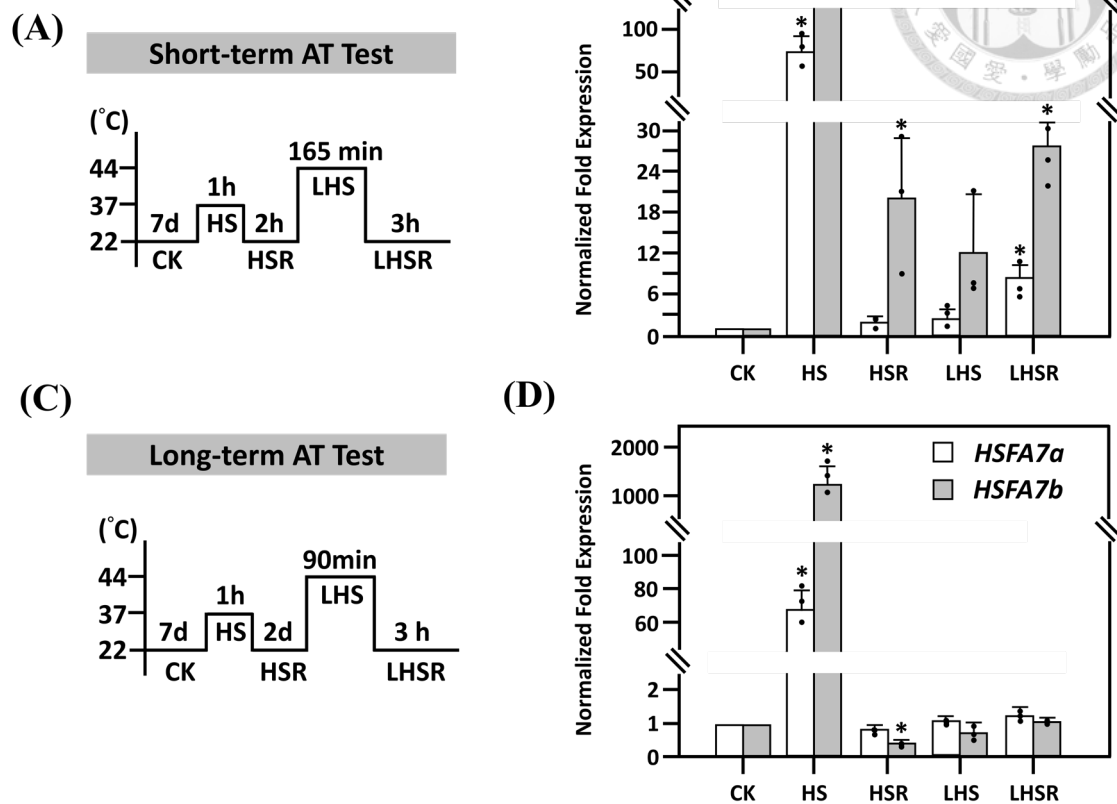
Figure 19. Expression of *HSFA7a* and *HSFA7b* in response to short-term AT test or long-term AT test.

The HS regimes are schematically shown on the left of each penal, as indicated. **(A and B)** Short-term AT test. **(C and D)** Long-term AT test. Gene expression level of *HSFA7a* and *HSFA7b* were normalized to the CK. Data were mean ± SD ($n = 3$). The qRT-PCR assays were repeated for three times. The asterisk (*****) indicated significance at $P < 0.05$ (Student's *t* test) compared to the CK. *PP2A* was used as reference gene.
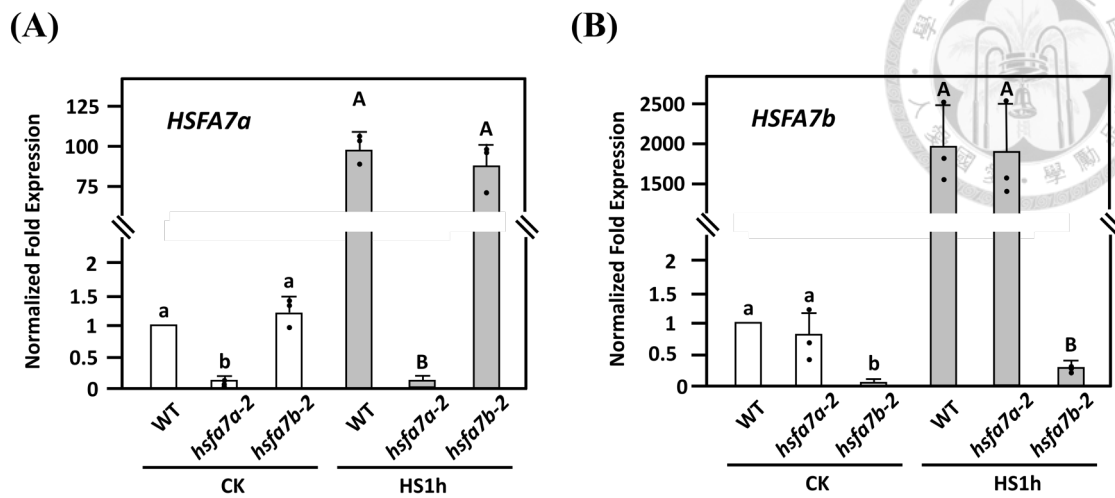
Figure 20. Expression level of *HSFA7a* and *HSFA7b* in *hsfa7a-2* and *hsfa7b-2* knockout mutant, respectively.

(A) The expression of *HSFA7a* in *hsfa7a-2* and *hsfa7b-2* knockout mutants under CK or after HS. **(B)** The expression of *HSFA7b* in *hsfa7a-2* and *hsfa7b-2* knockout mutants under CK or after HS. Data were mean ± SD ($n = 3$). The qRT-PCR assays were repeated for three times. Statistically significant differences between each line were represented by different letters (One-way ANVOA, Tukey-Kramer test, $P < 0.05$). *PP2A* was used as reference gene.
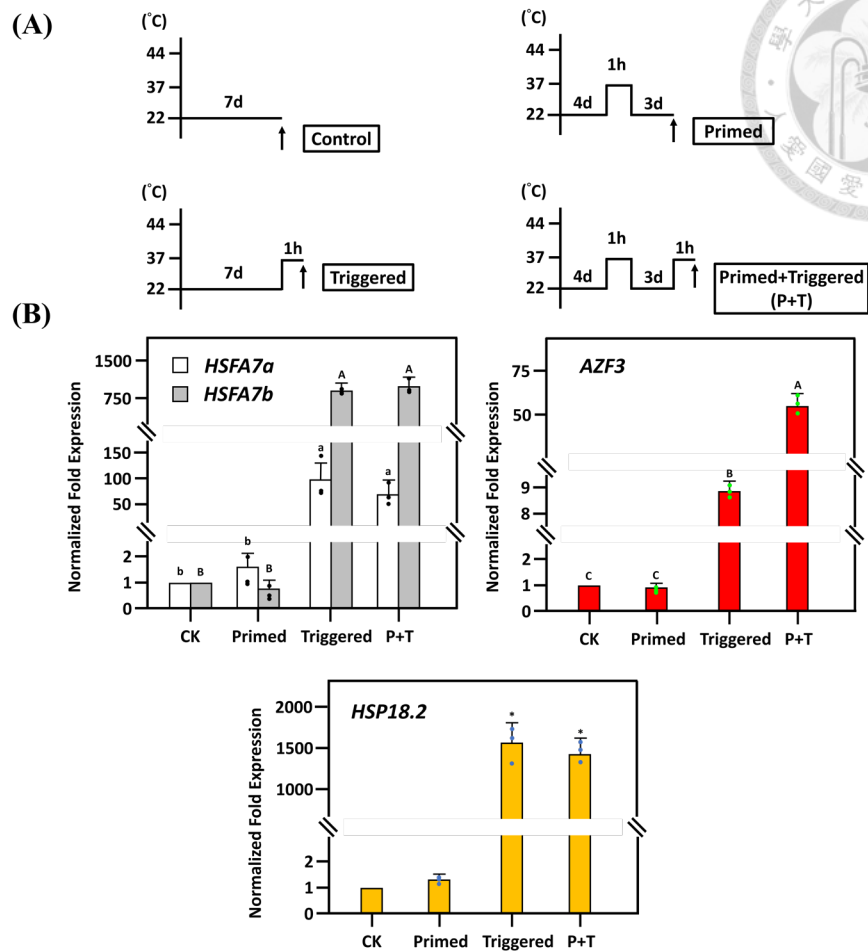
Figure 21. Transcriptional memory analysis of *HSFA7a* and *HSFA7b*.

(A) The HS regimes of control (CK), heat-primed (P), heat-triggered (T), and heat-primed and triggered (P+T) are schematically shown here. **(B)** The expression patterns of *HSFA7a*, *HSFA7b*, *AZF3*, and *HSP18.2* of CK, P, T, and P+T are shown here. Data were mean ± SD (n = 3). The qRT-PCR assays were repeated for three times. Statistically significant differences between each line were represented by different upper and lower letters (One-way ANVOA, Tukey-Kramer test, $P < 0.05$). The asterisk (*****) indicated significance at $P < 0.05$ (Student's t test) compared to the CK. *PP2A* was used as reference gene. *AZF3*, a HS-memory gene, was used as a positive control.

Supplemental Figures
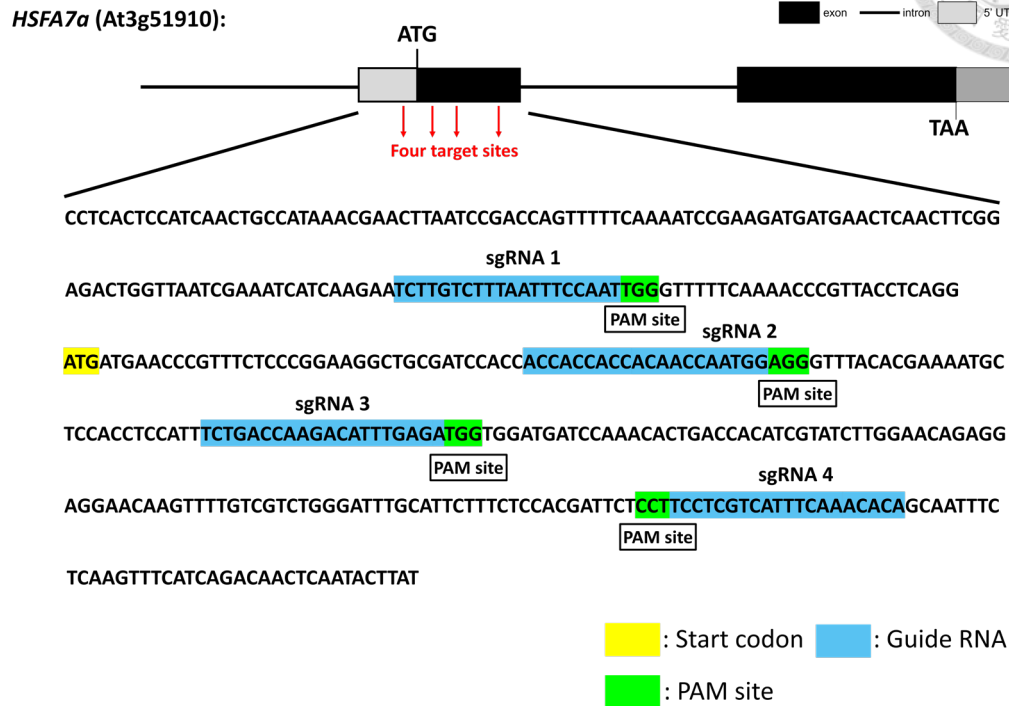
Supplemental Figure S1. Four sgRNAs responsible for generation of *hsfa7a^cas9-1*.

The figure exhibited four sgRNAs responsible for generation of *hsfa7a^cas9-1*. The sequence began at the 5'-UTR of *HSFA7a* and extended to the first exon of *HSFA7a*. The yellow box represented start codon, and blue boxes represented four sgRNAs. Green boxes represented protospacer-adjacent motif (PAM) sequences of each sgRNA.
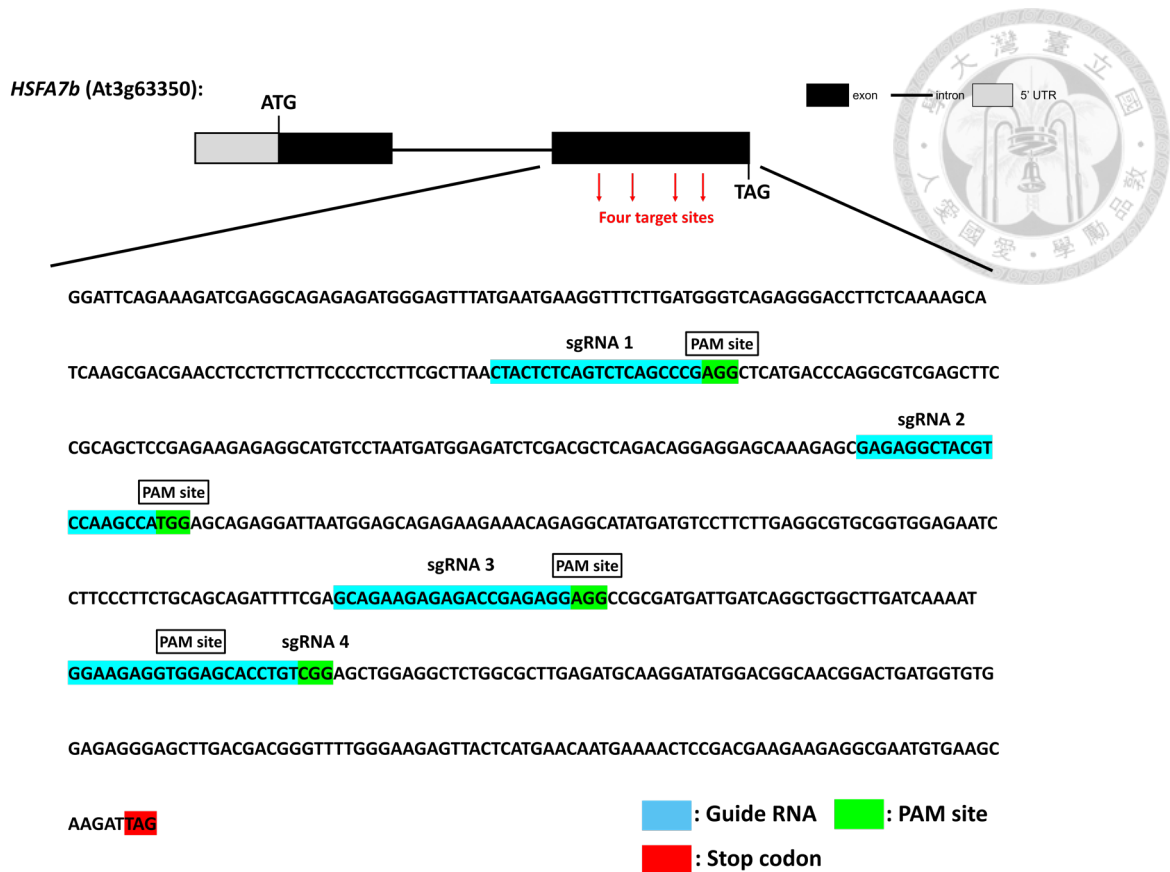
Supplemental Figure S2. Four sgRNAs responsible for generation of *hsfa7b^cas9-1*.

The figure exhibited four sgRNAs responsible for generation of *hsfa7b_cas9-1*. The sequence began at the second exon of *HSFA7b* and extended to the end of second exon. Blue boxes represented four sgRNAs, and green boxes represented protospacer-adjacent motif (PAM) sequences of each sgRNA. Red box represented stop codon of the second exon.
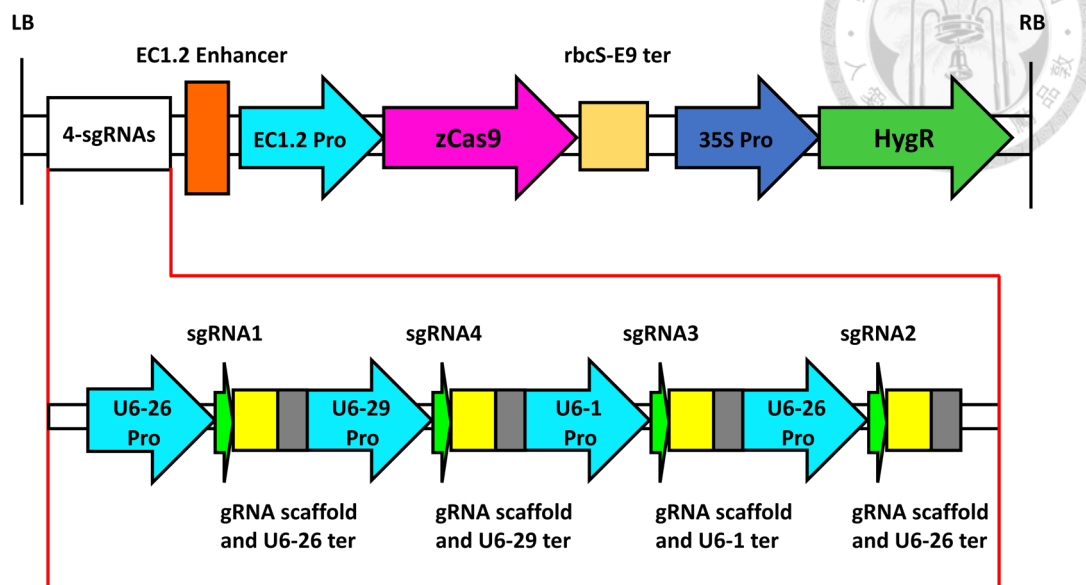
Supplemental Figure S3. The construction of pHEE401E/*HSFA7a*.

Physical maps illustrated CRISPR/Cas9 binary vector pEE401E/*HSFA7a,* harboring Cas9 driven by the egg-cell specific promoter EC1.2 Pro and four sgRNAs driven by Pol-III promoters U6-1Pro U6-26 Pro, and U6-29 Pro, respectively. RB/LB, T-DNA right/left border; EC1.2 Pro, EC1.2 promoter; rbcS-E9t, rbcS E9 terminator; zCas9, Zea mays codon-optimized Cas9; U6-1 Pro, U6-26 Pro, and U6-29 Pro, three Arabidopsis U6 gene promoter; HygR, hygromycin-resistance gene. For the sgRNAs, the green parts represented 20-bp target and the yellow part represented 76-bp sgRNA scaffold; U6-1 ter, U6-26 ter, and U6-29 ter, three terminators with downstream sequence.

106
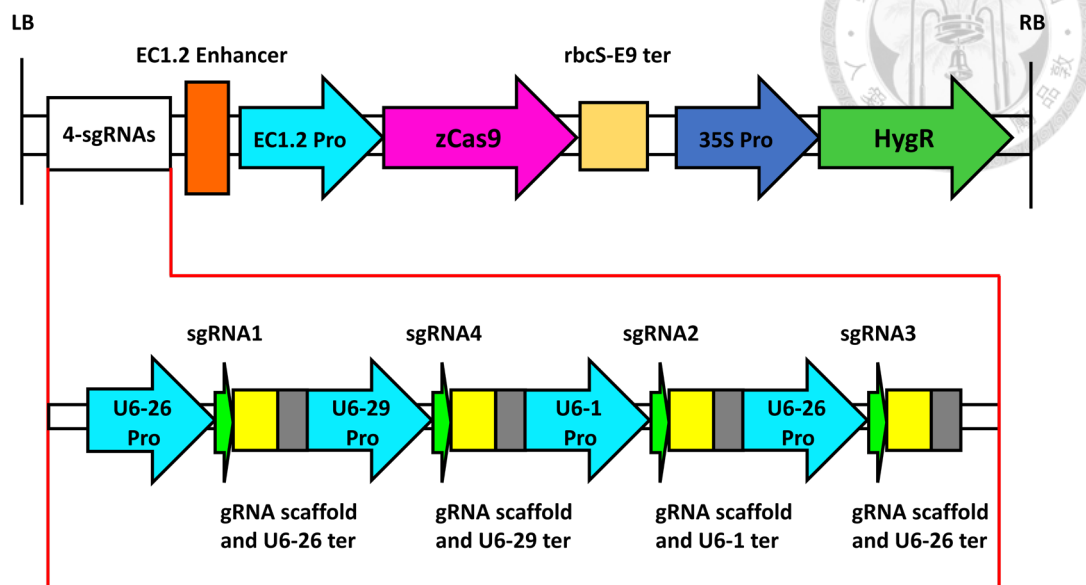
pHEE401E/*HSFA7b*:

Supplemental Figure S4. The construction of pHEE401E/*HSFA7b*.

Physical maps illustrated CRISPR/Cas9 binary vector pEE401E/*HSFA7b,* harboring Cas9 driven by the egg-cell specific promoter EC1.2 Pro and four sgRNAs driven by Pol-III promoters U6-1Pro U6-26 Pro, and U6-29 Pro, respectively. RB/LB, T-DNA right/left border; EC1.2 Pro, EC1.2 promoter; rbcS-E9t, rbcS E9 terminator; zCas9, Zea mays codon-optimized Cas9; U6-1 Pro, U6-26 Pro, and U6-29 Pro, three Arabidopsis U6 gene promoter; HygR, hygromycin-resistance gene. For the sgRNAs, the green parts represented 20-bp target and the yellow part represented 76-bp sgRNA scaffold; U6-1 ter, U6-26 ter, and U6-29 ter, three terminators with downstream sequence.
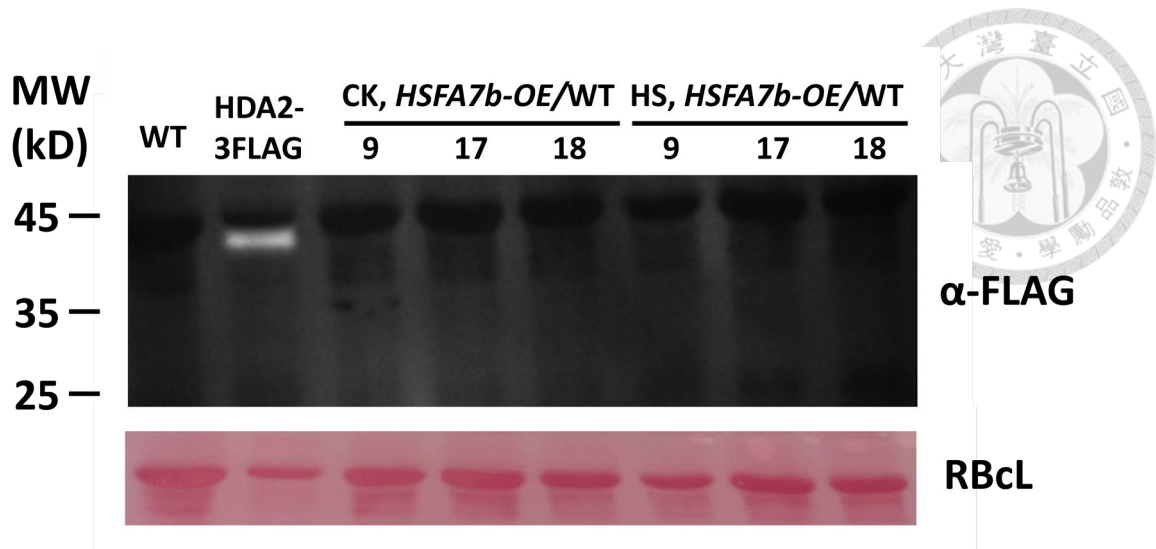
Supplemental Figure S5. Characterization of *HSFA7b*-overexpression plants.

10-d-old Col, *HSFA7b*-overexpression (*HSFA7b-OE*) lines in Col background were analyzed. Immunoblotting used α-FLAG antibody. HDA2-3FLAG (42 kD) from lab member was used for positive control. The MW of *HSFA7b*-3xFLAG is 36 kD. Ponceau S staining blots showed the ribulose bisphosphate carboxylase large subunit (RbcL) was used as an input control.

Supplemental Figure S6. Predicted *cis*-element in 2.0-kb *HSFA7a* promoter region.
The HSEs, ABREs, and DREs were characterized and annotated by using the *Arabidopsis thaliana* Plant Promoter Analysis Navigator (PlantPAN4.0; http://plantpan.itps.ncku.edu.tw/plantpan4/index.html), a database for transcription regulatory networks (Chow et al., 2016). The start codons (ATG) were highlighted in bold letters.

Supplemental Figure S7. Predicted *cis*-element in 2.0-kb *HSFA7b* promoter region.

The HSEs, ABREs, and DREs were characterized and annotated by using the *Arabidopsis thaliana* Plant Promoter Analysis Navigator (PlantPAN4.0; http://plantpan.itps.ncku.edu.tw/plantpan4/index.html), a database for transcription regulatory networks (Chow et al., 2016). The start codons (ATG) were highlighted in bold letters.
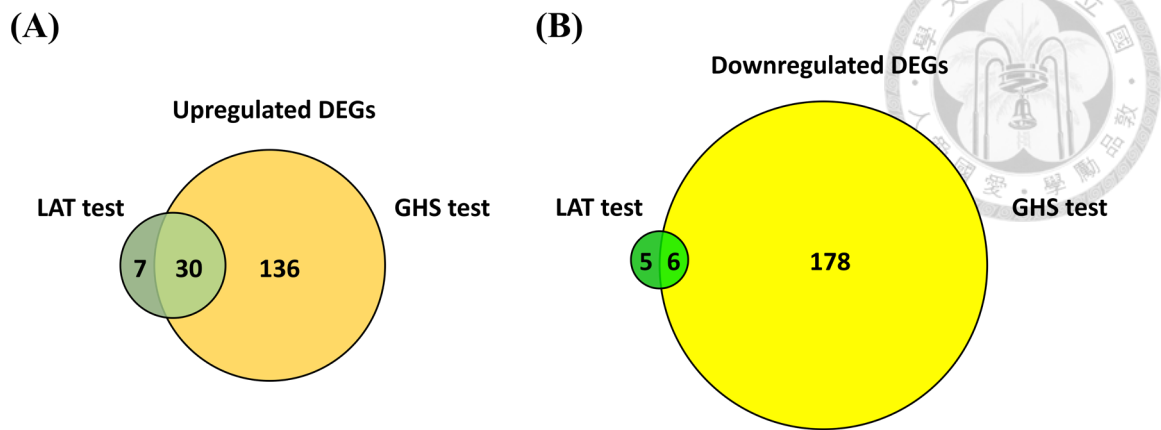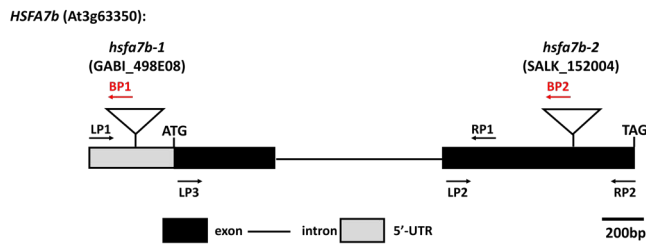
Supplemental Figure S8. The Vann diagram of DEGs in *hsfa7a^cas9-1* after LAT and GHS tests. (A) Vann diagram exhibited the upregulated DEGs in *hsfa7a^cas9-1* after LAT and GHS test. Among all the upregulated DEGs, 30 DEGs were overlapped in two datasets. **(B)** Vann diagram exhibited the downregulated DEGs in *hsfa7a^cas9-1* after LAT and GHS test. Among all the downregulated DEGs, only 6 DEGs were overlapped in two datasets.
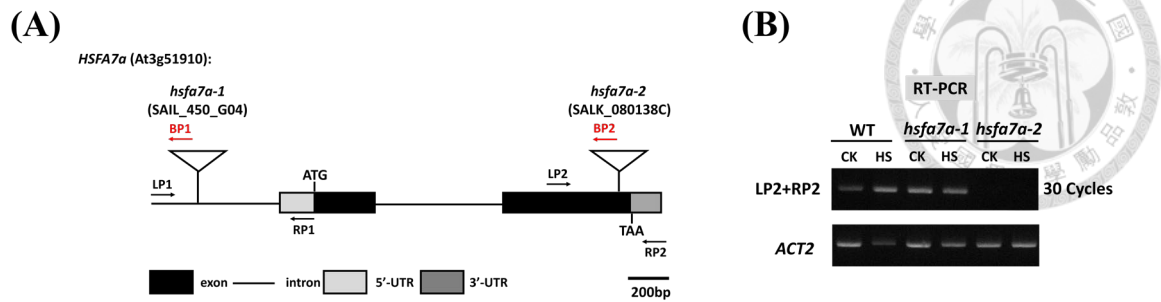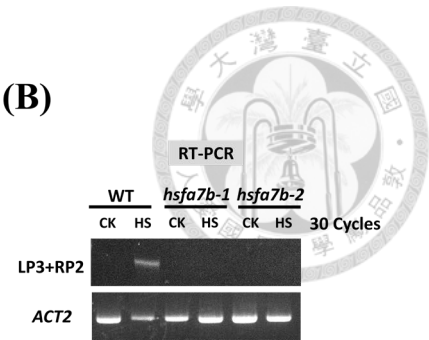
Supplemental Figure S9. The RT-PCR results of *HSFA7a* expression in *hsfa7a-1* and *hsfa7a-2*. (A) The inverted triangle represented the T-DNA insertion site in *hsfa7a-1* (SAIL_450_G04) and *hsfa7a-2* (SALK_080138C) lines. ATG and TAG showed the position of the start and stop codons, respectively. Arrows indicated the positions of the specific primers designed for RT-PCR and genotyping. **(B)** The expression levels of *HSFA7a* in *hsfa7a-1* and *hsfa7a-2* were analyzed by semiquantitative RT-PCR, respectively.

(A)

HSFA7b (At3g63350):

hsfa7b-1
(GABI_498E08)

BP1

LP1 ATG

LP3

exon — intron 5'-UTR

hsfa7b-2
(SALK_152004)

BP2

RP1 TAG

LP2 RP2

200bp

(B)

RT-PCR
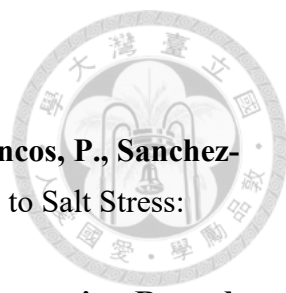
WT   hsfa7b-1 hsfa7b-2
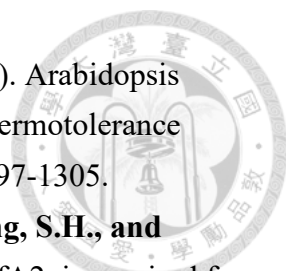
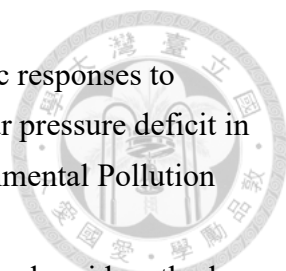CK HS CK HS CK HS   30 Cycles

LP3+RP2

ACT2

Supplemental Figure S10. The RT-PCR results of *HSFA7b* expression in *hsfa7b-1* and *hsfa7b-2*. (A) The inverted triangle represented the T-DNA insertion site in *hsfa7b-1* (GABI_498E08) and *hsfa7b-2* (SALK_152004) lines. ATG and TAG showed the position of the start and stop codons, respectively. Arrows indicated the positions of the specific primers designed for RT-PCR and genotyping. **(B)** The expression levels of *HSFA7b* in *hsfa7b-1* and *hsfa7b-2* were analyzed by semiquantitative RT-PCR, respectively.
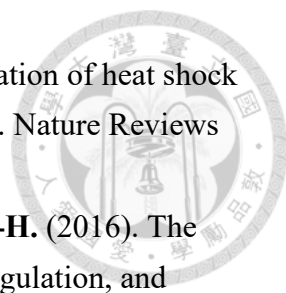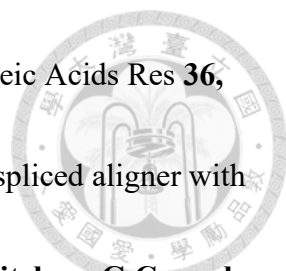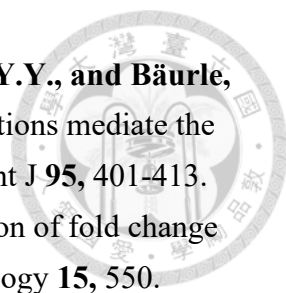
113

References

Acosta-Motos, J.R., Ortuño, M.F., Bernal-Vicente, A., Diaz-Vivancos, P., Sanchez-Blanco, M.J., and Hernandez, J.A. (2017). Plant Responses to Salt Stress: Adaptive Mechanisms. Agronomy **7,** 18.

Allakhverdiev, S.I., Kreslavski, V.D., Klimov, V.V., Los, D.A., Carpentier, R., and Mohanty, P. (2008). Heat stress: an overview of molecular responses in photosynthesis. Photosynthesis research **98,** 541-550.

Anders, S., McCarthy, D.J., Chen, Y., Okoniewski, M., Smyth, G.K., Huber, W., and Robinson, M.D. (2013). Count-based differential expression analysis of RNA sequencing data using R and Bioconductor. Nat Protoc **8,** 1765-1786.

Andrási, N., Pettkó-Szandtner, A., and Szabados, L. (2020). Diversity of plant heat shock factors: regulation, interactions, and functions. Journal of Experimental Botany **72,** 1558-1575.

Apse, M.P., Aharon, G.S., Snedden, W.A., and Blumwald, E. (1999). Salt tolerance conferred by overexpression of a vacuolar Na+/H+ antiport in Arabidopsis. Science **285,** 1256-1258.

Baniwal, S.K., Chan, K.Y., Scharf, K.-D., and Nover, L. (2007). Role of heat stress transcription factor HsfA5 as specific repressor of HsfA4. Journal of Biological Chemistry **282,** 3605-3613.

Begum, T., Reuter, R., and Schöffl, F. (2013). Overexpression of AtHsfB4 induces specific effects on root development of Arabidopsis. Mech Dev **130,** 54-60.

Bhuiyan, N.H., Rowland, E., Friso, G., Ponnala, L., Michel, E.J.S., and van Wijk, K.J. (2020). Autocatalytic Processing and Substrate Specificity of Arabidopsis Chloroplast Glutamyl Peptidase. Plant Physiol **184,** 110-129.

Blum, A. (2005). Drought resistance, water-use efficiency, and yield potential—are they compatible, dissonant, or mutually exclusive? Australian Journal of Agricultural Research **56,** 1159-1168.

Bolger, A.M., Lohse, M., and Usadel, B. (2014). Trimmomatic: a flexible trimmer for Illumina sequence data. Bioinformatics **30,** 2114-2120.

Bonetta, D., and McCourt, P. (1998). Genetic analysis of ABA signal transduction pathways. Trends in Plant Science **3,** 231-235.

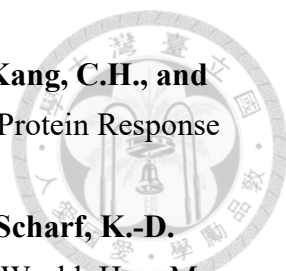**Bray, E.A.** (1997). Plant responses to water deficit. Trends in Plant Science **2,** 48-54.

Charng, Y.Y., Liu, H.C., Liu, N.Y., Hsu, F.C., and Ko, S.S. (2006). Arabidopsis Hsa32, a novel heat shock protein, is essential for acquired thermotolerance during long recovery after acclimation. Plant Physiol **140,** 1297-1305.

Charng, Y.Y., Liu, H.C., Liu, N.Y., Chi, W.T., Wang, C.N., Chang, S.H., and Wang, T.T. (2007). A heat-inducible transcription factor, HsfA2, is required for extension of acquired thermotolerance in Arabidopsis. Plant Physiol **143,** 251-262.

Cheeseman, J.M. (1988). Mechanisms of Salinity Tolerance in Plants Plant Physiology **87,** 547-550.

Chow, C.N., Zheng, H.Q., Wu, N.Y., Chien, C.H., Huang, H.D., Lee, T.Y., Chiang-Hsieh, Y.F., Hou, P.F., Yang, T.Y., and Chang, W.C. (2016). PlantPAN 2.0: an update of plant promoter analysis navigator for reconstructing transcriptional regulatory networks in plants. Nucleic Acids Res **44,** D1154-1160.

Clos, J., Westwood, J.T., Becker, P.B., Wilson, S., Lambert, K., and Wu, C. (1990). Molecular cloning and expression of a hexameric Drosophila heat shock factor subject to negative regulation. Cell **63,** 1085-1097.

Clough, S.J., and Bent, A.F. (1998). Floral dip: a simplified method for Agrobacterium-mediated transformation of Arabidopsis thaliana. The plant journal **16,** 735-743.

Cortijo, S., Charoensawan, V., Brestovitsky, A., Buning, R., Ravarani, C., Rhodes, D., van Noort, J., Jaeger, K.E., and Wigge, P.A. (2017). Transcriptional regulation of the ambient temperature response by H2A. Z nucleosomes and HSF1 transcription factors in Arabidopsis. Molecular plant **10,** 1258-1273.

Czechowski, T., Stitt, M., Altmann, T., Udvardi, M.K., and Scheible, W.R. (2005). Genome-wide identification and testing of superior reference genes for transcript normalization in Arabidopsis. Plant Physiol **139,** 5-17.

Deinlein, U., Stephan, A.B., Horie, T., Luo, W., Xu, G., and Schroeder, J.I. (2014). Plant salt-tolerance mechanisms. Trends in Plant Science **19,** 371-379.

Demidchik, V. (2015). Mechanisms of oxidative stress in plants: from classical chemistry to cell biology. Environmental and experimental botany **109,** 212-228.

Ding, Y., Fromm, M., and Avramova, Z. (2012). Multiple exposures to drought 'train' transcriptional responses in Arabidopsis. Nat Commun **3,** 740.

Ding, Y., Shi, Y., and Yang, S. (2020). Molecular Regulation of Plant Responses to Environmental Temperatures. Mol Plant **13,** 544-564.
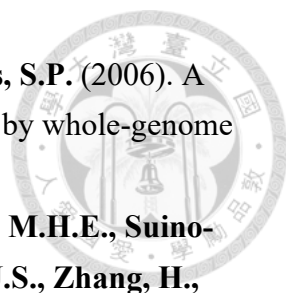
Eamus, D., Duff, G.A., and Berryman, C.A. (1995). Photosynthetic responses to temperature, light flux-density, CO_2 concentration and vapour pressure deficit in Eucalyptus tetrodonta grown under CO_2 enrichment. Environmental Pollution **90,** 41-49.

Edwards, K., Johnstone, C., and Thompson, C. (1991). A simple and rapid method for the preparation of plant genomic DNA for PCR analysis. Nucleic Acids Research **19,** 1349-1349.

Engler, C., Kandzia, R., and Marillonnet, S. (2008). A One Pot, One Step, Precision Cloning Method with High Throughput Capability. PLOS ONE **3,** e3647.

Ewels, P., Magnusson, M., Lundin, S., and Käller, M. (2016). MultiQC: summarize analysis results for multiple tools and samples in a single report. Bioinformatics **32,** 3047-3048.

Fahad, S., Bajwa, A.A., Nazir, U., Anjum, S.A., Farooq, A., Zohaib, A., Sadia, S., Nasim, W., Adkins, S., Saud, S., Ihsan, M.Z., Alharby, H., Wu, C., Wang, D., and Huang, J. (2017). Crop Production under Drought and Heat Stress: Plant Responses and Management Options. Front Plant Sci **8,** 1147.

Fang, Y., and Xiong, L. (2015). General mechanisms of drought response and their application in drought resistance improvement in plants. Cellular and molecular life sciences **72,** 673-689.

Franklin, K.A., Lee, S.H., Patel, D., Kumar, S.V., Spartz, A.K., Gu, C., Ye, S., Yu, P., Breen, G., Cohen, J.D., Wigge, P.A., and Gray, W.M. (2011). Phytochrome-interacting factor 4 (PIF4) regulates auxin biosynthesis at high temperature. Proc Natl Acad Sci U S A **108,** 20231-20235.

Friedrich, T., Oberkofler, V., Trindade, I., Altmann, S., Brzezinka, K., Lamke, J., Gorka, M., Kappel, C., Sokolowska, E., Skirycz, A., Graf, A., and Baurle, I. (2021). Heteromeric HSFA2/HSFA3 complexes drive transcriptional memory after heat stress in Arabidopsis. Nat Commun **12,** 3426.

Giesguth, M., Sahm, A., Simon, S., and Dietz, K.-J. (2015). Redox-dependent translocation of the heat shock transcription factor AtHSFA8 from the cytosol to the nucleus in Arabidopsis thaliana. FEBS letters **589,** 718-725.

Goldenberg, E.P. (1988). Mathematics, metaphors, and human factors: Mathematical, technical, and pedagogical challenges in the educational use of graphical representation of functions. The Journal of Mathematical Behavior.

Golldack, D., Li, C., Mohan, H., and Probst, N. (2014). Tolerance to drought and salt stress in plants: Unraveling the signaling networks. Frontiers in Plant Science **5.**
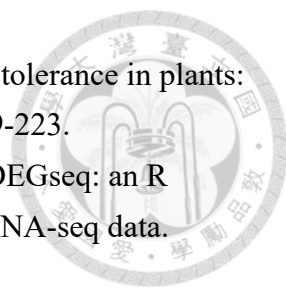
Gomez-Pastor, R., Burchfiel, E.T., and Thiele, D.J. (2018). Regulation of heat shock transcription factors and their roles in physiology and disease. Nature Reviews Molecular Cell Biology **19,** 4-19.

Guo, M., Liu, J.-H., Ma, X., Luo, D.-X., Gong, Z.-H., and Lu, M.-H. (2016). The Plant Heat Stress Transcription Factors (HSFs): Structure, Regulation, and Function in Response to Abiotic Stresses. Frontiers in Plant Science **7.**

Hasanuzzaman, M., Nahar, K., Alam, M.M., Roychowdhury, R., and Fujita, M. (2013). Physiological, biochemical, and molecular mechanisms of heat stress tolerance in plants. Int J Mol Sci **14,** 9643-9684.

Hayes, S., Schachtschabel, J., Mishkind, M., Munnik, T., and Arisz, S.A. (2021). Hot topic: Thermosensing in plants. Plant Cell Environ **44,** 2018-2033.

Howell, S.H. (2021). Evolution of the unfolded protein response in plants. Plant Cell Environ **44,** 2625-2635.

Hu, S., Ding, Y., and Zhu, C. (2020). Sensitivity and Responses of Chloroplasts to Heat Stress in Plants. Frontiers in Plant Science **11.**

Huang, G.-T., Ma, S.-L., Bai, L.-P., Zhang, L., Ma, H., Jia, P., Liu, J., Zhong, M., and Guo, Z.-F. (2012). Signal transduction during cold, salt, and drought stresses in plants. Molecular Biology Reports **39,** 969-987.

Huang, Y.C., Niu, C.Y., Yang, C.R., and Jinn, T.L. (2016). The Heat Stress Factor HSFA6b Connects ABA Signaling and ABA-Mediated Heat Responses. Plant Physiol **172,** 1182-1199.

Hwang, S.M., Kim, D.W., Woo, M.S., Jeong, H.S., Son, Y.S., Akhter, S., Choi, G.J., and Bahk, J.D. (2014). Functional characterization of A rabidopsis HsfA6a as a heat-shock transcription factor under high salinity and dehydration conditions. Plant, cell & environment **37,** 1202-1222.

Ikeda, M., Mitsuda, N., and Ohme-Takagi, M. (2011). Arabidopsis HsfB1 and HsfB2b Act as Repressors of the Expression of Heat-Inducible Hsfs But Positively Regulate the Acquired Thermotolerance   Plant Physiology **157,** 1243-1254.

Kanehisa, M., Sato, Y., Furumichi, M., Morishima, K., and Tanabe, M. (2019). New approach for understanding genome variations in KEGG. Nucleic Acids Res **47,** D590-d595.

Kanehisa, M., Araki, M., Goto, S., Hattori, M., Hirakawa, M., Itoh, M., Katayama, T., Kawashima, S., Okuda, S., Tokimatsu, T., and Yamanishi, Y. (2008).

117

KEGG for linking genomes to life and the environment. Nucleic Acids Res **36,** D480-484.

Kim, D., Langmead, B., and Salzberg, S.L. (2015). HISAT: a fast spliced aligner with low memory requirements. Nature Methods **12,** 357-360.

Koini, M.A., Alvey, L., Allen, T., Tilley, C.A., Harberd, N.P., Whitelam, G.C., and Franklin, K.A. (2009). High temperature-mediated adaptations in plant architecture require the bHLH transcription factor PIF4. Curr Biol **19,** 408-413.

Kotak, S., Vierling, E., Bäumlein, H., and Koskull-Döring, P.v. (2007). A Novel Transcriptional Cascade Regulating Expression of Heat Stress Proteins during Seed Development of Arabidopsis. The Plant Cell **19,** 182-195.

Kumar, S.V., and Wigge, P.A. (2010). H2A. Z-containing nucleosomes mediate the thermosensory response in Arabidopsis. Cell **140,** 136-147.

Lamke, J., Brzezinka, K., Altmann, S., and Baurle, I. (2016). A hit-and-run heat shock factor governs sustained histone methylation and transcriptional stress memory. EMBO J **35,** 162-175.

Larkindale, J., Hall, J.D., Knight, M.R., and Vierling, E. (2005). Heat stress phenotypes of Arabidopsis mutants implicate multiple signaling pathways in the acquisition of thermotolerance. Plant physiology **138,** 882-897.

Li, L., Foster, C.M., Gan, Q., Nettleton, D., James, M.G., Myers, A.M., and Wurtele, E.S. (2009). Identification of the novel protein QQS as a component of the starch metabolic network in Arabidopsis leaves. Plant J **58,** 485-498.

Liao, Y., Smyth, G.K., and Shi, W. (2014). featureCounts: an efficient general purpose program for assigning sequence reads to genomic features. Bioinformatics **30,** 923-930.

Lin, K.F., Tsai, M.Y., Lu, C.A., Wu, S.J., and Yeh, C.H. (2018). The roles of Arabidopsis HSFA2, HSFA4a, and HSFA7a in the heat shock response and cytosolic protein response. Bot Stud **59,** 15.

Liu, H., Able, A.J., and Able, J.A. (2022). Priming crops for the future: rewiring stress memory. Trends in Plant Science **27,** 699-716.

Liu, H.C., and Charng, Y.Y. (2013). Common and distinct functions of Arabidopsis class A1 and A2 heat shock factors in diverse abiotic stress responses and development. Plant Physiol **163,** 276-290.

Liu, H.C., Liao, H.T., and Charng, Y.Y. (2011). The role of class A1 heat shock factors (HSFA1s) in response to heat and other stresses in Arabidopsis. Plant Cell Environ **34,** 738-751.

118

Liu, H.C., Lämke, J., Lin, S.Y., Hung, M.J., Liu, K.M., Charng, Y.Y., and Bäurle, I. (2018). Distinct heat shock factors and chromatin modifications mediate the organ-autonomous transcriptional memory of heat stress. Plant J **95,** 401-413.

Love, M.I., Huber, W., and Anders, S. (2014). Moderated estimation of fold change and dispersion for RNA-seq data with DESeq2. Genome Biology **15,** 550.

Ma, X., Zhang, Q., Zhu, Q., Liu, W., Chen, Y., Qiu, R., Wang, B., Yang, Z., Li, H., Lin, Y., Xie, Y., Shen, R., Chen, S., Wang, Z., Chen, Y., Guo, J., Chen, L., Zhao, X., Dong, Z., and Liu, Y.-G. (2015). A Robust CRISPR/Cas9 System for Convenient, High-Efficiency Multiplex Genome Editing in Monocot and Dicot Plants. Molecular Plant **8,** 1274-1284.

Manghwar, H., and Li, J. (2022). Endoplasmic Reticulum Stress and Unfolded Protein Response Signaling in Plants. Int J Mol Sci **23**.

Mesihovic, A., Ullrich, S., Rosenkranz, R.R.E., Gebhardt, P., Bublak, D., Eich, H., Weber, D., Berberich, T., Scharf, K.-D., Schleiff, E., and Fragkostefanakis, S. (2022). HsfA7 coordinates the transition from mild to strong heat stress response by controlling the activity of the master regulator HsfA1a in tomato. Cell Reports **38,** 110224.

Misra, S., Wu, Y., Venkataraman, G., Sopory, S.K., and Tuteja, N. (2007). Heterotrimeric G-protein complex and G-protein-coupled receptor from a legume (Pisum sativum): role in salinity and heat stress and cross-talk with phospholipase   C. The Plant Journal **51,** 656-669.

Mittler, R., Finka, A., and Goloubinoff, P. (2012). How do plants feel the heat? Trends in Biochemical Sciences **37,** 118-125.

Msanne, J., Lin, J., Stone, J.M., and Awada, T. (2011). Characterization of abiotic stress-responsive Arabidopsis thaliana RD29A and RD29B genes and evaluation of transgenes. Planta **234,** 97-107.

Munemasa, S., Hauser, F., Park, J., Waadt, R., Brandt, B., and Schroeder, J.I. (2015). Mechanisms of abscisic acid-mediated control of stomatal aperture. Current Opinion in Plant Biology **28,** 154-162.

Narusaka, Y., Nakashima, K., Shinwari, Z.K., Sakuma, Y., Furihata, T., Abe, H., Narusaka, M., Shinozaki, K., and Yamaguchi-Shinozaki, K. (2003). Interaction between two cis-acting elements, ABRE and DRE, in ABA-dependent expression of Arabidopsis rd29A gene in response to dehydration and high-salinity stresses. Plant J **34,** 137-148.

Nawkar, G.M., Lee, E.S., Shelake, R.M., Park, J.H., Ryu, S.W., Kang, C.H., and Lee, S.Y. (2018). Activation of the Transducers of Unfolded Protein Response in Plants. Front Plant Sci **9,** 214.

Nover, L., Bharti, K., Döring, P., Mishra, S.K., Ganguli, A., and Scharf, K.-D. (2001). Arabidopsis and the Heat Stress Transcription Factor World: How Many Heat Stress Transcription Factors Do We Need? Cell stress & chaperones **6,** 177.

Ohama, N., Sato, H., Shinozaki, K., and Yamaguchi-Shinozaki, K. (2017). Transcriptional Regulatory Network of Plant Heat Stress Response. Trends Plant Sci **22,** 53-65.

Ohama, N., Kusakabe, K., Mizoi, J., Zhao, H., Kidokoro, S., Koizumi, S., Takahashi, F., Ishida, T., Yanagisawa, S., Shinozaki, K., and Yamaguchi-Shinozaki, K. (2015). The Transcriptional Cascade in the Heat Stress Response of Arabidopsis Is Strictly Regulated at the Level of Transcription Factor Expression. The Plant Cell **28,** 181-201.

Pick, T., Jaskiewicz, M., Peterhänsel, C., and Conrath, U. (2012). Heat Shock Factor HsfB1 Primes Gene Transcription and Systemic Acquired Resistance in Arabidopsis   Plant Physiology **159,** 52-55.

Quint, M., Delker, C., Franklin, K.A., Wigge, P.A., Halliday, K.J., and van Zanten, M. (2016). Molecular and genetic control of plant thermomorphogenesis. Nat Plants **2,** 15190.

Sakuma, Y., Maruyama, K., Qin, F., Osakabe, Y., Shinozaki, K., and Yamaguchi-Shinozaki, K. (2006). Dual function of an Arabidopsis transcription factor DREB2A in water-stress-responsive and heat-stress-responsive gene expression. Proc Natl Acad Sci U S A **103,** 18822-18827.

Salvucci, M.E., and Crafts-Brandner, S.J. (2004). Inhibition of photosynthesis by heat stress: the activation state of Rubisco as a limiting factor in photosynthesis. Physiol Plant **120,** 179-186.

Savchenko, G., Klyuchareva, E., Abramchik, L., and Serdyuchenko, E. (2002). Effect of periodic heat shock on the inner membrane system of etioplasts. Russian journal of plant physiology **49,** 349-359.

Schramm, F., Ganguli, A., Kiehlmann, E., Englich, G., Walch, D., and von Koskull-Doring, P. (2006). The heat stress transcription factor HsfA2 serves as a regulatory amplifier of a subset of genes in the heat stress response in Arabidopsis. Plant Mol Biol **60,** 759-772.

Singer, T., Fan, Y., Chang, H.S., Zhu, T., Hazen, S.P., and Briggs, S.P. (2006). A high-resolution map of Arabidopsis recombinant inbred lines by whole-genome exon array hybridization. PLoS Genet **2,** e144.

Soon, F.-F., Ng, L.-M., Zhou, X.E., West, G.M., Kovach, A., Tan, M.H.E., Suino-Powell, K.M., He, Y., Xu, Y., Chalmers, M.J., Brunzelle, J.S., Zhang, H., Yang, H., Jiang, H., Li, J., Yong, E.-L., Cutler, S., Zhu, J.-K., Griffin, P.R., Melcher, K., and Xu, H.E. (2012). Molecular Mimicry Regulates ABA Signaling by SnRK2 Kinases and PP2C Phosphatases. Science **335,** 85-88.

Sorger, P.K., and Pelham, H.R. (1988). Yeast heat shock factor is an essential DNA-binding protein that exhibits temperature-dependent phosphorylation. Cell **54,** 855-864.

Stavang, J.A., Gallego-Bartolomé, J., Gómez, M.D., Yoshida, S., Asami, T., Olsen, J.E., García-Martínez, J.L., Alabadí, D., and Blázquez, M.A. (2009). Hormonal regulation of temperature-induced growth in Arabidopsis. Plant J **60,** 589-601.

Tang, R.H., Han, S., Zheng, H., Cook, C.W., Choi, C.S., Woerner, T.E., Jackson, R.B., and Pei, Z.M. (2007). Coupling diurnal cytosolic Ca2+ oscillations to the CAS-IP3 pathway in Arabidopsis. Science **315,** 1423-1426.

Tasset, C., Singh Yadav, A., Sureshkumar, S., Singh, R., van der Woude, L., Nekrasov, M., Tremethick, D., van Zanten, M., and Balasubramanian, S. (2018). POWERDRESS-mediated histone deacetylation is essential for thermomorphogenesis in Arabidopsis thaliana. PLoS Genetics **14,** e1007280.

TEJEDOR-CANO, J., PRIETO-DAPENA, P., Almoguera, C., Carranco, R., Hiratsu, K., OHME-TAKAGI, M., and Jordano, J. (2010). Loss of function of the HSFA9 seed longevity program. Plant, Cell & Environment **33,** 1408-1417.

Tubiello, F.N., Soussana, J.-F., and Howden, S.M. (2007). Crop and pasture response to climate change. Proceedings of the National Academy of Sciences **104,** 19686-19690.

Vierling, E. (1991). The roles of heat shock proteins in plants PAnnual Review of Plant Physiology and Plant Molecular Biology **42,** 579-620.

von Koskull-Döring, P., Scharf, K.D., and Nover, L. (2007). The diversity of plant heat stress transcription factors. Trends Plant Sci **12,** 452-457.

Vu, L.D., Gevaert, K., and De Smet, I. (2019). Feeling the Heat: Searching for Plant Thermosensors. Trends Plant Sci **24,** 210-219.

Wahid, A., Gelani, S., Ashraf, M., and Foolad, M.R. (2007). Heat tolerance in plants: an overview. Environmental and experimental botany **61,** 199-223.

Wang, L., Feng, Z., Wang, X., Wang, X., and Zhang, X. (2010). DEGseq: an R package for identifying differentially expressed genes from RNA-seq data. Bioinformatics **26,** 136-138.

Wang, Z.P., Xing, H.L., Dong, L., Zhang, H.Y., Han, C.Y., Wang, X.C., and Chen, Q.J. (2015). Egg cell-specific promoter-controlled CRISPR/Cas9 efficiently generates homozygous mutants for multiple target genes in Arabidopsis in a single generation. Genome Biol **16,** 144.

Wenjing, W., Chen, Q., Singh, P.K., Huang, Y., and Pei, D. (2020). CRISPR/Cas9 edited HSFA6a and HSFA6b of Arabidopsis thaliana offers ABA and osmotic stress insensitivity by modulation of ROS homeostasis. Plant Signaling & Behavior **15,** 1816321.

Wu, C. (1995). Heat Shock Transcription Factors: Structure and Regulation. Annual Review of Cell and Developmental Biology **11,** 441-469.

Wunderlich, M., Groß-Hardt, R., and Schöffl, F. (2014). Heat shock factor HSFB2a involved in gametophyte development of Arabidopsis thaliana and its expression is controlled by a heat-inducible long non-coding antisense RNA. Plant molecular biology **85,** 541-550.

Yeh, C.H., Kaplinsky, N.J., Hu, C., and Charng, Y.Y. (2012). Some like it hot, some like it warm: phenotyping to explore thermotolerance diversity. Plant Sci **195,** 10-23.

Yoshida, T., Mogami, J., and Yamaguchi-Shinozaki, K. (2014). ABA-dependent and ABA-independent signaling in response to osmotic stress in plants. Current Opinion in Plant Biology **21,** 133-139.

Yoshida, T., Sakuma, Y., Todaka, D., Maruyama, K., Qin, F., Mizoi, J., Kidokoro, S., Fujita, Y., Shinozaki, K., and Yamaguchi-Shinozaki, K. (2008). Functional analysis of an Arabidopsis heat-shock transcription factor HsfA3 in the transcriptional cascade downstream of the DREB2A stress-regulatory system. Biochem Biophys Res Commun **368,** 515-521.

Yu, G., Wang, L.G., Han, Y., and He, Q.Y. (2012). clusterProfiler: an R package for comparing biological themes among gene clusters. Omics **16,** 284-287.

Yue, B., Xue, W., Xiong, L., Yu, X., Luo, L., Cui, K., Jin, D., Xing, Y., and Zhang, Q. (2006). Genetic basis of drought resistance at reproductive stage in rice:

separation of drought tolerance from drought avoidance. Genetics **172,** 1213-1228.

Zang, D., Wang, J., Zhang, X., Liu, Z., and Wang, Y. (2019). Arabidopsis heat shock transcription factor HSFA7b positively mediates salt stress tolerance by binding to an E-box-like motif to regulate gene expression. J Exp Bot **70,** 5355-5374.

Zhu, J.-K. (2001). Plant salt tolerance. Trends in Plant Science **6,** 66-71.

Zhu, J.-K. (2002). Salt and drought stress signal transduction in plants. Annual review of plant biology **53,** 247-273.

Zhu, J.-K., Liu, J., and Xiong, L. (1998). Genetic analysis of salt tolerance in Arabidopsis: evidence for a critical role of potassium nutrition. The Plant Cell **10,** 1181-1191.

張凌誌**.** (2021). 阿拉伯芥熱休克因子 HSFC1 在溫度逆境下的表達調控.

Appendix

Appendix 1. The map of pHEE401E vector for generation of double mutant lines.
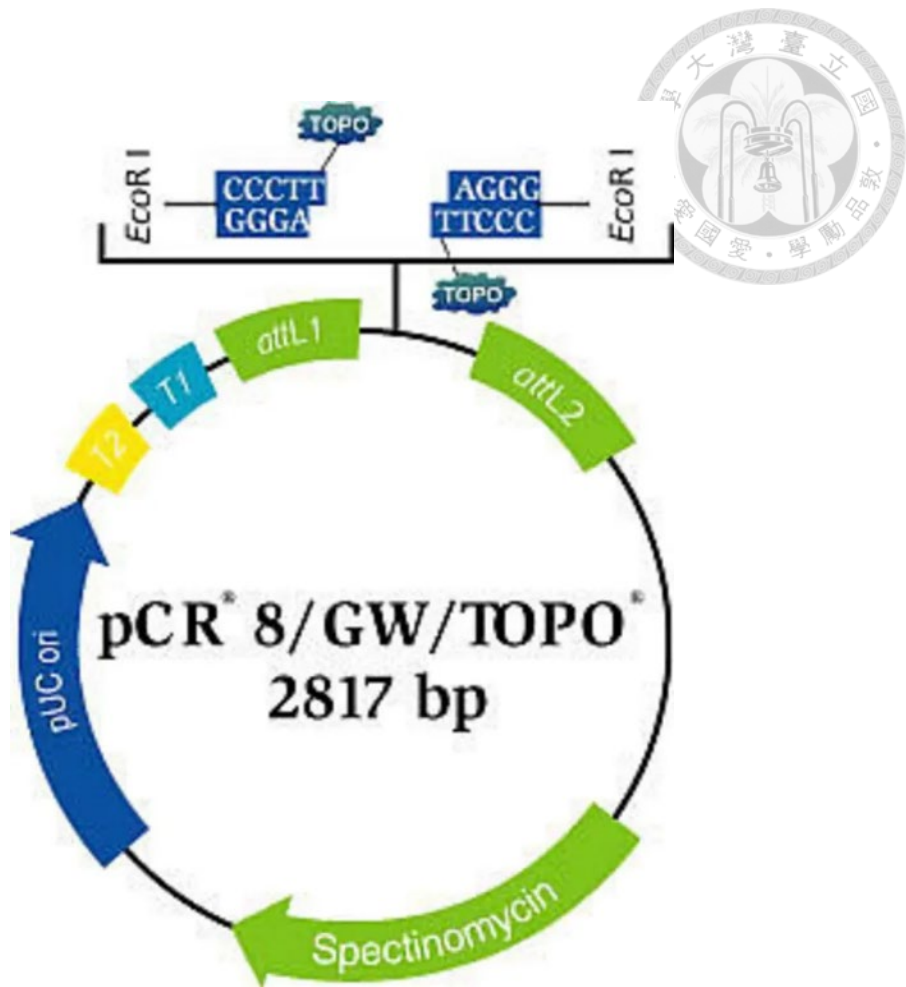
Appendix 2. The map of pCR8/GW/TOPO vector.

Appendix 3. The map of pEarleyGate 201 vector used for *HSFA7a* overexpression lines. Kanamycin is the bacterial resistance marker, while BASTA is the seedling selection marker in the pEarleyGate 201.

pCAMBIA3300-35S-GW-3xFLAG

Appendix 4. The map of a modified vector pCAMBIA3300-35S-GW-3xFLAG used

for *HSFA7b* overexpression lines. Kanamycin is the bacterial resistance marker, while

BASTA is the seedling selection marker in the pCMABIA-3300 backbone.